Assessing brain structure and function with diffusion-weighted MRI

Application to stroke

Filatova, Lena

DOI
10.4233/uuid:38dffcc5-11fb-45c1-8de9-1d9fba72a395

Publication date
2019

Document Version
Final published version

Citation (APA)
Filatova, L. (2019). *Assessing brain structure and function with diffusion-weighted MRI: Application to stroke*. [Dissertation (TU Delft), Delft University of Technology]. https://doi.org/10.4233/uuid:38dffcc5-11fb-45c1-8de9-1d9fba72a395

Assessing Brain Structure and Function with Diffusion-Weighted MRI: Application to Stroke

Assessing Brain Structure and Function with Diffusion-Weighted MRI: Application to Stroke

PROEFSCHRIFT

ter verkrijging van de graad van doctor
aan de Technische Universiteit Delft,
op gezag van de Rector Magnificus Prof. Dr. ir. T.H.J.J. van der Hagen,
voorzitter van het College voor Promoties,
in het openbaar te verdedigen op maandag 28 januari om 15:00 uur
door

Olena Grygorivna FILATOVA

Master of Science in Industrial and Applied Mathematics
Technische Universiteit Eindhoven, Nederland
geboren te Odessa, Oekraïne.

Dit proefschrift is goedgekeurd door de
promotoren: Prof. dr. ir. L.J. van Vliet
Prof. dr. F.C.T. van der Helm
copromotoren: Dr. F.M. Vos
Dr. ir. A.C. Schouten

Samenstelling promotiecommissie:

Rector Magnificus	chairman
Prof. dr. F.C.T. van der Helm	Technische Universiteit Delft, promotor
Prof. dr. ir. L.J. van Vliet	Technische Universiteit Delft, promotor
Dr. F. M. Vos	Technische Universiteit Delft, copromotor
Dr. ir. A.C. Schouten	Technische Universiteit Delft, copromotor

Onafhankelijke leden

Dr. L.J. O'Donnell	Harvard Medical School
Dr. A. Vilanova Bartroli	Technische Universiteit Delft
Prof.dr. A. van der Lugt	Erasmus MC, Rotterdam
Prof.dr.ir. B.P.F. Lelieveldt	Leiden University MC
Prof.dr.ir. J. Harlaar	Technische Universiteit Delft, reservelid

The work in this thesis was conducted at the Biomechanical Engineering (BME) Group, Faculty of 3mE and the Quantitative Imaging Group (QI), Faculty of Applied Sciences, Delft University of Technology.

The work was funded by the European Research Council under the European Union's Seventh Framework Program (FP/2007-2013) ERC Grant Agreement n. 291339, project 4D EEG: A new tool to investigate spatial and temporal activity patterns in the brain.

Keywords: diffusion MRI, stroke, brain, ADHD

Cover design: O.G. Filatova and O.I. Matveichuk

Printed by: Ridderprint BV

ISBN 978-94-6384-009-5

An electronic version of this dissertation is available at http://repository.tudelft.nl/.

Contents

1
Introduction

Beginnings are always messy.

John Galsworthy

1 Introduction

"The brain, and the brain alone, is the source of our pleasures, joys, laughter, and amusement, as well as our sorrow, pain, grief and tears. It is especially the organ we use to think and learn, see and hear, to distinguish the ugly from the beautiful, the bad from the good, and the pleasant from the unpleasant. The brain is also a seat of madness and delirium, of the fears and terrors that assail us, often at night, but sometimes even during the day, of insomnia, sleepwalking, elusive thoughts, forgetfulness, and eccentricities… In these ways I am of the opinion that the brain exercises the greatest power in the man. This is the interpreter to us of those things which emanate from the air, when it [the brain] happens to be in a sound state."

Hippocrates, ca. 400 BC

1.1 Human Brain

The first known reference to the brain dates back to the 17th century BC and was found in an Egyptian medical papyrus. From that time people have been fascinated and intrigued by the brain and its inner workings, which is frequently reflected in art and popular culture, e.g. Figure 1.1.

The human brain is a complex network of about 86 billion neurons (Herculano-

Figure 1.1 "Anatomy lesson of Dr. Deijman", Rembrandt, 1656. This painting shows a brain dissection being performed on the cadaver of an executed criminal (left); supervillain Krang, "Teenage Mutant Ninja Turtles" series.

Houzel, 2009). A neuron typically consists of a cell body, dendrites, and an axon, see Figure 1.2. An outer, folded layer of the brain is largely formed by neuronal cell bodies and is called the cerebral cortex, which is frequently referred to as the grey matter (GM). Dendrites are branching extensions of the cell body via which the neuron receives information from other neurons. An axon is a long extension via which electrical impulses are sent to surrounding cells from the neuron's cell body. A neuron has a large amount of dendrites, however there is only one axon originating from the neuron's cell body. Axons of multiple neurons form bundles connecting different parts of the grey matter. Such bundles are called tracts and constitute the so-called white matter (WM). Nerve fibers are surrounded by myelin, which mainly consists of fat (70-80%) and protein (20-30%). Myelin gives the white matter its color and acts as an electrical insulation improving the speed of electrical nerve signals transmission.

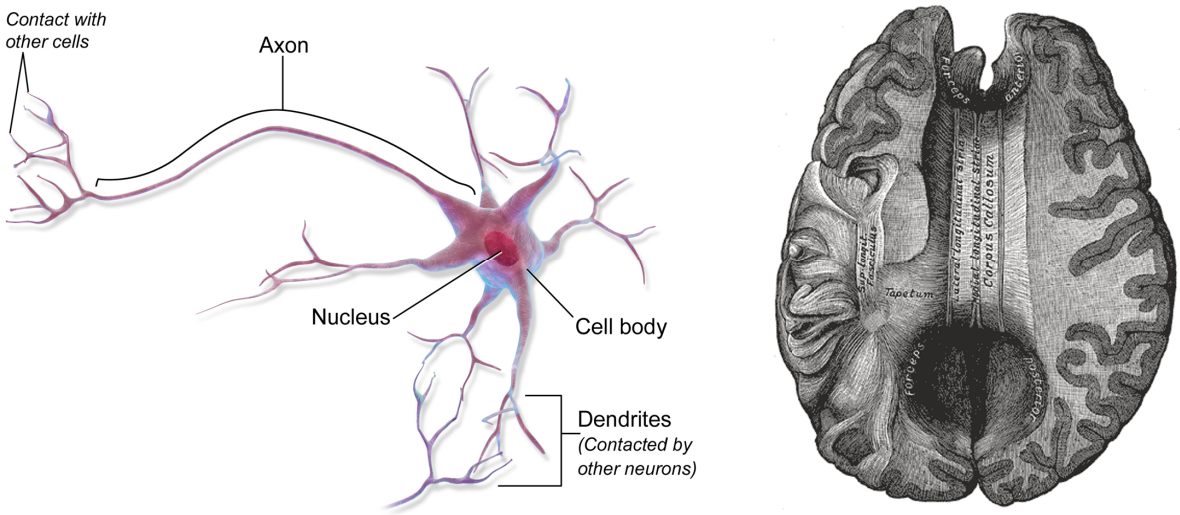

Figure 1.2 Left: Schematic of a neuron consisting of a cell body, dendrites and an axon, modified from (Blausen.com, 2014). Right: cerebral cortex and view of corpus callosum WM tract from above, adapted from (Bartleby.com, 2000). Cerebral cortex is frequently referred to as grey matter. Corpus callosum is a tract connecting right and left brain hemispheres.

1.2 Cardiovascular diseases and brain disorders

According to the factsheet of the (World Health Organization, 2017), cardiovascular diseases (CVDs) are the leading cause of death globally with estimated 17.7 million people or 31% of global deaths in 2015, of which 6.7 million were due to stroke. Ischemic stroke is an abrupt interruption of the blood

flow to certain brain areas, which results in brain cell death. Among the survivors, stroke is a major cause of disability in the developed world with up to 80% suffering from upper limb paresis (Kwakkel et al., 2003; Dobkin, 2005). In the Netherlands, societal cost per stroke survivor in the first year after stroke is estimated as €29500 (van Eeden et al., 2015). Three quarters of the costs are spent in the first six months, mainly due to hospital, rehabilitation and loss of productivity costs (van Eeden et al., 2015). As the population is aging, total economic burden of stroke is expected to grow, unless structure and costs of rehabilitation and treatment change.

Prognosis for upper limb motor recovery/outcome is mainly determined within the first hours and days after the onset of brain ischemia. Recently, (Winters et al., 2015) showed that outcome of motor recovery of the upper paretic limb measured at 6 months is predictable within the first 72 hours post stroke using clinical determinants (e.g. absence of finger extension, stroke size, low motion scores of both upper and lower extremities). The extent of recovery in the majority of the patients is an almost fixed amount of about 70% of the total ly possible change, defined as the difference between patient motor score and maximum possible score (Byblow et al., 2015). However, ~30% of the patients, called non-fitters, experience less recovery than predicted by this proportional recovery rule (Winters et al., 2015) and the reason for that is not well understood.

There is a number of mechanisms which can account for damage reversibility of infarcted motor control areas post stroke. For example, it can be achieved by salvation of the tissue bordering the ischemic lesion or recovery of function in anatomically separated, but functionally related areas (Buma et al., 2013). A better insight into how neuronal networks change, starting from the acute phase after stroke onset, could help to understand the underlying recovery mechanisms and explain lack of recovery in these non-fitters. Additionally, prognostic models might be improved by an enhanced understanding of these mechanisms. Furthermore, having improved biomarkers of spontaneous recovery early after stroke could support assessing the impact of applied rehabilitative interventions. To achieve this, analysis techniques able to assess neurological damage have to be carefully designed and tested first in chronic stages and then during the course of recovery.

While stroke is more prevalent in older population, Attention-Deficit/Hyperactivity Disorder (ADHD) is a neurodevelopmental disorder, which is most frequently diagnosed in children and adolescents. There is no global consensus on the number of people it affects. However, a pooled estimate, based on analysis of 175 studies, is 7.2% in children under 18 (Thomas et al., 2015) and 3.4% in adults under 44 years (Fayyad et al., 2007). Prevalence in young children under 6 years old and adults over 44 years old is less well studied. Usually, severe cases are diagnosed at an early age, under 5 years old, moderate cases – under 7 years old and mild cases at a later age. Boys are two to three times more frequently diagnosed with ADHD, depending on the disease type (Willcutt, 2012; Visser et al., 2014). The reason for this gender imbalance is not yet clear. As more and more children are diagnosed with ADHD and treated with stimulant medication, it is important to get a better insight into the effects this medication may have on the patients' brain. Specifically, learning whether these effects are age dependent would facilitate better treatment of afflicted children and teenagers.

1.3 Electric activity of the brain

The outer layer of the brain, cortex, with thickness varying between about 2 and 5 mm, has a folded structure formed from a smooth neuronal tube during fetal development. This process creates grooves, called sulci, and ridges, called gyri, with a total cortex surface area of roughly 2000 cm^2. Electrical current in the brain is the flow of ions through channels in neuronal membranes, the direction of which is determined by the membrane potential. Existence of this current was discovered by Richard Caton in 1875 and first measured on the human scalp by Hans Berger in 1924, (Teplan, 2002). Such measurements, achieved by placing a number of electrodes on the scalp, are called electroencephalography (EEG) and normally have amplitude ranging between 0.5 and 100 μV. Typically, between 32 and 256 electrodes are used for measuring EEG, but in some cases even signal from one or two electrodes placed over a region of interest can be employed.

The potential generated by a single neuron is not sufficient to be picked up by the EEG electrodes. However, a measurable signal results from synchronized activity of cortical neuron populations (da Silva, 2009), where the active neurons must be

arranged parallel to each other. A configuration in which a region of positive charge is spatially separated from a region of negative charge is referred to as a dipole. EEG can measure two major types of dipoles: tangential and radial with respect to the scalp surface. Tangential dipoles generally originate from the cortical gyri and radial ones from the sulci. See (Jackson and Bolger, 2014) for the review of neurophysiological bases and details of EEG measurement.

With typical sampling rates ranging between 250 and 2000 Hz, and in some cases even higher (Weiergräber et al., 2016), EEG has high temporal resolution. However, even in the case of high density EEG set-ups, there exist more potential sources of brain activity than the number of EEG electrodes measuring that activity. Therefore, distribution of the electrical potentials recorded at the scalp does not uniquely translate into a configuration of dipoles, because multiple source distributions could explain the recorded potentials. This is known as an *inverse* problem and forms one of the main challenges in EEG analysis: finding an approach to solve this ill-posed problem (Koenig, 2014). Clearly, it requires making assumptions regarding the distribution and origin of brain activity. In practice, this is usually done in one of the following ways: assuming a limited number of active sources, direct search of the optimal source positions over the source space or introducing regularization methods/priors of the solution (Baillet et al., 2001; Darvas et al., 2004). The other part of EEG source estimation, also called source localization, is the conduction problem, which allows to calculate the potential field values given the source distribution. This is essentially the *forward* part of the inverse problem. To solve it, again several assumptions are needed (i.e., the skull can be assumed spherical or modeled based on MRI information) in search of a balance between model accuracy and computational complexity (Baillet et al., 2001).

1.4 Brain imaging

Since the first human body magnetic resonance imaging (MRI) scan was recorded in 1977 (Damadian et al., 1977), its clinical applications and our technical abilities have come a long way. Nowadays, images can be created with widely varying tissue contrasts, high resolution and high SNR. An important factor enabling this has

been the increased strengths of the main magnetic field of scanners. The main magnetic field of commercially available MRI scanners for clinical purpose ranges up to 3 T, whereas for research purposes 7 T or even 11.7 T could be used. What is more, scanners with up to 23.5 T exist for nuclear magnetic resonance spectrometry. To put these enormous fields into perspective, a souvenir refrigerator magnet is hundreds of times weaker with 5 mT and the Earth's magnetic field varies between about 30 and 70 μT, depending on the latitude[1].

These magnetic fields are used to manipulate and measure the magnetization of the nuclear spins – typically, H^+ ions – in the body. First of all, the nuclear spins tend to align in the direction of a strong static magnetic field, the B_0 field. Furthermore, the nuclear spins will start to precess around this B_0 field at a frequency proportional to the field strength, known as the Larmor frequency and given by:

$$\omega = \gamma B_0, \tag{1.1}$$

where γ is the gyromagnetic ratio and B_0 is the strength of the static magnetic field.

Gradient coils are used to generate gradients in the static magnetic field and introduce a positional dependency of the precession frequencies, which makes it possible to differentiate between signals coming from different positions in the body. Finally, radio frequency (RF) pulses are used to flip the magnetization into a plane that is transverse to the B_0 field. In this way weak RF fields generated by the precessing spins can be measured using receive coils. As the precession frequency is location-dependent, this signal is at the basis to form an image. Conventional MRI is an established technique for assessment of patients, which allows to exploit different tissue contrasts depending on the specific acquisition sequence.

Molecules of gases and liquids are involved in constant random motion associated with their thermal energy. This process is also called diffusion. The MR signal can be made sensitive to molecular diffusion, which causes a decrease in signal amplitude. This sensitivity is exploited to acquire diffusion-weighted images. The

[1] https://en.wikipedia.org/wiki/Orders_of_magnitude_(magnetic_field)

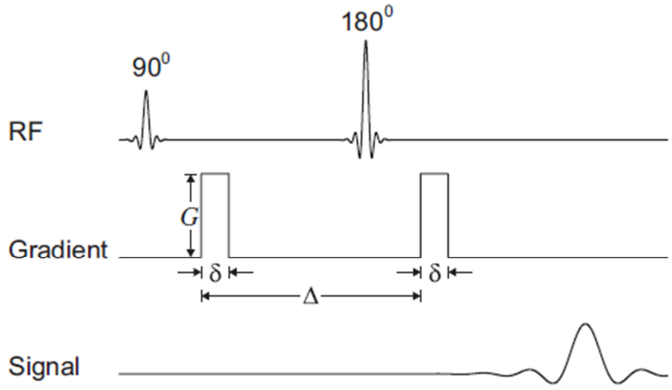

Figure 1.3 A schematic of the pulsed field gradient spin echo MR technique introduced by Stejskal and Tanner (1965). Figure is adapted from (Basser and Özarslan, 2009). In contrast with the acquisition sequence containing only RF pulses and the echo (signal recording), two gradients are applied after flipping the spins into a transverse plane with the 90^0 pulse and after rephrasing with the 180^0 pulse. When a water molecule diffuses during the sequence, it is exposed to varying gradient strength and dephases. This occurs at a much smaller scale than a single voxel and reduces the amount of the measured signal.

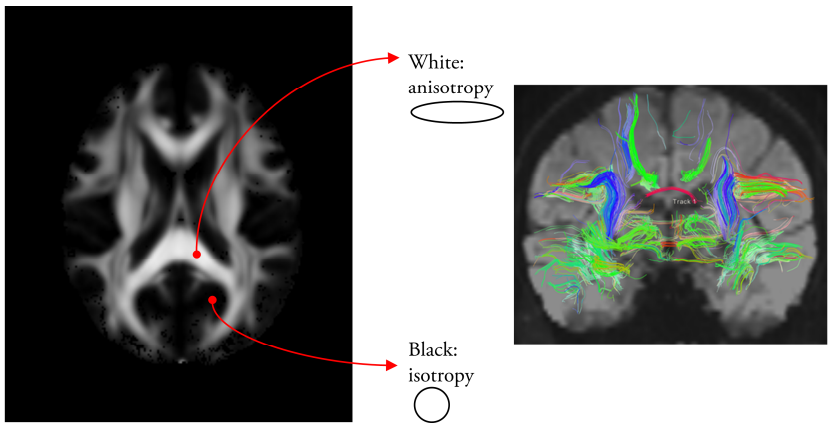

Figure 1.4 The diffusion is typically modelled by a mathematical construct called a tensor, which is visualized by an ellipsoid. It basically represents the shape of the local diffusion, from which scalar measures are derived such as, for example, the fractional anisotropy (FA), left. Fiber tracts are streamlines throughout the tensor field, indicating the WM bundles, right.

classical diffusion weighted MRI (dMRI) acquisition scheme introduced by (Stejskal and Tanner, 1965) is presented in Figure 1.3.

The level of induced sensitivity to diffusion is called a b-value. Quantitatively, it can be expressed via parameters of the MR acquisition:

$$b = (\gamma \delta G)^2 (\Delta - \delta / 3), \tag{1.2}$$

where G is the magnetic gradient amplitude, δ is the gradient duration and Δ is the time between two diffusion synthesizing gradients.

Complementary to conventional, anatomical MRI, diffusion weighted MRI (dMRI) reflects tissue structure. Particularly, it measures the ability of water molecules to move freely in the surrounding tissue. Human white matter (WM) bundles have a structure due to which water molecules both inside and outside the axons can diffuse easier along the tracts than perpendicular to them. Importantly, normal WM shows high diffusivity along and low across axons, whereas in gray matter (GM) the diffusion is more isotropic, i.e. direction-independent (see Figure 1.4). Frequently, dMRI studies compare *fractional anisotropy* (FA) maps between subject groups. Here FA is a scalar measure describing the degree of anisotropy of a diffusion process and ranging between zero (equal diffusion in all directions) and one (diffusion along one direction only). FA and other diffusion measures give indication of microstructural tissue properties, c.q. neuronal integrity More recently, dMRI has also been used to study prevalent networks in the brain: structural connectivity analysis.

1.5 Connectivity: structure and function

White matter tracts connect grey matter areas with each other, forming an anatomical brain network. By following the diffusion directions, modeled based on dMRI, we can infer the orientations of the WM bundles and their properties. Reconstruction of such inferred connections is called tractography (Behrens and Jbabdi, 2009). To explore brain networks, they can be modelled as graphs composed of nodes (vertices) denoting brain regions that are linked by edges representing physical connections. Structural networks of the human brain, also known as the human connectome, can be either studied as binary graphs (connection is present/absent) or weighted graphs. In the latter case, properties of the tracts such as their length or mean diffusivity measures over the tracts can be used as weights for the graph edges, describing the *structural* connectivity (SC) (Bullmore and Sporns, 2009).

The structural connection formed between pairs of brain areas may be at the basis of some kind of activity interaction between them (Rubinov and Sporns, 2010).

Conventionally, these interactions are defined as temporal correlation (statistical dependence) or causal relation between activity of brain areas. In general this is referred to as *functional* connectivity (FC), which can be derived, for example, from EEG or functional MRI measurements (Bastos and Schoffelen, 2016). Such recordings can be performed either in the 'resting state' condition or while subjects perform certain tasks.

In the past years both SC and FC have been investigated in healthy population and animal models to reveal architecture and characteristics of brain network organization (Bassett et al., 2011a; Bullmore and Bassett, 2011; Azadbakht et al., 2015; van den Heuvel et al., 2015). Based on various studies it is clear that changes in the connectome (either structural or functional) are associated with brain development or its deterioration due to diseases. Such changes can be indicative of human learning (Bassett et al., 2011b) or help predict effects of lesions (Alstott et al., 2009). In simulated and healthy subjects' data, a strong interrelation between structural and resting state functional connectivity was demonstrated, even though functional connectivity can be present between regions without direct anatomical linkage (Honey et al., 2009). In clinical population of schizophrenia patients, it was found that coupling between SC and FC is disrupted (Cocchi et al., 2014). Therefore, it is becoming increasingly clear that brain structure and function should be studied together to capture the complex nature of neurological alterations during aging or disease development.

1.6 4D-EEG: a new tool to investigate the spatial and temporal activity patterns in the brain

The 4D-EEG project was a collaboration among Delft University of Technology, VU University Medical Center, VU University, and Northwestern University, and was funded by the European Research Council (Advanced ERC grant, n. 291339). The aim of the 4D-EEG project was to develop a new methodology allowing to assess the dynamics of neural processing during motor control in healthy individuals and in stroke survivors. Different research directions within the project included: system identification techniques on EEG recordings, source localization methodology, and analysis of dMRI. This thesis mainly focuses on dMRI analysis.

1.7 Problem statement and goal

Clinically, most of recovery after stroke occurs in the first months after the incident and varies greatly between patients. Predicting functional outcome from initial patient status is difficult as it depends on many factors including direct nerve fiber damage and subsequent degeneration of areas more distal to the lesion. The role of different cerebral structures in motor deficits and impact of stroke on them are not exactly known. The assessment of the neural dynamics both in healthy subjects and in stroke population could increase our understanding of the sensorimotor system.

Accordingly, the overall objective of this thesis is to enhance understanding of the neurological alterations in patients using diffusion-weighted MRI modeling. We intend to investigate influence of stroke on the human brain by measuring structural features with dMRI and combining them with functional properties obtained by EEG. Evaluation of the WM integrity using brain imaging may in the future enable to set realistic therapeutic goals and selection of particular rehabilitation approaches.

1.8 Thesis Outline

Chapter 2 presents an example of how diffusion-weighted MRI can be used in a randomized clinical trial. It is investigated whether effects of medication used to mitigate ADHD on the brain WM are modulated by age.

In **Chapter 3** properties estimated by different diffusion-tensor models are related to the motor function of the upper limb of stroke survivors. Additionally, the asymmetry of these diffusion characteristics in lesional/contralesional hemisphere in stroke patients is compared to that of healthy subjects.

Chapter 4 introduces a framework for probabilistic tractography based on spatially varying diffusion models: in each voxel the best fitting diffusion model is selected.

Chapter 5 describes an advanced computational approach to track the information flow in the brain based on Bayesian hierarchical modeling of EEG sources with constraints derived from anatomical and diffusion-weighted MRI. This method is then validated using in-vivo sensorimotor evoked potentials' measurements.

Chapter 6 assesses evolution of diffusion properties in major white matter tracts during the recovery period for six case studies. No clear relation between the changes in the diffusivity properties of the patient WM and their motor outcome was found. The results suggest that the rapid decrease of the brain swelling in the first weeks post-stroke is associated with motor recovery.

The thesis is concluded by discussing advantages and limitations of the current work and presenting an outlook on future research in this field.

References

Alstott, J., Breakspear, M., Hagmann, P., Cammoun, L., and Sporns, O. (2009). Modeling the impact of lesions in the human brain. *PLoS Comput Biol* 5(6), e1000408. doi: 10.1371/journal.pcbi.1000408.

Azadbakht, H., Parkes, L.M., Haroon, H.A., Augath, M., Logothetis, N.K., de Crespigny, A., et al. (2015). Validation of High-Resolution Tractography Against In Vivo Tracing in the Macaque Visual Cortex. *Cereb Cortex*. doi: 10.1093/cercor/bhu326.

Baillet, S., Mosher, J.C., and Leahy, R.M. (2001). Electromagnetic brain mapping. *IEEE Signal Processing Magazine* 18(6), 14-30. doi: 10.1109/79.962275.

Bartleby.com (2000). (New York).

Basser, P.J., and Özarslan, E. (2009). "Chapter 1 - Introduction to Diffusion MR A2 - Johansen-Berg, Heidi," in *Diffusion MRI,* ed. T.E.J. Behrens. (San Diego: Academic Press), 2-10.

Bassett, D.S., Brown, J.A., Deshpande, V., Carlson, J.M., and Grafton, S.T. (2011a). Conserved and variable architecture of human white matter connectivity. *Neuroimage* 54(2), 1262-1279. doi: 10.1016/j.neuroimage.2010.09.006.

Bassett, D.S., Wymbs, N.F., Porter, M.A., Mucha, P.J., Carlson, J.M., and Grafton, S.T. (2011b). Dynamic reconfiguration of human brain networks during learning. *Proc Natl Acad Sci U S A* 108(18), 7641-7646. doi: 10.1073/pnas.1018985108.

Bastos, A.M., and Schoffelen, J.-M. (2016). A Tutorial Review of Functional Connectivity Analysis Methods and Their Interpretational Pitfalls. *Frontiers in Systems Neuroscience* 9(175). doi: 10.3389/fnsys.2015.00175.

Behrens, T.E.J., and Jbabdi, S. (2009). "Chapter 15 - MR Diffusion Tractography," in *Diffusion MRI*. (San Diego: Academic Press), 333-351.

Blausen.com (2014). "Medical gallery of Blausen Medical 2014", in: *WikiJournal of Medicine.*).

Bullmore, E., and Sporns, O. (2009). Complex brain networks: graph theoretical analysis of structural and functional systems. *Nat Rev Neurosci* 10(3), 186-198. doi: 10.1038/nrn2575.

Bullmore, E.T., and Bassett, D.S. (2011). Brain graphs: graphical models of the human brain connectome. *Annu Rev Clin Psychol* 7, 113-140. doi: 10.1146/annurev-clinpsy-040510-143934.

Buma, F., Kwakkel, G., and Ramsey, N. (2013). Understanding upper limb recovery after stroke. *Restor Neurol Neurosci* 31(6), 707-722. doi: 10.3233/RNN-130332.

Byblow, W.D., Stinear, C.M., Barber, P.A., Petoe, M.A., and Ackerley, S.J. (2015). Proportional recovery after stroke depends on corticomotor integrity. *Annals of Neurology* 78(6), 848-859. doi: 10.1002/ana.24472.

Cocchi, L., Harding, I.H., Lord, A., Pantelis, C., Yucel, M., and Zalesky, A. (2014). Disruption of structure-function coupling in the schizophrenia connectome. *Neuroimage Clin* 4, 779-787. doi: 10.1016/j.nicl.2014.05.004.

da Silva, F.L. (2009). EEG: Origin and Measurement. 19-38. doi: 10.1007/978-3-540-87919-0_2.

Damadian, R.V., Goldsmith, M., and Minkoff, L. (1977). NMR in cancer: XVI. FONAR image of the live human body. *Physiol. Chem. Phys.* 9(1), 97-100.

Darvas, F., Pantazis, D., Kucukaltun-Yildirim, E., and Leahy, R.M. (2004). Mapping human brain function with MEG and EEG: methods and validation. *NeuroImage* 23, S289-S299. doi: https://doi.org/10.1016/j.neuroimage.2004.07.014.

Dobkin, B.H. (2005). Clinical practice. Rehabilitation after stroke. *N Engl J Med* 352(16), 1677-1684. doi: 10.1056/NEJMcp043511.

Fayyad, J., De Graaf, R., Kessler, R., Alonso, J., Angermeyer, M., Demyttenaere, K., et al. (2007). Cross–national prevalence and correlates of adult attention–deficit hyperactivity disorder. *The British Journal of Psychiatry* 190(5), 402.

Herculano-Houzel, S. (2009). The human brain in numbers: a linearly scaled-up primate brain. *Frontiers in Human Neuroscience* 3, 31.

Honey, C.J., Sporns, O., Cammoun, L., Gigandet, X., Thiran, J.P., Meuli, R., et al. (2009). Predicting human resting-state functional connectivity from

structural connectivity. *Proc Natl Acad Sci U S A* 106(6), 2035-2040. doi: 10.1073/pnas.0811168106.

Jackson, A.F., and Bolger, D.J. (2014). The neurophysiological bases of EEG and EEG measurement: A review for the rest of us. *Psychophysiology* 51(11), 1061-1071. doi: 10.1111/psyp.12283.

Koenig, T. (2014). "Basic Principles of EEG and MEG Analysis".).

Kwakkel, G., Kollen, B.J., van der Grond, J., and Prevo, A.J. (2003). Probability of regaining dexterity in the flaccid upper limb: impact of severity of paresis and time since onset in acute stroke. *Stroke* 34(9), 2181-2186. doi: 10.1161/01.STR.0000087172.16305.CD.

Rubinov, M., and Sporns, O. (2010). Complex network measures of brain connectivity: uses and interpretations. *Neuroimage* 52(3), 1059-1069. doi: 10.1016/j.neuroimage.2009.10.003.

Stejskal, E.O., and Tanner, J.E. (1965). Spin Diffusion Measurements: Spin Echoes in the Presence of a Time - Dependent Field Gradient. *The Journal of Chemical Physics* 42(1), 288-292. doi: 10.1063/1.1695690.

Teplan, M. (2002). Fundamentals of EEG Measurement. *IEEE Measurement Science Review* 2, 1-11.

Thomas, R., Sanders, S., Doust, J., Beller, E., and Glasziou, P. (2015). Prevalence of Attention-Deficit/Hyperactivity Disorder: A Systematic Review and Meta-analysis. *Pediatrics*. doi: 10.1542/peds.2014-3482.

van den Heuvel, M.P., de Reus, M.A., Feldman Barrett, L., Scholtens, L.H., Coopmans, F.M., Schmidt, R., et al. (2015). Comparison of diffusion tractography and tract-tracing measures of connectivity strength in rhesus macaque connectome. *Hum Brain Mapp* 36(8), 3064-3075. doi: 10.1002/hbm.22828.

van Eeden, M., van Heugten, C., van Mastrigt, G.A.P.G., van Mierlo, M., Visser-Meily, J.M.A., and Evers, S.M.A.A. (2015). The burden of stroke in the Netherlands: estimating quality of life and costs for 1 year poststroke. *BMJ Open* 5(11).

Visser, S.N., Danielson, M.L., Bitsko, R.H., Holbrook, J.R., Kogan, M.D., Ghandour, R.M., et al. (2014). Trends in the Parent-Report of Health Care Provider-Diagnosed and Medicated Attention-Deficit/Hyperactivity Disorder: United States, 2003–2011. *Journal of the American Academy of Child & Adolescent Psychiatry* 53(1), 34-46.e32. doi: 10.1016/j.jaac.2013.09.001.

Weiergräber, M., Papazoglou, A., Broich, K., and Müller, R. (2016). Sampling rate, signal bandwidth and related pitfalls in EEG analysis. *Journal of Neuroscience Methods* 268, 53-55. doi: https://doi.org/10.1016/j.jneumeth.2016.05.010.

Willcutt, E.G. (2012). The Prevalence of DSM-IV Attention-Deficit/Hyperactivity Disorder: A Meta-Analytic Review. *Neurotherapeutics* 9(3), 490-499. doi: 10.1007/s13311-012-0135-8.

Winters, C., van Wegen, E.E.H., Daffertshofer, A., and Kwakkel, G. (2015). Generalizability of the Proportional Recovery Model for the Upper Extremity After an Ischemic Stroke. *Neurorehabilitation and Neural Repair* 29(7), 614-622. doi: 10.1177/1545968314562115.

World Health Organization (2017). *Cardiovascular diseases Fact Sheet* [Online]. http://www.who.int/mediacentre/factsheets/fs317/en/. [Accessed 24 October 2017].

2

DTI application in ADHD

The successful person places more attention on doing the right thing rather than doing things right.

Peter F. Drucker

2 Effects of Methylphenidate on White Matter in Children and Adults With Attention-Deficit/Hyperactivity Disorder

Objective Although methylphenidate (MPH) is highly effective in treating attention-deficit/hyperactivity disorder (ADHD), not much is known about its effect on the development of human brain white matter (WM).

Method To determine whether MPH modulates WM age-dependently, we set up a randomized, double-blind, placebo-controlled trial (ePOD-MPH) among ADHD referral centers (NTR3103). Fifty male stimulant treatment naïve boys (aged 10-12 years of age) and 49 adult men (23-40 years of age) diagnosed with ADHD (all types) according to DSM-IV criteria were randomized to treatment with MPH or a placebo for 16 weeks. Before and one week after treatment cessation, patients underwent MR imaging including diffusion tensor imaging (DTI). The main outcome measure was change in fractional anisotropy (FA), which was assessed in three regions of interest (ROIs) as well as voxel-based in the whole WM. Data was analysed using intention to treat using linear mixed models for ROI analysis and a permutation-based methods for voxel based analysis.

Results Analysis of the ROIs yielded no main effect of time in any of the conditions. However, voxel-based analysis revealed significant time-by-medication-by-age interaction effects in several association tracts of the left hemisphere as well as lateral aspect of the truncus of the corpus callosum, due to more rapid increase in FA in MPH treated children, and not so in children receiving a placebo, nor adults.

Interpretation Our findings suggest that, at least on the short-term and in boys with ADHD, the effects of MPH on specific tracts in brain WM are modulated by age.

2.1 Introduction

Attention-deficit/hyperactivity disorder (ADHD) is the most frequently diagnosed neurodevelopmental disorder, with symptoms arising in childhood and often persisting into adulthood (Merikangas et al., 2010). Methylphenidate (MPH) is a commonly prescribed psychotropic drug for treatment of ADHD and its efficacy is very high (MTA Cooperative Group, 1999). ADHD has been associated with alterations in white matter (WM) tract development. A meta-analysis (van Ewijk et al., 2012) identified compromised WM integrity in several tracts in both pediatric and adult ADHD patients, including right anterior corona radiata containing fibers from the superior longitudinal fasciculus, forceps minor close to the genu of the corpus callosum (CC), right and left legs of internal capsule, and left cerebellar WM. However, the studies included in this meta-analysis were all retrospective in nature and the possible confounding effects of medication were not taken into account.

For instance, the initial paper by (Castellanos et al., 2002) reported an (+8.9%) increase, or rather normalization, of WM volume in medicated ADHD children compared to unmedicated children. However, in that retrospective study, medication status of the subjects was not well accounted for, and most subjects were already on ADHD medication. Interestingly, in a preclinical study in rats we observed an increase in FA only in the CC of adolescent rats treated with MPH, but not in adult rats or rats treated with a saline solution (van der Marel et al., 2014). These preclinical findings suggest that the effect of MPH on brain WM are modulated by age. Indeed, the adolescent brain is a rapidly developing system maintaining high levels of plasticity. For instance, the maturation and development of WM continues well into adulthood (Yap et al., 2013). Therefore, brain WM may be particularly vulnerable to drugs such as ADHD medication that interfere with these processes or modify the specific genes involved.

Evidently, increasing the knowledge about the effects of MPH on human brain development may result in better treatment of children and adolescents with ADHD. Therefore, we designed a randomized clinical trial (RCT) entitled the "Effects of Psychotropic medication On brain Development - Methylphenidate (ePOD-MPH) (Bottelier et al., 2014) study". This paper aims to investigate

whether the effects of MPH on human brain including WM are indeed modulated by age. Based on the available (preclinical) literature, we expected increased FA values in children treated with MPH but not in children treated with placebo, nor adults.

2.2 Materials and Methods

2.2.1 Experimental design

ePOD-MPH was a 16-week double-blind, RCT with MPH. A blinded end-point evaluation in stimulant-treatment naïve children and adults with ADHD was performed (Bottelier et al., 2014). Subjects were randomly assigned to either a placebo or treatment with MPH. The effect of age and MPH treatment on WM structure was assessed by means of DTI at baseline and at the end of the trial, after a one-week washout in week 18 to ensure drug clearance (half-life time of MPH is 2-3 hours). The trial protocol adhered to the Declaration of Helsinki (2013) and was registered by the Central Committee on Research Involving Human Subjects (an independent registry) on March 24, 2011 (identifier NL34509.000.10) and subsequently at The Netherlands National Trial Register (identifier NTR3103). The primary outcome measure of ePOD-MPH was to report on the modification by age of MPH treatment on the outgrowth of the DA system using pharmacological MRI, and second primary outcome measures included diffusion tensor imaging (DTI) for WM assessment. This RCT is the first study that examines the effects of MPH on the brain in children and young adults using MRI. This means that there is only limited and indirect data available to perform a sample size calculation. Our goal for this research was to be able to detect differences in the age-dependent effect of MPH on the outgrowth of the dopaminergic system if these differences were in the magnitude of a standardized effect size of 1.25. As we pointed out in our study protocol (online Supplementary), there are several pieces of evidence supporting the view that the expected differences will lead to standardized effect sizes of at least 1.25, including the DTI assessments we report here. Our findings on DA function (assessed using pharmacological MRI) have been reported elsewhere (Schrantee et al., 2016). The trial was monitored by the Clinical Research Unit of the Academic Medical Center.

2.2.2 Randomization and blinding

After baseline MRI assessment, every patient was stratified by age and randomized to receiving either MPH or placebo treatment (1:1) using a permuted block scheme generated by the local Clinical Research Unit. The hospital pharmacy (Alkmaar) received the information sealed and prepared the assigned treatment, i.e. MPH or placebo. Patients as well as the treating physician as well as research personnel were blinded to the type of treatment. The treating physician prescribed the study medication on clinical guidance (change of ADHD symptoms), in accordance with Dutch treatment guidelines. The placebo tablet matched the MPH tablet in appearance and was manufactured and labelled according to GMP guidelines (2003/94/EG). Therapy compliance was monitored on five control visits.

2.2.3 Participants

The included study subjects were 50 stimulant treatment-naive boys (10-12 years of age) and 48 stimulant treatment-naive men (23-40 years of age), of which baseline DTI values were published elsewhere (Bouziane et al., 2018). They were recruited in the outpatient clinics of the Child and Adolescent Psychiatry Center Triversum (Alkmaar), department of Child and Adolescent Psychiatry at the Bascule/AMC (Amsterdam), Adult ADHD program at PsyQ, psycho-medical programs clinical programs at the PsyQ mental health facility (The Hague) and from the department of Psychiatry of the AMC (Amsterdam). All subjects were diagnosed by an experienced psychiatrist based on the criteria of the Diagnostic and Statistical Manual of Mental Disorders (DSM-IV, 4th edition). The diagnosis was subsequently confirmed with a structured interview: the Diagnostic Interview Schedule for Children (National Institute of Mental Health Diagnostic Interview Schedule for Children Version IV, DISC-IV (Ferdinand and van der Ende, 2000)) and the Diagnostic Interview for ADHD (DIVA 2.0 (Kooij and Francken, 2010)) for adults. Inclusion criteria were at least 6 of 9 symptoms of inattention or hyperactivity/impulsivity on the DISC-IV (for children) and on the DIVA 2.0 (for adults). Patients were excluded if diagnosed with a co-morbid axis I psychiatric disorder requiring pharmacological treatment at study entry or having general contraindications for MRI such as implanted electric and electronic devices, metal implants or claustrophobia. Adult patients received coaching sessions, and parents of children received psychoeducation. All patients, and for the children also either both parents or their legal representatives, provided written informed consent.

2.2.4 Image Acquisition

DTI is a powerful non-invasive technique that enables assessment of micro-structural features of WM and microfiber neuronal pathways by measuring the diffusion of water molecules. Fractional anisotropy (FA) is a scalar measure that provides information about the degree of fiber organization and integrity (Feldman et al., 2010). Processes that lead to alterations in axonal architecture, such as altered axonal outgrowth, can result in FA changes (Reneman et al., 2001; Moeller et al., 2005; de Win et al., 2006). All MR imaging was performed on a 3.0T Philips MR scanner equipped with a SENSE 8-channel head coil and body coil transmission (Philips Medical Systems, Best, The Netherlands). DTI scans were obtained at baseline (week 0) and post-treatment . The scan parameters were: field of view: 224x224 mm, slice thickness: 2 mm, TR/TE: 8135/94 ms, scan time: 6m47s, SENSE: 2, slices: 60, 46 gradient directions with b=1000 s/mm^2, four averaged images with b=0 s/mm^2, half-scan: 0.797, fat suppression SPIR: 250 Hz.

2.2.5 DTI processing

Pre-processing of Diffusion Weighted Images (DWIs) is discussed in detail in the Supplementary Materials. Briefly, DWIs were corrected for distortions due to eddy currents and head motion (Mohammadi et al., 2010). Based on the latter correction, an overall motion score was calculated for each subject representing the degree of patient movement during scanning (Ling et al., 2012). Diffusion tensors were estimated from the DWIs after which the tensors' FA statistic was calculated. The pre-processing of the DTI data was partially performed using in-house developed software, written in Matlab (The MathWorks, Natick, MA). This was done using the AMC Neuroscience Gateway, using resources of the Dutch e-Science Grid with the support of SURF Foundation (Shahand et al., 2015). Average values of the diffusion statistics were computed over the whole WM (Castellanos et al., 2002), within a ROI central in the truncus of the CC (van der Marel et al., 2014), as well as well as in the bilateral anterior thalamic radiation (ATR) as determined by the JHU white-matter tractography atlas (Mori et al., 2005). The choice of whole brain FA and CC was based upon previous findings, while we included the ATR because it is an important tract in the frontal lobe, and one of the latest to mature (Klingberg et al., 1999; Barnea-Goraly et al., 2005; Yap et al., 2013). Therefore, a WM skeleton representation was generated with TBSS

software (Tract-Based Spatial Statistics) (de Groot et al., 2013). The whole brain and ROIs mean FA values were computed based on the WM skeleton.

2.2.6 Statistical analysis

All ROI analyses were intent-to-treat, with significance level set at $p<0.05$ (two-sided). Linear mixed models (using SPSS version 22.0 (IBM, 2013)) were used to estimate the effect of time, group and age and the corresponding interaction effects in the three ROIs. A compound symmetry covariance matrix and a fixed intercept were asserted; the model parameters were estimated using a maximum likelihood approach. Demeaned motion was added as a covariate to the model. Further, missing values (dropout and technical failure, see below) were imputed by population averages. The data were analyzed in IBM SPSS Statistics (Version 22.0. Armonk, NY). In addition, an exploratory voxel-wise statistical analysis was performed on the TBSS created WM skeleton to evaluate differences in FA using non parametric permutation testing with Randomise (500 permutations) (Winkler et al., 2014). All analyses were initially thresholded at *P*-value < 0.05 (two-sided) with a family wise error (FWE) correction for multiple comparisons using threshold free cluster enhancement (TFCE) (Smith and Nichols, 2009). Conditions were compared over time with demeaned motion scores as covariates, similar to the ROI analyses.

2.3 Results

2.3.1 Demographics and treatment

The children nor the adult groups differed in age, ADHD symptom severity nor extent of clinical impairment prior to treatment administration. No serious adverse events were noted in any of the subjects studied. An overview of the demographics and clinical scores of the subjects is presented in

Table 2.1. The CONSORT flow diagram of the trial is presented in Figure 2.1. Seven missing datasets were imputed due to dropout (no follow-up), and one due to technical failure of the scan (at baseline), amounting to 4.1% (8 of 196) in total. The voxel-wise analysis involved 47 children and 43 adults (Appendix, Table 2.2).

Table 2.1. Characteristics of the study groups

	Children MPH	placebo	Adults MPH	placebo
	n=25	n=25	n=24	n=24
	mean±SD	mean±SD	mean±SD	mean±SD
Age (y)	11.4±0.8	11.3±0.9	28.6±4.6	29.0±4.9
Estimated IQ[1]	104.8±21.0	103.4±15.1	107.9±8.8	107.9±6.4
ADHD subtype				
Inattentive	14	14	11	5
Hyperactive/impulsive	0	1	0	0
Combined	11	10	13	19
ADHD symptoms				
DBD-RS Inattention	21.7±3.2	22.8±3.4	-	-
DBD-RS Hyperactivity	15.0±5.0	16.4±6.3	-	-
ADHD-SR	-	-	30.6±10.0	30.4±9.3
Adherence	84%±15	80%±18	90%±8	86±8

	Motion scores			
	Children		Adults	
	Baseline	Follow-up	Baseline	Follow-up
	mean±SD	mean±SD	mean±SD	mean±SD
	0.16±0.42	0.098±0.43	-0.18±0.24	-0.09±0.27

[1]For children: Wechsler Intelligence Scale for Children (WISC); for adults: National Adults Reading Test (NART); DBD-RS=disruptive behavior disorder rating scale; ADHD-SR=Attention Deficit Hyperactivity Disorder-Self Report

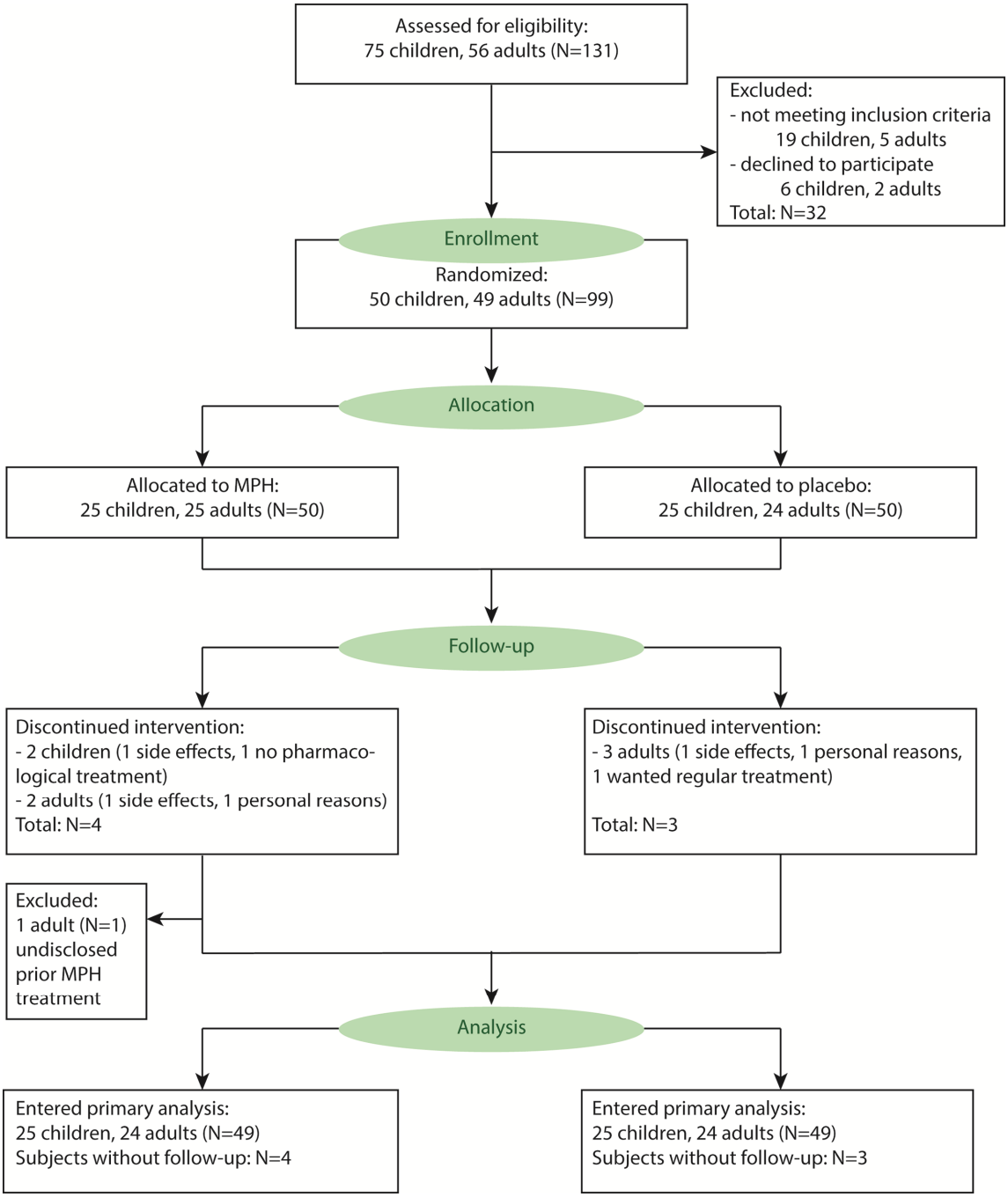

Figure 2.1 CONSORT diagram.

2.3.2 ROI-based analysis

At baseline, no differences were observed in the children nor in the adult group between the two medication groups for any of the ROIs (all P>0.2). We found no three-way interaction between time, age and medication in any of the ROIs (whole brain: F[1,88.6]=0.43 P=0.51; ATR: F[1,85.7]=0.03 P=0.86; CC: F[1,90.9]=0.13 P=0.72) (Figure 2.2). After splitting the age groups, we also did not find a two-way

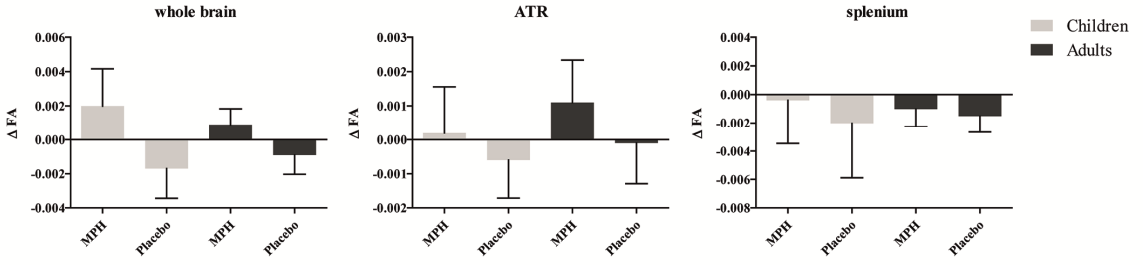

Figure 2.2 ROI analysis. Change in FA values from baseline to post-treatment in whole brain WM, ATR and splenium. Error bars represent standard error of the mean.

interaction between time and medication in either the young or adult patients (children: whole brain: F[1,46.78]=2.23 *P*=0.13; ATR: F[1,46.34]=0.30 *P*=0.59; CC: F[1,47.60]=0.33 *P*=0.57; adults: whole brain: F[1,42.40]=1.86 *P*=0.18; ATR: F[1,39.43]=0.58 *P*=0.45; CC: F[1,43.24]=0.09 *P*=0.76). Finally, no main effect of time was found on FA in any of the ROIs (all *P*>0.2).

2.3.3 Voxel-based analysis

In line with the ROI analyses, there were no differences between the medication groups in either the children or adults at baseline. Additionally, no significant changes in FA were observed between baseline and post-treatment in any age group and treatment condition (all *P*>0.2). Interestingly, in contrast with the ROI analyses, we found several clusters with significant differences in the *changes* from baseline to post-treatment between children and adults in which MPH was administered (see Figure 2.3(left) for the time-by-medication-by-age interaction effects), illustrating small but significant increases in FA in MPH children. The change in mean FA of all the significant voxels was extracted and plotted in Figure 2.3(right).

2.4 Discussion

In this RCT we studied for the first time whether the effects of MPH treatment on WM of stimulant naïve ADHD patients are modulated by age. We did not find a significant age by time by treatment interaction in the ROI analyses. However, our voxel-based analyses demonstrated a different *change* in FA values in children after treatment with MPH than the *change* in adults treated with MPH in specific brain regions. This suggests that the effects of MPH on brain WM are modulated by age. As such, additional evidence is provided that, already during this relatively short treatment time, MPH seems to affect the regional WM development.

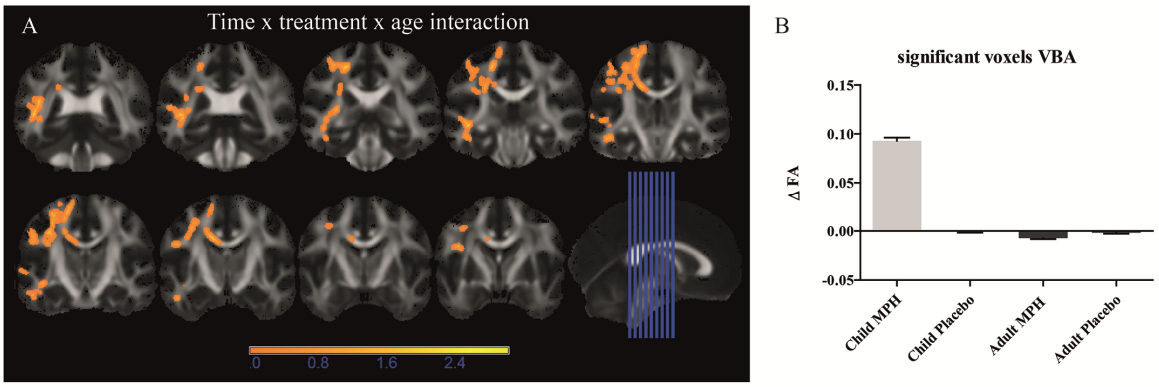

Figure 2.3 Voxel based analysis. Voxel-wise FA comparison by TBSS showing significant treatment-by-age interaction effects. A) The areas in which the difference between baseline and post-treatment in children treated with MPH is higher than in adults treated with MPH is color coded red ($P<0.05$), and located in several association fibers (parts of left superior longitudinal fasciculus, inferior longitudinal fasciculus, inferior fronto-occipital fasciculus) and commisural fibers (lateral in the truncus corpus callosum). B) FA of all significant voxels from panel A was extracted and plotted per group.

Our results are in line with the (limited) available literature on ADHD medications and brain WM. First, (Castellanos et al., 2002) also reported an (8.9%) increase of WM volume in ADHD medicated children compared to unmedicated children. Interestingly, also in a preclinical study in rats we observed an increase of 9.2% in FA (only) in the CC of adolescent rats treated with MPH, but not in adult rats nor saline treated rats (van der Marel et al., 2014). As such, there is some evidence that ADHD medication could affect brain WM development in an age-dependent manner, in which the effects differ between early and late exposure. The combined results of these studies and our current findings (albeit in a limited number of patients, but with the best possible study design), provides further evidence that MPH seems to affect WM maturation. The preclinical evidence also suggests that our current findings may be mediated, in part, by increased expression of striatal genes involved in the formation of new axons which were upregulated (fold change >1.5) by peri-adolescent MPH treatment (Adriani et al., 2006).

The fact that we observed the interaction effects only in voxel-wise comparisons and not in the selected ROIs, suggests the effects of MPH are particularly subtle. Furthermore, the locations in which significant interactions were found might indicate that other brain regions than ATR are more susceptible to the stimulating effects of MPH. As for our CC ROI: this ROI was placed central and more anteriorly in the truncus CC than where the voxel-based analysis detected an

interaction effect (lateral and more posteriorly in the truncus): the lack of overlap likely explains the discrepancy between the two analyses. Moreover, changes after such a short period of time are likely small and therefore restricted to subclusters of tracts rather than along the entire tract. Our voxel-based analyses suggests that the WM in several association fibers (parts of left superior longitudinal fasciculus, inferior longitudinal fasciculus, inferior fronto-occipital fasciculus) seem to be particularly sensitive to the modulating effects of age. However, it is well known that these regions are rich in crossing fibers. The diffusion weighted MRI acquisition used in this study was limited to a single b = 1000 s/mm^2 value. In future studies a more advanced protocol using multiple (at least two) b-values would allow to distinguish additional WM details, for example, fiber crossings, which cannot be reliably estimated otherwise.

As we did not include normal developing peers in this RCT, for evident medical ethical reasons, we do not know whether the increase in FA in children treated with MPH is a 'normalizing' effect. However, the study by (Castellanos et al., 2002) reported that the increase in FA in medicated children was in the direction of the healthy subjects. Similar findings were reported for cortical thickness, demonstrating more rapid cortical thinning in a group not taking psychostimulants when compared to a group taking psychostimulants (Shaw et al., 2009). Interestingly, similar to this RCT, the treatment groups in that study also did not differ regarding clinical outcome (which we reported elsewhere (Schrantee et al., 2016)). Although it is conceivable that we here provide further evidence for a positive/normalizing effect of MPH on brain WM maturation, the long-term effects hereof on clinical outcome remain to be established. This is especially relevant because it has been shown that the effects of stimulants like MPH on the developing brain are only fully expressed later in life, in early adulthood (Andersen, 2005).

The clinical implications of our study are considerable in view of the importance brain WM maturation plays in the development of cognitive function. For instance, it has been shown that lower FA values are associated with lower cognitive function (Vernooij et al., 2009). Safety studies on the effect of MPH on the immature brain in general are scarce in children. This has led to considerable debate and concern, e.g. amongst parents, about the consequences or possible side effects of MPH

prescriptions to children. High non-compliance is attributed in part to apprehension about the safety of MPH on human brain development. In this respect, our data may provide some direction, as we provide evidence that MPH seems to have positive effects on brain WM in children with ADHD, in that it increases FA values, presumably to normal levels, at least on the short term. Importantly, MPH is being prescribed not only to increasing numbers of children, but also to children of increasingly younger ages. In addition, a substantial proportion of the patients fails to meet criteria for ADHD (Elder, 2010), or use stimulants such as MPH to improve school performance (Lakhan and Kirchgessner, 2012). Although we did not investigate the effects of MPH treatment in normally developing children, it is conceivable that lasting alterations to WM by MPH in normal developing children may not be beneficial, and could potentially induce behavioral and psychiatric problems later in life. As such our findings provide comfort to treatment with MPH of patients with ADHD, but at the same time urge for tighter regulations of prescribing ADHD medications.

A major strength of our current study is its design, in which effects of confounders, such as age and gender, are very small. Also, we included only male patients to limit subject variation as girls and boys differ considerably in brain WM development(Giedd et al., 1999). The selective inclusion of stimulant-treatment naive patients was also critical for addressing our objective. Clearly, there are important ethical considerations for medication studies in children and in our case, the most important restriction was the time that a child would not receive adequate treatment (but a placebo). Because the waiting list for treatment in the Netherlands was typically four months, this dictated the design of this RCT. Ideally, we would have used a longer wash-out period, as pointed out above. Also, future studies should investigate whether our findings can be extrapolated to the female gender and young/older children and/or adolescents. Another potential weakness is the limited statistical power. Due to its complexity, the power of the study was limited, especially because we examined three different brain regions, which could have increased the risk of a type I error. The voxel-based analyses, however, were corrected for multiple comparisons. Our relatively low statistical power likely explains the lateralization of the effects in the left hemisphere (Figure 2.3): when we increase the statistical threshold from $P<0.05$ to $P<0.2$, we also observe interaction

effects in the right hemisphere. Alternatively, since nearly all children were righted handed, handedness could also explain the lateralization of our MPH effect.

2.5 Conclusion

In line with clinical and preclinical data, we provide further evidence that the effects of MPH on brain WM are modulated by age. The group difference was due to more rapid increase in FA in MPH treated children, and not so in children receiving a placebo nor adults.

Funding

This study was funded by faculty resources of the Academic Medical Center, University of Amsterdam, and grant 11.32050.26 from the European Research Area Network Priority Medicines for Children (Sixth Framework Programme).

Appendix

A. Pre-processing

Head motion and deformations induced by eddy currents were corrected for by affine registration of the Diffusion Weighted Images (DWIs) to the non-diffusion weighted (b0) image. The gradient directions were corrected by the rotation component of the transformation. These corrections were performed using the artefact correction in diffusion MRI (ACID) toolbox of SPM software (Mohammadi et al., 2010). The affine transformation between consecutive DWI's was derived from their respective registrations to the b0 image. Subsequently, patient displacement from one DWI to the next was represented by the magnitude of the translation component (discarding potential skewing or rotation components). The motion score for a patient was defined as the logarithm of the mean patient displacement (to compensate for the skewed distribution of displacements). When compared within the same age and medication group (e.g. initial and follow-up scans of children treated with MPH), motion scores were demeaned for that specific group. Rician noise in the DWIs was reduced by an adaptive noise filtering method (Caan et al., 2010), which was applied after eddy current and motion correction. Subsequently, diffusion tensors were estimated in a non-linear least squares sense facilitating computation of the outcome parameters:

FA, MD, and RD. FA maps of *all* patients were aligned to a 1x1x1 mm3 standard MNI152 space using *elastix* (Klein et al., 2010) instead of the standard nonlinear registration step included in the TBSS pipeline of the FSL package (Andersson et al., 2007). The following settings were used for the registration setup:

- normalised cross correlation as the cost function;
- affine transformation with 12 degrees of freedom served as the starting point for the B-spline non-linear transformation;
- adaptive stochastic gradient descent optimization procedure was applied;
- random coordinate sampler was selected for the cost function calculation;
- four resolutions in combination with the Gaussian scale space were used as a hierarchical strategy.

Subsequently, the transformed images were averaged to create a mean FA image, from which a skeleton was generated. This allows to reduce risk of partial volume effects as the analysis focuses on the central parts of the WM tracts. A threshold of 0.2 was applied to represent tracts common for all subjects and to avoid including regions of too high inter-subject

variability where good alignment could not be attained. FA values were projected on the same skeleton for each patient to minimize bias of FA comparisons between groups caused by possible residual misalignment. Average values of diffusion statistics were computed over the entire WM skeleton and within the CC and the left and right ATR as determined by the JHU white-matter tractography atlas(Mori et al., 2005). Furthermore, a voxelwise statistical analysis of the FA data was carried out using TBSS (Tract-Based Spatial Statistics) (Smith et al., 2004; Smith et al., 2006).

B. Demographics

Table 2.2. Demographic and clinical information of 47 children and 43 adults with both baseline and post treatment scans. These subjects are considered in the voxel-wise analysis.

	Children	Adults
Age (median), years	10.06-13.08 (11.05)	22.44-39.37 (27.48)
Age IQR, years	10.63-11.77	25.67-31.38
ADHD scores (median)	22-50 (38)	9-48 (33)
ADHD score IQR	33-44	24-38.5

IQ total score (median)*	71-145 (99)	92-124 (108)
IQ total score IQR*	92-111	101.75-111.25
Treated with MPH/placebo	23/24	22/21

*Score is not available for 2 children and 3 adults

References

Adriani, W., Leo, D., Greco, D., Rea, M., di Porzio, U., Laviola, G., et al. (2006). Methylphenidate Administration to Adolescent Rats Determines Plastic Changes on Reward-Related Behavior and Striatal Gene Expression. *Neuropsychopharmacology* 31(9), 1946-1956. doi: http://www.nature.com/npp/journal/v31/n9/suppinfo/1300962s1.html.

Andersen, S.L. (2005). Stimulants and the developing brain. *Trends in Pharmacological Sciences* 26(5), 237-243. doi: http://dx.doi.org/10.1016/j.tips.2005.03.009.

Andersson, J., Jenkinson, M., and Smith, S. (2007). Non-linear registration aka Spatial normalisation FMRIB Technial Report TR07JA2.

Barnea-Goraly, N., Menon, V., Eckert, M., Tamm, L., Bammer, R., Karchemskiy, A., et al. (2005). White Matter Development During Childhood and Adolescence: A Cross-sectional Diffusion Tensor Imaging Study. *Cerebral Cortex* 15(12), 1848-1854. doi: 10.1093/cercor/bhi062.

Bottelier, M.A., Schouw, M.L.J., Klomp, A., Tamminga, H.G.H., Schrantee, A.G.M., Bouziane, C., et al. (2014). The effects of Psychotropic drugs On Developing brain (ePOD) study: methods and design. *BMC Psychiatry* 14, 48-48. doi: 10.1186/1471-244X-14-48.

Bouziane, C., Caan, M.W.A., Tamminga, H.G.H., Schrantee, A., Bottelier, M.A., de Ruiter, M.B., et al. (2018). ADHD and maturation of brain white matter: A DTI study in medication naive children and adults. *NeuroImage: Clinical* 17, 53-59. doi: https://doi.org/10.1016/j.nicl.2017.09.026.

Caan, M., Khedoe, G., Poot, D., den Dekker, A., Olabarriaga, S., Grimbergen, K., et al. (2010). "Adaptive Noise Filtering for Accurate and Precise Diffusion Estimation in Fiber Crossings," in *Medical Image Computing and Computer-Assisted Intervention – MICCAI 2010: 13th International Conference, Beijing, China, September 20-24, 2010, Proceedings, Part I,* eds. T. Jiang, N. Navab, J.P.W. Pluim & M.A. Viergever. (Berlin, Heidelberg: Springer Berlin Heidelberg), 167-174.

Castellanos, F., Lee, P.P., Sharp, W., and et al. (2002). Developmental trajectories of brain volume abnormalities in children and adolescents with attention-deficit/hyperactivity disorder. *JAMA* 288(14), 1740-1748. doi: 10.1001/jama.288.14.1740.

de Groot, M., Vernooij, M.W., Klein, S., Ikram, M.A., Vos, F.M., Smith, S.M., et al. (2013). Improving alignment in Tract-based spatial statistics: Evaluation and optimization of image registration. *NeuroImage* 76, 400-411. doi: http://dx.doi.org/10.1016/j.neuroimage.2013.03.015.

de Win, M.M.L., Reneman, L., Jager, G., Vlieger, E.-J.P., Olabarriaga, S.D., Lavini, C., et al. (2006). A Prospective Cohort Study on Sustained Effects of Low-Dose Ecstasy Use on the Brain in New Ecstasy Users. *Neuropsychopharmacology* 32(2), 458-470.

Elder, T.E. (2010). The importance of relative standards in ADHD diagnoses: Evidence based on exact birth dates. *Journal of Health Economics* 29(5), 641-656. doi: https://doi.org/10.1016/j.jhealeco.2010.06.003.

Feldman, H.M., Yeatman, J.D., Lee, E.S., Barde, L.H.F., and Gaman-Bean, S. (2010). Diffusion Tensor Imaging: A Review for Pediatric Researchers and Clinicians. *Journal of developmental and behavioral pediatrics : JDBP* 31(4), 346-356. doi: 10.1097/DBP.0b013e3181dcaa8b.

Ferdinand, R.F., and van der Ende, J. (2000). NIMH DISC-IV: Diagnostic Interview Schedule for Children [in Dutch]. *Rotterdam, the Netherlands: Erasmus MC-Sophia*.

Giedd, J.N., Blumenthal, J., Jeffries, N.O., Castellanos, F.X., Liu, H., Zijdenbos, A., et al. (1999). Brain development during childhood and adolescence: a longitudinal MRI study. *Nat Neurosci* 2(10), 861-863.

Klein, S., Staring, M., Murphy, K., Viergever, M.A., and Pluim, J.P. (2010). elastix: a toolbox for intensity-based medical image registration. *IEEE Trans Med Imaging* 29(1), 196-205. doi: 10.1109/TMI.2009.2035616.

Klingberg, T., Vaidya, C.J., Gabrieli, J.D.E., Moseley, M.E., and Hedehus, M. (1999). Myelination and organization of the frontal white matter in children: a diffusion tensor MRI study. *NeuroReport* 10(13).

Kooij, J., and Francken, M. (2010). Diagnostic Interview for ADHA in Adults (DIVA).

Lakhan, S.E., and Kirchgessner, A. (2012). Prescription stimulants in individuals with and without attention deficit hyperactivity disorder: misuse, cognitive impact, and adverse effects. *Brain and Behavior* 2(5), 661-677. doi: 10.1002/brb3.78.

Ling, J., Merideth, F., Caprihan, A., Pena, A., Teshiba, T., and Mayer, A.R. (2012). Head injury or head motion? Assessment and quantification of motion artifacts in diffusion tensor imaging studies. *Hum Brain Mapp* 33(1), 50-62. doi: 10.1002/hbm.21192.

Merikangas, K.R., He, J.-P., Brody, D., Fisher, P.W., Bourdon, K., and Koretz, D.S. (2010). Prevalence and Treatment of Mental Disorders Among US Children in the 2001–2004 NHANES. *Pediatrics* 125(1), 75.

Moeller, F.G., Hasan, K.M., Steinberg, J.L., Kramer, L.A., Dougherty, D.M., Santos, R.M., et al. (2005). Reduced anterior corpus callosum white matter integrity is related to increased impulsivity and reduced discriminability in

cocaine-dependent subjects: diffusion tensor imaging. *Neuropsychopharmacology* 30(3), 610-617. doi: 10.1038/sj.npp.1300617.

Mohammadi, S., Möller, H.E., Kugel, H., Müller, D.K., and Deppe, M. (2010). Correcting eddy current and motion effects by affine whole-brain registrations: Evaluation of three-dimensional distortions and comparison with slicewise correction. *Magnetic Resonance in Medicine* 64(4), 1047-1056. doi: 10.1002/mrm.22501.

Mori, S., Wakana, S., van Zijl, P.C.M., and and Nagae-Poetscher, L.M. (2005). *MRI Atlas of Human White Matter*. Amsterdam: Elsevier.

MTA Cooperative Group (1999). A 14-month randomized clinical trial of treatment strategies for attention-deficit/hyperactivity disorder. *Archives of General Psychiatry* 56(12), 1073-1086. doi: 10.1001/archpsyc.56.12.1073.

Reneman, L., Majoie, C.B.L.M., Habraken, J.B.A., and den Heeten, G.J. (2001). Effects of Ecstasy (MDMA) on the Brain in Abstinent Users: Initial Observations with Diffusion and Perfusion MR Imaging. *Radiology* 220(3), 611-617. doi: 10.1148/radiol.2202001602.

Schrantee, A., Tamminga, H.G.H., Bouziane, C., Bottelier, M.A., Bron, E.E., Mutsaerts, H.-J.M.M., et al. (2016). Age-Dependent Effects ofMethylphenidate on the Human Dopaminergic System in Young vs Adult Patients With Attention-Deficit/Hyperactivity Disorder A Randomized Clinical Trial. *JAMA Psychiatry* 73(9), 8. doi: 10.1001/jamapsychiatry.2016.1572.

Shahand, S., Benabdelkader, A., Jaghoori, M.M., Mourabit, M.a., Huguet, J., Caan, M.W.A., et al. (2015). A data-centric neuroscience gateway: design, implementation, and experiences. *Concurrency and Computation: Practice and Experience* 27(2), 489-506. doi: 10.1002/cpe.3281.

Shaw, P., Sharp, W., Morrison, M., Eckstrand, K., Greenstein, D., Clasen, L., et al. (2009). Psychostimulant treatment and the developing cortex in Attention-Deficit/Hyperactivity Disorder. *The American journal of psychiatry* 166(1), 58-63. doi: 10.1176/appi.ajp.2008.08050781.

Smith, S.M., Jenkinson, M., Johansen-Berg, H., Rueckert, D., Nichols, T.E., Mackay, C.E., et al. (2006). Tract-based spatial statistics: voxelwise analysis of multi-subject diffusion data. *Neuroimage* 31(4), 1487-1505. doi: 10.1016/j.neuroimage.2006.02.024.

Smith, S.M., Jenkinson, M., Woolrich, M.W., Beckmann, C.F., Behrens, T.E.J., Johansen-Berg, H., et al. (2004). Advances in functional and structural MR image analysis and implementation as FSL. *NeuroImage* 23, Supplement 1, S208-S219. doi: http://dx.doi.org/10.1016/j.neuroimage.2004.07.051.

Smith, S.M., and Nichols, T.E. (2009). Threshold-free cluster enhancement: Addressing problems of smoothing, threshold dependence and localisation in cluster inference. *NeuroImage* 44(1), 83-98. doi: https://doi.org/10.1016/j.neuroimage.2008.03.061.

van der Marel, K., Klomp, A., Meerhoff, G.F., Schipper, P., Lucassen, P.J., Homberg, J.R., et al. (2014). Long-Term Oral Methylphenidate Treatment in Adolescent and Adult Rats: Differential Effects on Brain Morphology and Function. *Neuropsychopharmacology* 39(2), 263-273. doi: 10.1038/npp.2013.169.

van Ewijk, H., Heslenfeld, D.J., Zwiers, M.P., Buitelaar, J.K., and Oosterlaan, J. (2012). Diffusion tensor imaging in attention deficit/hyperactivity disorder: A systematic review and meta-analysis. *Neuroscience & Biobehavioral Reviews* 36(4), 1093-1106. doi: http://dx.doi.org/10.1016/j.neubiorev.2012.01.003.

Vernooij, M.W., Ikram, M., Vrooman, H.A., and et al. (2009). White matter microstructural integrity and cognitive function in a general elderly population. *Archives of General Psychiatry* 66(5), 545-553. doi: 10.1001/archgenpsychiatry.2009.5.

Winkler, A.M., Ridgway, G.R., Webster, M.A., Smith, S.M., and Nichols, T.E. (2014). Permutation inference for the general linear model. *NeuroImage* 92, 381-397. doi: http://dx.doi.org/10.1016/j.neuroimage.2014.01.060.

Yap, Q.J., Teh, I., Fusar-Poli, P., Sum, M.Y., Kuswanto, C., and Sim, K. (2013). Tracking cerebral white matter changes across the lifespan: insights from diffusion tensor imaging studies. *Journal of Neural Transmission* 120(9), 1369-1395. doi: 10.1007/s00702-013-0971-7.

3

Diffusion Models in Chronic Stroke

Comparison is the great force which motivates

us to compete and to improve ourselves.

Aleksandr Vertinsky

3 Comparison of Multi-Tensor Diffusion Models' Performance for White Matter Integrity Estimation in Chronic Stroke

Better insight into white matter (WM) alterations after stroke onset could help to understand the underlying recovery mechanisms and improve future interventions. MR diffusion imaging enables to assess such changes. Our goal was to investigate the relation of WM diffusion characteristics derived from diffusion models of increasing complexity with the motor function of the upper limb. Moreover, we aimed to evaluate the variation of such characteristics across different WM structures of chronic stroke patients in comparison to healthy subjects. Subjects were scanned with a two b-value diffusion-weighted MRI protocol to exploit multiple diffusion models: single tensor, single tensor with isotropic compartment, bi-tensor model, bi-tensor with isotropic compartment. From each model we derived the mean tract fractional anisotropy (FA), mean (MD), radial (RD) and axial (AD) diffusivities outside the lesion site based on a WM tracts atlas. Asymmetry of these measures was correlated with the Fugl-Meyer upper extremity assessment (FMA) score and compared between patient and control groups. Eighteen chronic stroke patients and eight age-matched healthy individuals participated in the study. Significant correlation of the outcome measures with the clinical scores of stroke recovery was found. The lowest correlation of the corticospinal tract $FA_{asymmetry}$ and FMA was with the single tensor model ($r=-0.3$, $p=0.2$) whereas the other models reported results in the range of $r=-0.79 \div -0.81$ and $p=4 \cdot 10^{-5} \div 8 \cdot 10^{-5}$. The corticospinal tract and superior longitudinal fasciculus showed most alterations in our patient group relative to controls. Multiple compartment models yielded superior correlation of the diffusion measures and FMA compared to the single tensor model.

3.1 Introduction

Unilateral loss of motor function is a frequent consequence of stroke. White matter changes in the corticospinal tract (CST) and the posterior limb of the internal capsule (PLIC) are known to correlate to motor impairment in stroke patients (Cho et al., 2007; Schaechter et al., 2008; Jang et al., 2010; Park et al., 2013; Song et al., 2014). Therefore, accurate measurements of white matter changes could be an indicator of stroke severity.

A commonly used technique to assess white matter integrity is diffusion Magnetic Resonance Imaging (dMRI). Specifically, it measures the ability of water molecules to move freely in the surrounding tissue. Importantly, normal white matter (WM) shows high diffusivity along axons and low across axons, whereas gray matter (GM) shows more isotropic diffusion patterns(Neil, 2008). The diffusion is conventionally modeled by a mathematical construct called a tensor, which can be visualized by an ellipsoid. It represents the shape of the local diffusion, from which measures are derived such as the mean diffusivity (MD) and the fractional anisotropy (FA). FA is a measure of anisotropy or pointedness of a diffusion ellipsoid and MD represents the mean diffusion in a voxel.

dMRI has proven to be a versatile tool and used in a wide range of applications. Particularly, $FA_{asymmetry}$ was utilized by (Byblow et al., 2015) who aimed to predict which patients will have spontaneous recovery. In a severe patient category without transcranial magnetic stimulation (TMS) evoked potentials, patients with initially small $FA_{asymmetry}$ would still show some recovery, in contrast to patients with a large $FA_{asymmetry}$. For the purpose of building a linear regression model, $FA_{asymmetry}$ was binarized (< >0.15) and became the only significant predictor of change in the FMA score. Therefore, $FA_{asymmetry}$ could be a good predictor of the stroke severity and potential recovery.

Several studies with animal models of stroke found that structural white matter changes in both the ipsi- and contralesional hemispheres play an important role in motor recovery (Dancause et al., 2005; Brus-Ramer et al., 2007). Furthermore, many studies have employed measures of brain asymmetry to study stroke outcome (Bhagat et al., 2008; Lindenberg et al., 2010; Puig et al., 2010; Park et al., 2013; Cunningham et al., 2015). For example, the asymmetry of FA along the PLIC in

the ipsi- versus contralesional hemisphere had higher correlation to upper limb motor functioning than functional MRI responses of cortical motor areas in chronic stroke patients (three to nine months post stroke) (Qiu et al., 2011). Ratios of FA between the affected and unaffected hemispheres were also used to study neuronal alterations immediately after stroke in hyper-acute ischemic stroke patients (Bhagat et al., 2008) and longitudinally from 1 week to 1 year (Yu et al., 2009). In the hyper-acute phase, the fractional anisotropy in the lesion relative to the healthy side was not consistent among patients, but elevated in some of them. After the first 24 h this FA ratio showed more consistent reductions (Bhagat et al., 2008). Subsequently, after three months, changes in the anisotropy ratio stabilized (Yu et al., 2009). Still, the exact patterns of change in diffusion properties of WM after stroke remain unclear.

Although white matter alterations are well-known to correlate with motor functioning in stroke patients, the exact etiology of these changes remains unknown. It has been observed, for example, in (Buma et al., 2013) that after stroke a general white matter deterioration takes place. However, as described above, most previous studies have merely focused on the CST and PLIC. Furthermore, a single diffusion ellipsoid was classically used to model the local diffusion of the water molecules. This conventional model is known to be inadequate for the characterization of diffusion in complex structures such as crossing fibers found, for example, at the intersection of the CST and corpus callosum. Importantly, (Jeurissen et al., 2013) showed that crossing fibers are present in 60 to 90% of the diffusion data. The benefit of more sophisticated diffusion modeling has already been reported for other applications (Caan et al., 2010b; Arkesteijn et al., 2015; Yang et al., 2015) and in a recent work of (Archer et al., 2017), where a two-compartment model representing free water and white matter tissue is used to study a relation between FAasymmetry and grip strength in chronic stroke subjects.

A single-tensor model is often applied to analyze dMRI in both chronic and longitudinal stroke studies (Lindenberg et al., 2012; Ma et al., 2014). A systematic review was presented by (Kumar et al., 2016). We hypothesize that more complex diffusion models are better equipped to detect subtle WM changes after stroke. This hypothesis also underlies the use of a two-compartment model in (Archer et al.,

2017), which adapted an approach by (Pasternak et al., 2009) to model a tissue and a free water compartment.

Multi-tensor models are a logical extension of the traditional single tensor model. Certainly, other higher order models exist, such as spherical deconvolution (SD) approaches. Instead of assuming a specific number of fibers, these models assume a distribution of fiber orientations. This allows to express the diffusion weighted signal as the spherical convolution of the fiber orientation distribution function and a response function representing the signal of a single fiber population (Tournier et al., 2004). However, a response function is unknown and generally assumed to be the same for the whole brain possibly leading to spurious results (Parker et al., 2013).

This paper aims to evaluate four diffusion models of increasing complexity based on the strength of the relation between the estimated WM properties and the clinical outcomes of chronic stroke patients. One of the motivating factors for the choice of these models is to validate their suitability for stroke patients and the feasibility of a model comparison per model parameter. The outcome parameters of the diffusion models are physically meaningful and directly comparable to each other. Moreover, the asymmetry between the healthy and afflicted hemispheres in the patient group is compared with the asymmetry in healthy controls in order to assess which WM properties are most relevant for such a comparison. We start with an application of the traditional single tensor model and build up to a so-called bi-tensor model with isotropic compartment in order to identify the smallest differences in diffusivities. This bi-tensor model especially takes into account that the diffusion may be affected by free water due to a cerebrovascular accident. We hypothesize that there are significant differences in diffusivity measures in several tracts between the two hemispheres. Furthermore, we anticipate that the application of sophisticated models allows a more sensitive analysis than the conventional approach.

3.2 Methods

3.2.1 Cohort

Subjects were included after informed consent and with permission of the Medical Ethics Committee of the Vrije Universiteit Medical Center, Amsterdam. The trial

protocol was registered on 23 October 2013 at the Netherlands Trial Register (identifier NTR4221). Inclusion criteria for the subjects suffering from chronic stroke were: upper limb paresis, ability to sit without support (National Institutes of Health Stroke Scale item 5 a/b > 0), age >18, first-ever ischemic hemispheric stroke, >6 months post stroke. Exclusion criteria were: previously existing pathological neurological conditions or orthopedic limitations of the upper limb that would affect the results, botuline-toxine injections or medication that may have influenced upper limb function in the past three months, general MRI contra indications (claustrophobia, pacemaker or other metallic implants), high risk of epilepsy.

Patients (n=18) were consecutively included from April 22, 2015 to February 29, 2016. Additionally, 8 controls with matching mean age were recruited for comparison in the period between April 9, 2015 and November 22, 2016. Post-hoc sample size analysis for this unmatched case-control study at the two-sided significance level of 0.05 indicated the power (chance of detecting) of 90% assuming a proportion of 44% of controls and an effect size of 0.5 (Kelsey et al., 1996; Charan and Biswas, 2013). Based on this analysis we stopped inclusion as we reached the mentioned number of patients and controls.

The patient population consisted of 18 first-ever ischemic stroke patients (12 men); median age: 60 (IQR: 51 – 67); 8/18 patients had an impaired left hand; for 9/18 patients the dominant hand was impaired; median FMA score: 57 (IQR: 24.75 – 61.5); median Action Research Arm Test (ARAT) score: 54 (IQR: 16.25 – 56.75). The control group consisted of 8 healthy subjects (7 men); median age: 59.5 (IQR: 55.25 – 62.25).

3.2.2 MRI protocol

Image acquisition was performed with a 3T MRI scanner (Discovery MR750, GE Medical Systems). The diffusion-weighted MRI (dMRI) acquisition protocol involved 40 non-collinear gradient directions uniformly sampled over a sphere for each of two b-values: 1000 and 2000 s/mm^2; TE=100 ms, TR=7200 ms, field of view FOV = 240x240 mm2, imaging matrix = 96x64 (zero padded to 256x256), 52 consecutive slices with a thickness of 2.5 mm, acquisition time 12,5 min. This

allowed for whole brain coverage. Data for each b-value were acquired as separate

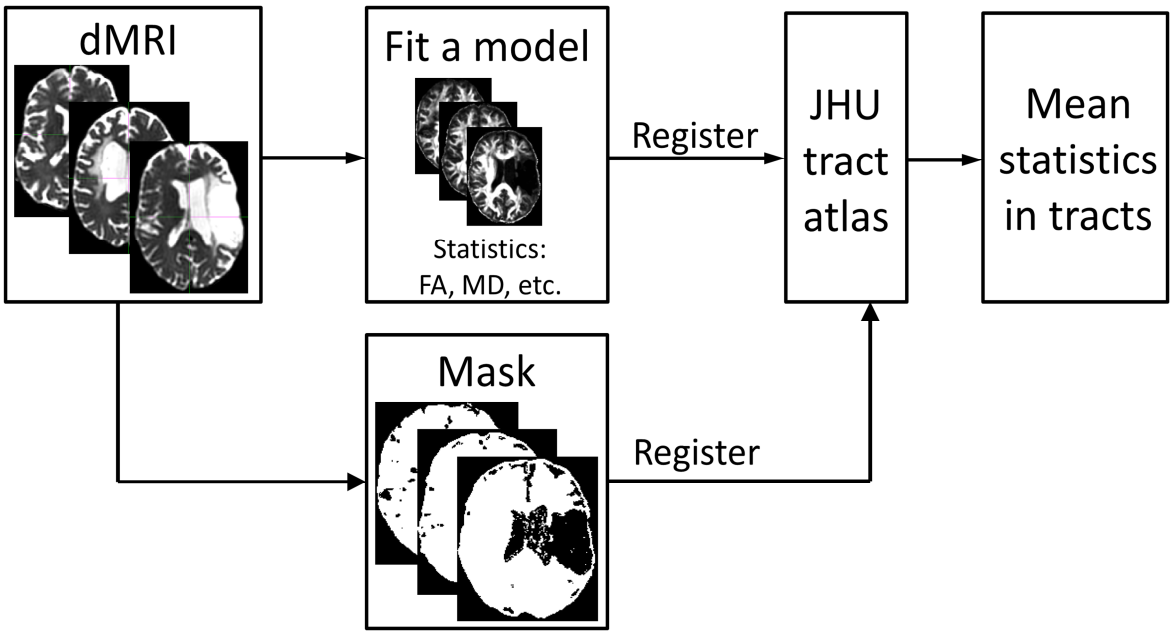

Figure 3.1 Overview of the analysis steps starting with the pre-processed dMR images. A diffusion tensor model is fitted to the data (four different diffusion models were used in this study). Masks excluding the subject-specific lesion site are created based on the thresholded isotropic compartment of the bi-tensor model with isotropic compartment. The results of this step are registered to the white-matter tract atlas (https://neurovault.org/media/images/264/JHU-ICBM-tracts-maxprob-thr25-1mm.nii.gz) and mean values of the outcome parameters are calculated for each tract.

scans together with five non-diffusion weighted images (i.e. per b-value).

3.2.3 Data processing

Figure 3.1 presents an overview of the analysis steps described below.

3.2.3.1 Pre-processing

dMRI data were preprocessed using FSL v5.0 (http://fsl.fmrib.ox.ac.uk/fsl/, (Jenkinson et al., 2012)). The acquired DWIs were corrected for motion and eddy current distortion by affine coregistration to the reference b0-image (using FSL eddy_correct). Gradient directions were reoriented according to the rotation component of the affine transformation. Datasets of the same subject with b=1000 and b=2000 s/mm2 different diffusion weighting were coregistered with each other using FSL flirt affine registration with six degrees of freedom.

3.2.3.2 Diffusion models

The following four diffusion models of increasing complexity were fitted to the diffusion data of each voxel using the so-called maximum likelihood estimation as described, for example, in (Caan et al., 2010b):

(1) Single-tensor model: A single tensor. The tensor shape is unconstrained. Images were generated representing FA, MD, axial diffusivity (AD) and radial diffusivity (RD). Axial diffusivity is the principal eigenvalue of the diffusion tensor and is often considered to represent the diffusion along a fiber tract. Radial diffusivity equals the mean of the secondary eigenvalues and is often taken to represent the diffusivity perpendicular to a tract.

(2) Single tensor with an isotropic compartment: A single tensor compartment accompanied by an isotropic, free water compartment. The shape of the tensor is unconstrained. Unlike in (Arkesteijn et al., 2015), not even a trace constraint is applied. This model yielded the same parameters as the single tensor model derived from the fiber compartment, and in addition a volume fraction characterizing the amount of free water in all voxels.

(3) Bi-tensor model (Caan et al., 2010b): A model consisting of two tensor compartments with the same shape (symmetric tensors with equal AD and RD, and thus same FA), but variable volume fractions (i.e. relative contribution to a voxel) and arbitrary orientations. This model represented two white matter bundles simultaneously present in a voxel. It yielded the same parameters as the single tensor model due to the presumed identical shape of the two tensors. The volume fraction was not considered for further analysis as it is affected by (arbitrary) partial volume effects.

(4) Bi-tensor model with an isotropic compartment (Yang et al., 2016): A model combining the representation of crossing nerve bundles and free water diffusion in a single voxel. The two estimated tensors are restricted to have the same shape as in the bi-tensor model. The free-water volume fraction is an additional parameter to the aforementioned parameters of the bi-tensor model.

In all of the models the maximum diffusivity of the tensor compartment is limited by the diffusivity of free water at body temperature. For an illustration of these

models see . Mathematical details of specific model parametrizations and model fitting procedure are described in the Appendix.

It is important to notice that models with multiple compartments are capable of

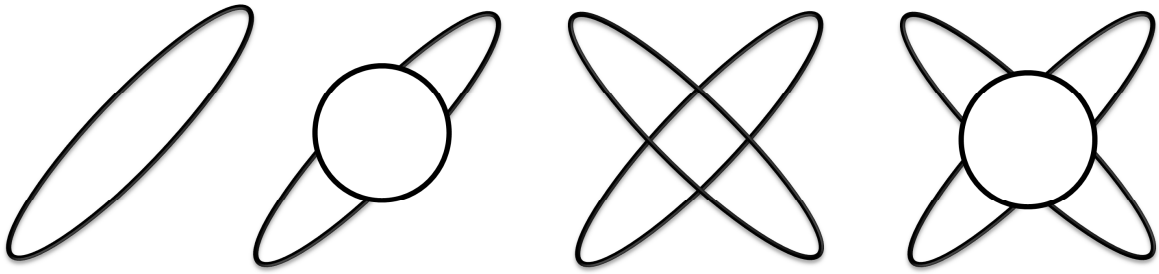

Figure 3.2 Illustration of the four diffusion models. From left to right: single tensor, single tensor with isotropic compartment, bi-tensor and bi-tensor with an isotropic compartment models.

modelling diffusion signals produced by several fiber populations leading to lower fit errors. However, applying these models to voxels containing a single fiber population may result in noise fitting and thus spurious fiber orientations' and erroneous model parameters.

3.2.3.3 Tract identification

The volume fraction of tissue in a stroke lesion was estimated to be less than 0.1 by (Latour and Warach, 2002). Reflecting this decreased parenchymal volume fraction, masks of stroke lesions were created by conservatively thresholding the volume fraction of the isotropic compartment estimated by model (4) at $f_{iso} = 0.9$. As such, regions with f_{iso} larger than this value were excluded from further analysis. The accuracy of the lesion delineation was visually checked by a research fellow (OF). The research fellow could adjust the threshold to obtain a more accurate delineation in case the mask was considered suboptimal.

Separate FA images were derived for each diffusion model and each subject. All FA images were co-registered to the MNI space using an affine registration with 12 degrees of freedom as implemented in FSL v5.0 (Jenkinson et al., 2012). To achieve an accurate registration of the non-lesional brain parts, the masked regions of the chronic stroke subjects were excluded in the registration process. Subsequently, the same transformation was applied to the parameter maps derived from the diffusion models (e.g. the volume fractions). Next, the JHU white-matter

tractography atlas, which is also defined in MNI space, was projected onto the data. This tractography atlas contains 20 labeled white matter structures. It was generated by averaging the results of deterministic tractography on 28 normal subjects (mean age 29, M:17, F:11) (Mori et al., 2005; Hua et al., 2008). Symmetric WM tracts in this atlas are considered in our analysis. Their functional roles are summarized in Table 3.1. Additionally, the atlas contains delineations of forceps major and forceps minor. For the median and interquartile range of the considered regions of interest computed in the atlas space after masking the lesion out see .

Registration to the atlas space is illustrated in Figure 3.3, showing that no significant warping occurs. Not even for the scans of a patient with a big lesion.

Table 3.1. White matter tracts of the JHU tractography atlas obtained from deterministic tractography on 28 normal subjects (https://neurovault.org/media/images/264/JHU-ICBM-tracts-maxprob-thr25-1mm.nii.gz, (Hua et al., 2008)), their approximate location and function.

Tract name	Location	Function
Anterior thalamic radiation (ATR)	Passes from thalamus to pre-frontal cortex	As a part of thalamic radiations, relays sensory and motor data to pre- and post-central cortex
Corticospinal tract (CST)	Connects cerebral motor and somatosensory cortex to medulla and descends into contralateral spinal cord	Facilitates voluntary motor control of the limbs and trunk
Cingulum (all parts): Cingulum 1 -cingulate gyrus (CG); cingulum 2 – cingulate hippocampus (CH)	A collection of WM fibers connecting cingulate gyrus (cortex) to the entorhinal cortex	Part of the limbic system of the brain, associated with emotion, visual and spatial skills, working and general memory
Inferior fronto-occipital fasciculus (IFOF)	Connects the occipital lobe with the anterior part of the temporal lobe, running medially and above the optic fibers. It is a direct pathway connecting occipital, posterior temporal orbitofrontal areas	Integration of auditory and visual association cortices with prefrontal cortex. Function is still poorly understood.

Inferior longitudinal fasciculus (ILF)	Connects the occipital lobe with the anterior part of the temporal lobe, running above the optic radiation fibers	Integration of auditory and speech nuclei. Function is still poorly understood.
Superior longitudinal fasciculus (all parts): SLF and temporal part SLF-T	Major association fiber tract connecting frontal, parietal, and temporal lobes	As a major tract with projections to multiple lobes, it is involved with regulating motor behavior, spatial attention, visual and oculomotor functions, transfer of somatosensory information as well as language.
Uncinate fasciculus	A hook-shaped fiber bundle linking anterior parts of the temporal lobe with the lower surface of the frontal lobe	Part of the limbic system which takes part in memory integration

3.2.4 Data analysis and statistics

The mean parameter values of each model were calculated for every tract and for all subjects. After that, we determined ratios of the mean tract values between contralesional (healthy) and ipsilesional (impaired) hemispheres, which were normalized to the interval between -1 and 1. For example, for FA it was defined as $\left(FA_{healthy} - FA_{impaired}\right)/\left(FA_{healthy} + FA_{impaired}\right)$. In this way, WM properties that were balanced between the hemispheres resulted in values close to zero; positive values indicate that the contralesional side has higher FA than the ipsilesional side and vice versa for negative values. In the same manner, the asymmetry was calculated for MD, RD and AD. For the healthy controls asymmetry was defined between the dominant and non-dominant hemispheres based on the handedness of each subject.

The asymmetries were statistically analyzed using the two-sided Wilcoxon signed rank test. The Benjamini–Hochberg procedure was used to control the false discovery rate at the 5% level (Benjamini and Hochberg, 1995; Benjamini and Yekutieli, 2001), independently for each of the outcome parameters. Comparisons for each model and each diffusivity measure were done independently. WM asymmetries were correlated with the upper limb Fugl-Meyer assessment (FMA) score using Pearson correlation.

3.3 Results

Pearson correlations between FA, MD, AD and RD asymmetries estimated from the four diffusion models with Fugl-Meyer scores are presented in Figure 3.4.

The comparison of asymmetries in diffusion measures between patient and control groups for all four diffusion models is presented in Figure 3.5. After applying the Benjamini–Hochberg false discovery rate control procedure, the comparisons were deemed to be statistically significant at the 95% confidence level when p<=0.016 for FAasymmetry, p<=0.014 for $MD_{asymmetry}$, p<=0.003 for $AD_{asymmetry}$ and p<=0.012 for $RD_{asymmetry}$. Patients showed a significant difference from controls in CST asymmetries of FA, MD and RD for all models, but of AD only for model (3). Similarly, a difference between groups was found in SLF asymmetries of FA, MD and RD for all models, and of AD only for models (1) and (3). $AD_{asymmetry}$ did not identify other WM tracts as being different between the patient and control groups. None of the models identified statistically significant difference in the cingulum-1, inferior fronto-occipital fasciculus and uncinate fasciculus. For the inferior longitudinal fasciculus, only $RD_{asymmetry}$ for models (2) and (4) and $MD_{asymmetry}$ for model (2) differed significantly between patients and controls.

Table 3.2. Median and IQR over the study population of the considered regions of interest after masking lesions out, computed in the atlas space. Names and order of ROIs coincide with Table 3.1.

Tract name	Median (IQR), px	
	Right hemisphere	Left hemisphere
Anterior thalamic radiation	11716 (9928,5-12588)	10776 (7265,25-11320,75)
Corticospinal tract	8867 (8451,75-9057,5)	7991,5 (7302,75-8106,75)
Cingulum (all parts)	5021 (4992,75-5053,75)	3781,5 (3721,75-3792,75)
Inferior fronto-occipital fasciculus	11018 (10587,25-11097,5)	12036 (10976-12134,5)

Inferior longitudinal fasciculus	10359,5 (10314-10400)	6964 (6790,5-7004,25)
Superior longitudinal fasciculus (all parts)	14977,5 (14862,5-15017,5)	11881,5 (11186,75-11909,75)
Uncinate fasciculus	2627 (2551,5-2650,75)	1775,5 (1605-1810)

3.4 Discussion

In this study, we evaluated how WM diffusion properties estimated by four diffusion models of increasing complexity relate to the motor outcome of chronic stroke patients. Particularly, the influence of stroke on symmetric white matter structures was assessed based on the interhemispheric asymmetry of mean tract model parameters. We have not investigated the influence of lesion size and lesion location on motor recovery, which was presented in literature before (e.g. (Lo et al., 2010)), but focused on four diffusion measures: FA, MD, AD and RD.

Model comparison

Diffusion MRI has been used to derive characteristics of the corticospinal tract in chronic stroke using the single tensor model. (Archer et al., 2017) aimed to eliminate bias of free water contamination from the FA estimation with an approach by (Pasternak et al., 2009) for modeling a tissue and a free water compartment. We add to this previous work by not only investigating the $FA_{asymmetry}$, but other diffusivity measures (MD, AD and RD) as well. This is supported by our acquisition protocol with two b-values, as it was discussed in (Taquet et al., 2015) that estimation of the parameters in the two-compartment model by (Pasternak et al., 2009), NODDI (Zhang et al., 2012), CHARMED (Assaf and Basser, 2005) and DIAMOND (Scherrer et al., 2013)[2] is ineffective for a single b-value data, unless additional regularization or assumptions are enforced on the model fit. Two-compartment models were also previously applied to multi-shell

[2] NODDI = Neurite Orientation Dispersion and Density Imaging; CHARMED = Composite hindered and restricted model of diffusion; DIAMOND = DIstribution of 3-D Anisotropic MicrOstructural eNvironments in Diffusion-compartment imaging

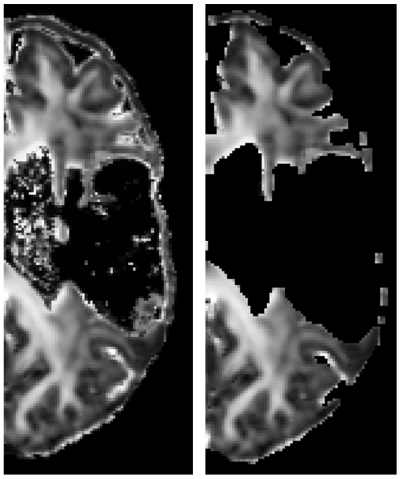

Figure 3.3 FA image of an affected hemisphere of a patient before (subject space, left) and after (atlas space, right) registration to the atlas space. Lesion mask was applied. The absence of large deformations indicates that the presence of the lesion hardly affected the registration outcome.

dMRI data by, for example, (Pierpaoli and Jones, 2004; Pasternak et al., 2012; Hoy et al., 2014).

The WM asymmetries were assessed using four diffusion models of increasing complexity: (1) single tensor, (2) single tensor with isotropic compartment, (3) bi-tensor and (4) bi-tensor with isotropic compartment. The addition of each compartment to the models in this study permits modeling of an additional physical phenomenon (i.e., free water and crossing fibers) and contributes to the interpretation of the results. It is important to notice that the outcome parameters of the selected diffusion models are directly comparable to each other. For example, the frequently used ball-and-stick model (Behrens et al., 2003) yields volume fractions of the fiber populations that cannot be directly compared to FA. However, more complex models do not everywhere in the brain reflect the underlying white matter anatomy. Applying a two tensor model to the diffusion data from a single fiber tract may lead to overfitting and meaningless outcome parameters. This is described in (Yang et al., 2016). Therefore, it cannot be taken for granted that more complex models are always performing better, especially in case of pathologies.

Damage to the CST after stroke has been extensively investigated in (Stinear et al., 2007; Schaechter et al., 2008; Schaechter et al., 2009; Cunningham et al., 2015). A linear correlation was found between the CST integrity and increased activation of the contralesional primary sensorimotor cortex (Schaechter et al., 2008). Qui and

coworkers (Qiu et al., 2011) showed a close relationship between the FA asymmetry and clinical outcome measures. The current study expands on this by exploring this relation for multiple WM properties assessed by four diffusion models. We did not find a significant Pearson correlation between the asymmetry of single tensor diffusion measures and the upper-limb FMA in most of the tracts, not even in the CST. The other models do show significant correlations between the CST asymmetry and the FMA score. The highest correlation and statistical significance are for FA and RD CST asymmetries. Except for the cingulum (tracts 3 and 4), MD, AD and RD asymmetry derived from models (2)-(4) showed significant correlation with the FMA for all other tracts. However, it was less consistent among tracts for the FA asymmetry. This may indicate that not only CST integrity, but also the state of other white matter tracts could be indicative of the patient's motor abilities after stroke. A similar conclusion was previously reached based on a voxel-wise FA analysis (Schaechter et al., 2009).

Our findings indicate that accounting for the free water by adding an isotropic compartment to the single tensor model already significantly increases the sensitivity of diffusion outcomes. Differences in the outcomes of different models may suggest that for specific tracts and especially in the areas hampered by partial volume effects, it can be beneficial to go beyond the single tensor model when relating the results to the patient motor function.

Affected white matter tracts

We investigated the asymmetry in FA, MD, AD and RD and tested whether the asymmetry was significantly different from the same measures for the control group and whether it correlated with the FMA score of the patients. As a higher FA may be related to a better quality of WM tracts (Huppi and Dubois, 2006; Teipel et al., 2010; Winston, 2012), statistically significant correlations of $FA_{asymmetry}$ with the motor score are negative. The rest of the diffusion properties have an inverse relation, e.g. lower MD indicates higher membrane density, leading to significant correlations of MD, AD and RD asymmetries with FMA being negative. Moreover, prior research predominantly focused on the CST in general and the posterior limb of the internal capsule in particular, because these structures are regularly associated with stroke damage (Jang, 2011; Park et al., 2013; Song et al., 2015). Instead, we

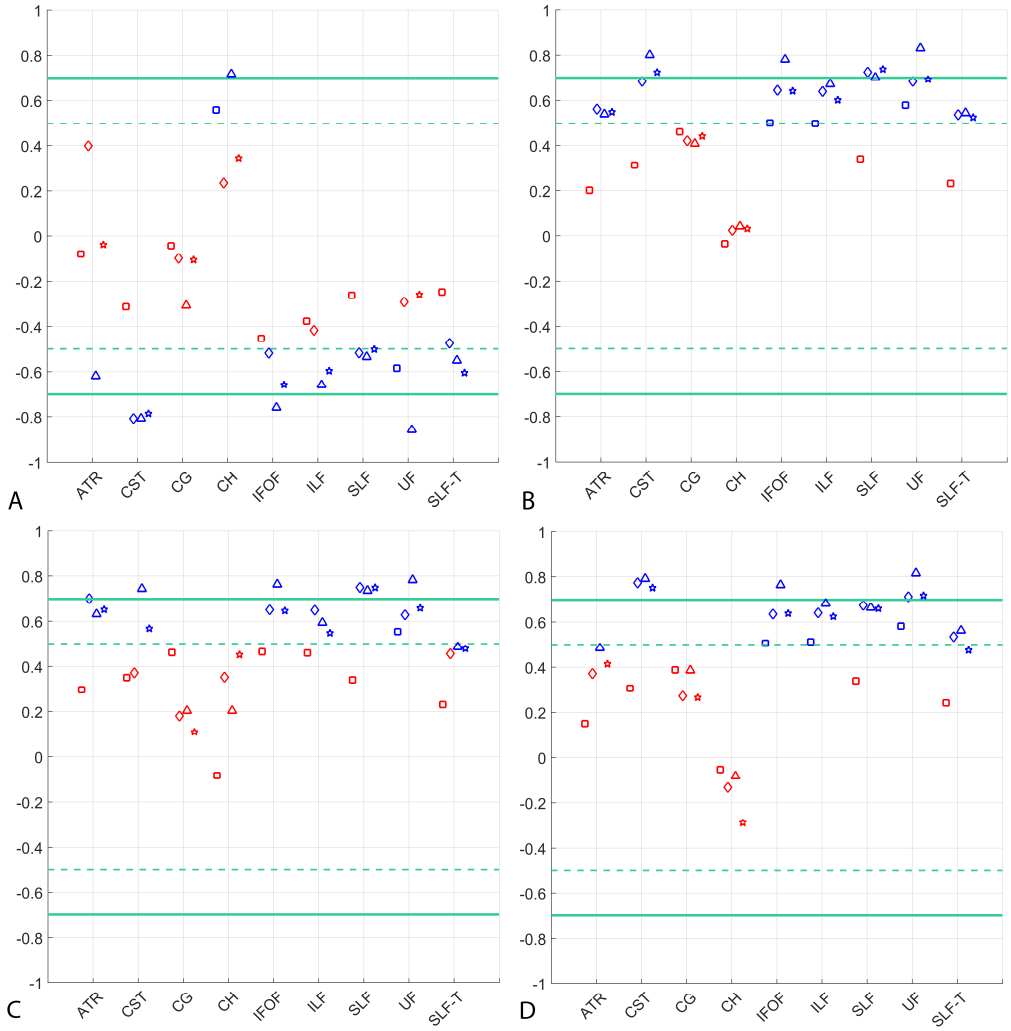

Figure 3.4 Correlation of the FMA score and asymmetry in (A) FA (top left), (B) MD (top right), (C) AD (bottom left) and (D) RD (bottom right) for the considered WM tracts. Statistically significant correlations ($p<0.05$) are depicted in blue, not significant correlations are shown in red. Models are denoted as follows: single tensor – square, single tensor with isotropic compartment –diamond, bi-tensor – triangle, bi-tensor with isotropic compartment – star. Horizontal dashed lines mark conditional boundaries of moderate (negative) linear relation (correlation of +/-0.5), solid lines – strong relation (correlation of +/-0.7).

chose to pursue a more comprehensive analysis involving diffusivity parameters in nine symmetric tracts as listed above.

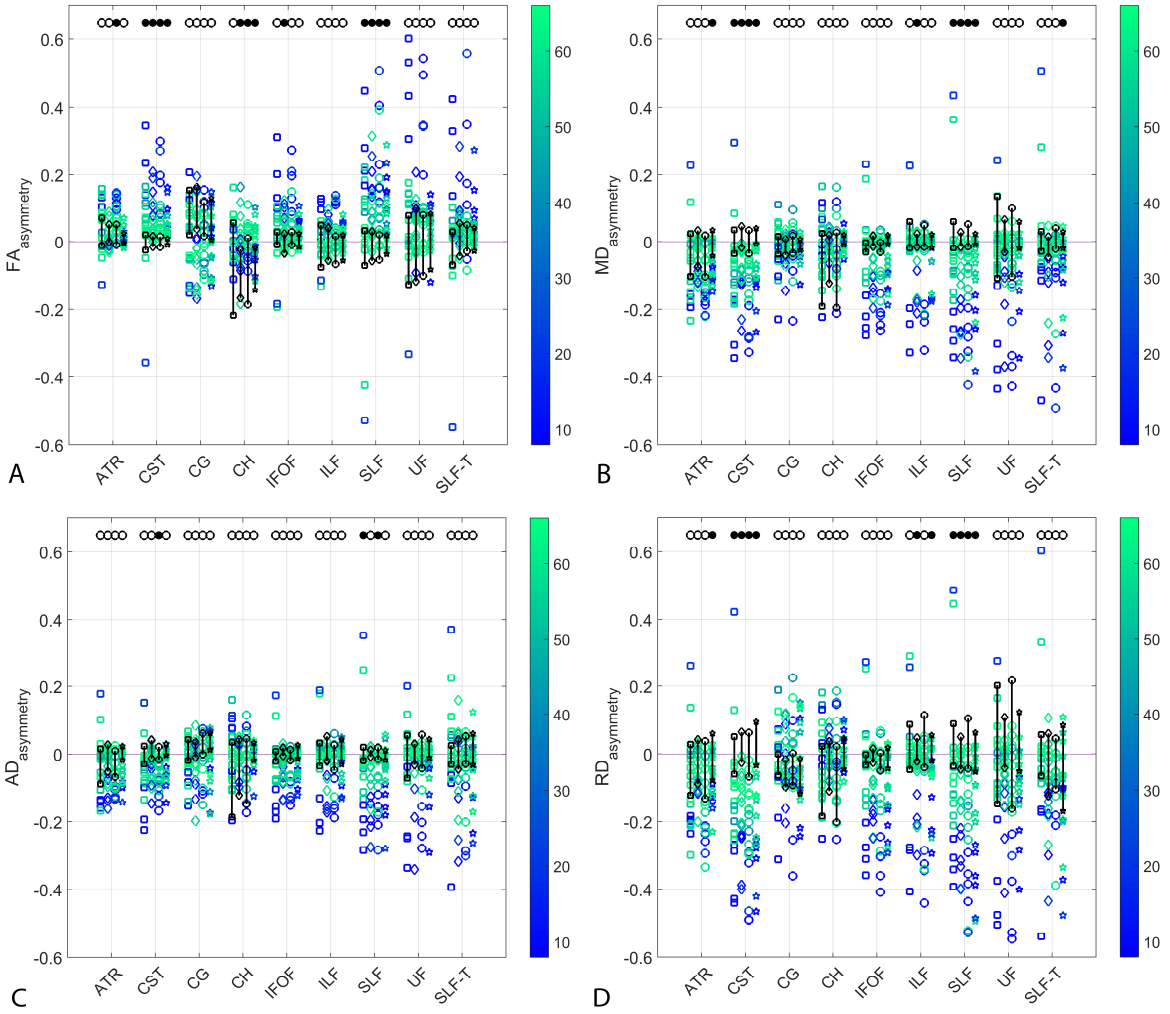

Figure 3.5 Comparison of the (A) FA (top left), (B) MD (top right), (C) AD (bottom left) and (D) RD (bottom right) asymmetries in the WM tracts between patients and controls (range indicated in black) estimated by the four diffusion models. Results for patients are color-coded with their FMA score. Models from left to right for each tract: single tensor (square), single tensor with isotropic compartment (diamond), bi-tensor (triangle), bi-tensor with isotropic compartment (star). Filled bullets at the top of each data series mark the tracts and models for which, after Benjamini-Hochberg correction, the asymmetry of patients is significantly different from the one of controls.

As might be expected, the WM tracts asymmetry in healthy controls fluctuated around zero. After false discovery rate correction, FA, MD and RD, but not AD, asymmetries differed between patients and controls in CST and SLF. Model (1) also failed to identify the $FA_{asymmetry}$ in SLF. Asymmetry in SLF has not been reported previously. However, the dorsal component of SLF originates in the superior and medial parietal cortex and terminates in the dorsal and medial cortex of the frontal lobe and in the supplementary motor cortex. Therefore, changes in the SLF with respect to the control group could have been expected as all patients in this study suffered from a certain extend of motor impairment. Overall, patients with more severe impairment, indicated by lower FMA scores, displayed indeed higher asymmetry of their WM properties.

Limitations

Diffusion properties of the cingulum (tracts 3 and 4) did not correlate with FMA and showed higher asymmetries even for the control group (Figure 3.4, Figure 3.5). Information about the dominant and the impaired hand of the patients may suggest that handedness of subjects could have influenced the sign of the WM asymmetry. A number of studies investigated the effects of handedness on the human brain. Differences in volumes of grey and white matter areas were detected by (Herve et al., 2006). A voxel-based statistical analysis found higher FA in the left arcuate fasciculus in consistent right-handers (Buchel et al., 2004). However, this was not confirmed in a similar study by (Park et al., 2004). Despite the fact that right hand preference might be expected to result from asymmetries in the motor cortex, it is stronger correlated with asymmetries in language-processing structures (Toga and Thompson, 2003). A more recent study by (Powell et al., 2012) suggests a greater effect of sex than handedness on FA asymmetry. (Luft et al., 2004) found significantly higher FA values for left-handed individuals in all major lobes and in the corpus callosum compared to the right-handed subjects. As such, results regarding handedness effects on WM have not been entirely consistent across different studies.

In our work we rely on an assumption that stroke causes a much larger asymmetry than the handedness of a person. We did compare the effect of stroke to the baseline asymmetries in diffusion properties of our control group, which are quite

symmetrically distributed around zero (except for the cingulum as mentioned above) and are in range that is at least twice smaller than that of the patient group. Although we are aware that this approach has drawbacks, it is frequently performed to avoid oversegmentation of the cohort, i.e. dividing it into groups based on handedness, (Luft et al., 2004; De Vico Fallani et al., 2013). Practically, it enabled us to include a sufficiently large subject group to achieve statistically valid results and conclusions. Such an approach is similar to the underlying assumption of many other stroke studies .

As a limitation we would also like to mention the absence of a ground truth, as the true diffusion properties of WM in stroke patients are unknown. This limits our ability to evaluate the performance of the diffusion models, but this is a common problem of in-vivo studies into brain structures, allowing only indirect assessments. Another factor is the smaller size of the control group compared to the patient group. We assume that the variation in the outcome parameters (e.g. $FA_{asymmetry}$, $MD_{asymmetry}$, etc.) of the controls is much smaller than those of the patients. Accordingly, the smaller group size of the controls should not hinder the comparison. This was confirmed in our power analysis, which indicated that the chance of detecting a large effect is 90%. That is why we consider our study design to be sufficient to fulfil its aims. However, a design with equal group size would have further enhanced the statistical power of the study.

Outlook

Differences in the parameter outcomes of different models may suggest that for specific tracts and especially in brain areas contaminated by partial volume effects, it can be beneficial to go beyond the single tensor model when relating the outcomes to the patients' motor function. Approaching stroke dMRI equipped with more sophisticated models could be helpful in studying scans at a more acute phase, when it is important to make a prediction of recovery and adjust therapy. This could be most beneficial for so-called non-fitters to the 70% recovery rule (see, for example, (Winters et al., 2015)) and differentiating between necrotic and still salvageable tissue. Our results suggest that employing multi-compartment diffusion models should be tested to investigate WM changes in stroke patients longitudinally, starting from the acute phase.

3.5 Conclusions

- FA and RD asymmetries are an indication of white matter alterations after stroke and related with the patients' motor outcome.
- As for selecting a diffusion model, the bi-tensor model with isotropic compartment should be used if permitted by the dMRI acquisition protocol (i.e., sufficient diffusion directions and multiple b-values). Otherwise, a single tensor model with isotropic compartment is a good alternative.
- Not only the cortical-spinal tract, but also the superior longitudinal fasciculus integrity values are significantly affected by stroke as indicated by the group comparison between patients and controls.
- Approaching dMRI in stroke patients with sophisticated diffusion models instead of a single tensor model leads to a higher sensitivity and should be tested in scans at a more acute phase, when it is important to make a prediction of recovery and adjust therapy. This could be most beneficial for so-called non-fitters to the 70% recovery rule (see, for example, (Winters et al., 2015)) and for differentiating between necrotic and still salvageable tissue.
- Employing multi-compartment diffusion models should be tested to detect WM changes in stroke patients longitudinally, starting from the acute phase.

Funding

This research was funded by the European Research Council under the European Union's Seventh Framework Programme (FP/2007-2013) ERC Grant Agreement n. 291339, project 4DEEG: A new tool to investigate the spatial and temporal activity patterns in the brain.

Acknowledgements. 4D-EEG consortium

In addition to the authors of the present study, the consortium consists of Jan de Munck, Carel Meskers, Mique Saes*, Luuk Haring*, Caroline Winters*, Aukje Andringa*, Dirk Hoevenaars*, Ines de Castro Fernandes, and Sarah Zandvliet from VU University Medical Centre; Andreas Daffertshofer and Erwin van Wegen from MOVE Research Institute Amsterdam; Jun Yao and Julius Dewald from

Northwestern University; Teodoro Solis-Escalante, Yuan Yang, Mark van de Ruit, Martijn Vlaar, and Konstantina Kalogianni from Delft University of Technology.

*These consortium members performed the measurements.

Ethics approval and consent to participate

This study was carried out in accordance with the recommendations of Medical Ethics Reviewing Committee of the VU Medical Center, Amsterdam with written informed consent from all subjects. All subjects gave written informed consent in accordance with the Declaration of Helsinki. The protocol was approved by the Medical Ethics Reviewing Committee of the VU Medical Center, Amsterdam (protocol number 2014.140, Dutch Central Committee on Research Involving Human Subjects, CCMO, protocol number NL47079.029.14).

Conflict of interest

The authors declare that they have no competing interests.

Appendix. Diffusion modeling

Assuming a mono-exponential and Gaussian diffusion along the principal directions (given by the eigenvectors) of the separate fiber compartments, the measured dMR signal S_j can be modeled as a sum of up to two fiber bundles and an isotropic compartment in the following way:

$$S_j = S_0\left(\sum_{i=1,2} f_i \exp\left(-\mathbf{b}_j \mathbf{g}_j^T \mathbf{D}_i \mathbf{g}_j\right) + f_{iso} \exp\left(-\mathbf{b}_j D_{iso}\right)\right) \qquad (3.1)$$

where S_0 is the signal without diffusion weighting, f_i and f_{iso} are the volume fractions of different compartments such that $\sum_{i=1,2} f_i + f_{iso} = 1$, g_j is a gradient direction, b_j is the diffusion weighting coefficient, D_i is the diffusion tensor of the i^{th} fiber, and D_{iso} is the scalar coefficient of isotropic diffusion. Here directions of diffusion sensitizing gradients and the amount of weighting are inputs, depending on the acquisition protocol. Different models are obtained by adjusting the number of fibers, constraints on diffusion tensors and presence or absence of the isotropic diffusion process. The assumption of the mono-exponential signal decay is valid up

to at least 2000 s/mm^2 (Yoshiura et al., 2001), or even up to 3000 s/mm^2 as reported in the multiple sclerosis study by (Assaf et al., 2002).

To estimate the unknowns, the diffusion tensor can be parametrized in polar coordinates. Parameters of the considered models are listed below.

Single tensor: $\theta_1, \phi_1, \psi_1, \lambda_1, \lambda_2, \lambda_3, S_0$.

Single tensor with an isotropic compartment: $\theta_1, \phi_1, \psi_1, \lambda_1, \lambda_2, \lambda_3, f_{iso}, S_0$.

Bi-tensor model: $f_1, \lambda_\parallel, \lambda_\perp, \theta_1, \phi_1, \theta_2, \phi_2, S_0$.

Bi-tensor with an isotropic compartment: $f_{iso}, f_1, \lambda_\parallel, \lambda_\perp, \theta_1, \phi_1, \theta_2, \phi_2, S_0$.

Here $\lambda_1, \lambda_2, \lambda_3$ are eigenvalues of the diffusion tensor, $\lambda_\parallel, \lambda_\perp$ denote the axial and perpendicular diffusion respectively, ψ_i , θ_i and ϕ_i determine the ith fiber orientation in polar coordinates.

The parameter vector is obtained by maximizing the log likelihood of the joint probability density function for diffusion-weighted signals with independent noise realizations. It is done using our constrained non-linear optimization routine in Matlab (The MathWorks, Natick, MA). The optimization problem can be formulated as follows.

Let $\tilde{\mathrm{S}}_{j,\sigma}$ be the measured diffusion weighted image (DWI) with diffusion weighting $\mathbf{b}_j$ in direction $\mathbf{g}_j$. It is affected by Rician noise with standard deviation σ (Gudbjartsson and Patz, 1995). Therefore, for the parameter vector $\boldsymbol{\theta}$, the probability density function (PDF) of the measured signal is given by

$$p(\tilde{\mathrm{S}}_{j,\sigma} \mid \boldsymbol{\theta}) = \frac{\tilde{\mathrm{S}}_{j,\sigma}}{\sigma^2} \exp\left(\frac{\tilde{\mathrm{S}}_{j,\sigma}{}^2 + S_{\boldsymbol{\theta},j}{}^2}{2\sigma^2} \right) I_0\left(\frac{\tilde{\mathrm{S}}_{j,\sigma} S_{\boldsymbol{\theta},j}}{\sigma^2} \right), \qquad (3.2)$$

where $I_0(\cdot)$ is the zeroth order modified Bessel function of the first kind, . Due to statistical independence of the DWIs, the joint probability density function $p(\tilde{\mathbf{S}}_\sigma \mid \boldsymbol{\theta})$ of the signal profile $\tilde{\mathbf{S}}_\sigma$ is equal to the product of the marginal distributions for the measured signals $\tilde{\mathrm{S}}_{j,\sigma}$ in each of the N_g diffusion weighted directions $\mathbf{g}_j$:

$$p\left(\tilde{\mathbf{S}}_\sigma \mid \boldsymbol{\theta}\right) = \prod_{j=1}^{N_g} p\left(\tilde{\mathrm{S}}_{j,\sigma} \mid \boldsymbol{\theta}\right) \tag{3.3}$$

The parameter values can be estimated by maximizing the log likelihood function of $\boldsymbol{\theta}$ given $\tilde{\mathbf{S}}_\sigma$ (Sijbers et al., 2004):

$$\hat{\boldsymbol{\theta}}_{\mathrm{MLE}} = \arg\max_{\boldsymbol{\theta}} \left\{ \ln\left(p(\tilde{\mathbf{S}}_\sigma \mid \boldsymbol{\theta}) \right) \right\}. \tag{3.4}$$

Maximum likelihood estimation (MLE) has a number of beneficial properties for diffusion estimation in crossing fiber bundles (Caan et al., 2010a). First of all, under very general conditions, MLE asymptotically reaches the Cramér-Rao lower bound (CRLB). This is a theoretical lower bound on the variance of any unbiased estimator. Secondly, the MLE is consistent, which means that it asymptotically ($N_g \to \infty$) converges to the true value of the parameter in a statistically well-defined way (Van den Bos, 2007). Optimization is performed using Levenberg–Marquardt algorithm.

References

Archer, D.B., Patten, C., and Coombes, S.A. (2017). Free-water and free-water corrected fractional anisotropy in primary and premotor corticospinal tracts in chronic stroke. *Human Brain Mapping* 38(9), 4546-4562. doi: 10.1002/hbm.23681.

Arkesteijn, G.A.M., Poot, D.H.J., de Groot, M., Vernooij, M.W., Niessen, W.J., van Vliet, L.J., et al. (Year). "CSF contamination-invariant statistics in diffusion-weighted MRI", in: *Biomedical Imaging (ISBI), 2015 IEEE 12th International Symposium on*), 454-457.

Assaf, Y., and Basser, P.J. (2005). Composite hindered and restricted model of diffusion (CHARMED) MR imaging of the human brain. *NeuroImage* 27(1), 48-58. doi: https://doi.org/10.1016/j.neuroimage.2005.03.042.

Assaf, Y., Ben-Bashat, D., Chapman, J., Peled, S., Biton, I.E., Kafri, M., et al. (2002). High b-value q-space analyzed diffusion-weighted MRI: Application to multiple sclerosis. *Magnetic Resonance in Medicine* 47(1), 115-126. doi: 10.1002/mrm.10040.

Behrens, T.E., Woolrich, M.W., Jenkinson, M., Johansen-Berg, H., Nunes, R.G., Clare, S., et al. (2003). Characterization and propagation of uncertainty in diffusion-weighted MR imaging. *Magn Reson Med* 50(5), 1077-1088. doi: 10.1002/mrm.10609.

Benjamini, Y., and Hochberg, Y. (1995). Controlling the False Discovery Rate: a Practical and Powerful Approach to Multiple Testing. *Journal of the Royal Statistical Society. Series B (Methodological)* 57(1), 289-300.

Benjamini, Y., and Yekutieli, D. (2001). The Control of the False Discovery Rate in Multiple Testing under Dependency. *The Annals of Statistics* 29(4), 1165-1188.

Bhagat, Y.A., Hussain, M.S., Stobbe, R.W., Butcher, K.S., Emery, D.J., Shuaib, A., et al. (2008). Elevations of diffusion anisotropy are associated with hyper-acute stroke: a serial imaging study. *Magnetic Resonance Imaging* 26(5), 683-693. doi: 10.1016/j.mri.2008.01.015.

Brus-Ramer, M., Carmel, J.B., Chakrabarty, S., and Martin, J.H. (2007). Electrical stimulation of spared corticospinal axons augments connections with ipsilateral spinal motor circuits after injury. *Journal of Neuroscience* 27(50), 13793-13801. doi: 10.1523/JNEUROSCI.3489-07.2007.

Buchel, C., Raedler, T., Sommer, M., Sach, M., Weiller, C., and Koch, M.A. (2004). White matter asymmetry in the human brain: a diffusion tensor MRI study. *Cereb Cortex* 14(9), 945-951. doi: 10.1093/cercor/bhh055.

Buma, F., Kwakkel, G., and Ramsey, N. (2013). Understanding upper limb recovery after stroke. *Restor Neurol Neurosci* 31(6), 707-722. doi: 10.3233/RNN-130332.

Byblow, W.D., Stinear, C.M., Barber, P.A., Petoe, M.A., and Ackerley, S.J. (2015). Proportional recovery after stroke depends on corticomotor integrity. *Annals of Neurology* 78(6), 848-859. doi: 10.1002/ana.24472.

Caan, M.W., Khedoe, H., Poot, D., Den Dekker, A., Olabarriaga, S., Grimbergen, K., et al. (2010a). Estimation of diffusion properties in crossing fiber bundles. *IEEE Trans Med Imaging* 29(8), 1504-1515.

Caan, M.W.A., Khedoe, H.G., Poot, D.H.J., den Dekker, A.J., Olabarriaga, S.D., Grimbergen, K.A., et al. (2010b). Estimation of Diffusion Properties in Crossing Fiber Bundles. *IEEE Transactions on Medical Imaging* 29(8), 1504-1515.

Charan, J., and Biswas, T. (2013). How to Calculate Sample Size for Different Study Designs in Medical Research? *Indian Journal of Psychological Medicine* 35(2), 121-126. doi: 10.4103/0253-7176.116232.

Cho, S.H., Kim, D.G., Kim, D.S., Kim, Y.H., Lee, C.H., and Jang, S.H. (2007). Motor outcome according to the integrity of the corticospinal tract determined by diffusion tensor tractography in the early stage of corona radiata infarct. *Neuroscience Letters* 426(2), 123-127. doi: 10.1016/j.neulet.2007.08.049.

Cunningham, D.A., Machado, A., Janini, D., Varnerin, N., Bonnett, C., Yue, G., et al. (2015). Assessment of inter-hemispheric imbalance using imaging and noninvasive brain stimulation in patients with chronic stroke. *Archives of physical medicine and rehabilitation* 96(4 Suppl), S94-103. doi: 10.1016/j.apmr.2014.07.419.

Dancause, N., Barbay, S., Frost, S.B., Plautz, E.J., Chen, D., Zoubina, E.V., et al. (2005). Extensive cortical rewiring after brain injury. *Journal of Neuroscience* 25(44), 10167-10179. doi: 10.1523/JNEUROSCI.3256-05.2005.

De Vico Fallani, F., Pichiorri, F., Morone, G., Molinari, M., Babiloni, F., Cincotti, F., et al. (2013). Multiscale topological properties of functional brain networks during motor imagery after stroke. *Neuroimage* 83, 438-449. doi: 10.1016/j.neuroimage.2013.06.039.

Gudbjartsson, H., and Patz, S. (1995). The Rician Distribution of Noisy MRI Data. *Magnetic resonance in medicine : official journal of the Society of Magnetic Resonance in Medicine / Society of Magnetic Resonance in Medicine* 34(6), 910-914.

Herve, P.Y., Crivello, F., Perchey, G., Mazoyer, B., and Tzourio-Mazoyer, N. (2006). Handedness and cerebral anatomical asymmetries in young adult

males. *Neuroimage* 29(4), 1066-1079. doi: 10.1016/j.neuroimage.2005.08.031.

Hoy, A.R., Koay, C.G., Kecskemeti, S.R., and Alexander, A.L. (2014). Optimization of a Free Water Elimination Two-Compartment Model for Diffusion Tensor Imaging. *NeuroImage* 103, 323-333. doi: 10.1016/j.neuroimage.2014.09.053.

Hua, K., Zhang, J., Wakana, S., Jiang, H., Li, X., Reich, D.S., et al. (2008). Tract probability maps in stereotaxic spaces: Analyses of white matter anatomy and tract-specific quantification. *NeuroImage* 39(1), 336-347. doi: https://doi.org/10.1016/j.neuroimage.2007.07.053.

Huppi, P.S., and Dubois, J. (2006). Diffusion tensor imaging of brain development. *Seminars in Fetal & Neonatal Medicine* 11(6), 489-497. doi: 10.1016/j.siny.2006.07.006.

Jang, S.H. (2011). A review of diffusion tensor imaging studies on motor recovery mechanisms in stroke patients. *NeuroRehabilitation* 28(4), 345-352. doi: 10.3233/NRE-2011-0662.

Jang, S.H., Ahn, S.H., Sakong, J., Byun, W.M., Choi, B.Y., Chang, C.H., et al. (2010). Comparison of TMS and DTT for predicting motor outcome in intracerebral hemorrhage. *Journal of Neurological Sciences* 290(1-2), 107-111. doi: 10.1016/j.jns.2009.10.019.

Jenkinson, M., Beckmann, C.F., Behrens, T.E., Woolrich, M.W., and Smith, S.M. (2012). Fsl. *Neuroimage* 62(2), 782-790. doi: 10.1016/j.neuroimage.2011.09.015.

Jeurissen, B., Leemans, A., Tournier, J.-D., Jones, D.K., and Sijbers, J. (2013). Investigating the prevalence of complex fiber configurations in white matter tissue with diffusion magnetic resonance imaging. *Human Brain Mapping* 34(11), 2747-2766. doi: 10.1002/hbm.22099.

Kelsey, J.L., Whittemore, A.S., Evans, A.S., and Thompson, W.D. (1996). *Methods in Observational Epidemiology.* New York: Oxford University ress.

Kumar, P., Kathuria, P., Nair, P., and Prasad, K. (2016). Prediction of Upper Limb Motor Recovery after Subacute Ischemic Stroke Using Diffusion Tensor Imaging: A Systematic Review and Meta-Analysis. *Journal of Stroke* 18(1), 50-59. doi: 10.5853/jos.2015.01186.

Latour, L.L., and Warach, S. (2002). Cerebral spinal fluid contamination of the measurement of the apparent diffusion coefficient of water in acute stroke. *Magnetic Resonance in Medicine* 48(3), 478-486. doi: 10.1002/mrm.10238.

Lindenberg, R., Renga, V., Zhu, L.L., Betzler, F., Alsop, D., and Schlaug, G. (2010). Structural integrity of corticospinal motor fibers predicts motor

impairment in chronic stroke. *Neurology* 74(4), 280-287. doi: 10.1212/WNL.0b013e3181ccc6d9.

Lindenberg, R., Zhu, L.L., Ruber, T., and Schlaug, G. (2012). Predicting functional motor potential in chronic stroke patients using diffusion tensor imaging. *Human Brain Mapping* 33(5), 1040-1051. doi: 10.1002/hbm.21266.

Lo, R., Gitelman, D., Levy, R., Hulvershorn, J., and Parrish, T. (2010). Identification of critical areas for motor function recovery in chronic stroke subjects using voxel-based lesion symptom mapping. *Neuroimage* 49(1), 9-18. doi: 10.1016/j.neuroimage.2009.08.044.

Luft, A.R., Waller, S., Forrester, L., Smith, G.V., Whitall, J., Macko, R.F., et al. (2004). Lesion location alters brain activation in chronically impaired stroke survivors. *NeuroImage* 21(3), 924-935. doi: https://doi.org/10.1016/j.neuroimage.2003.10.026.

Ma, C., Liu, A., Li, Z., Zhou, X., and Zhou, S. (2014). Longitudinal study of diffusion tensor imaging properties of affected cortical spinal tracts in acute and chronic hemorrhagic stroke. *Journal of Clinical Neuroscience* 21(8), 1388-1392. doi: 10.1016/j.jocn.2013.11.032.

Mori, S., Wakana, S., van Zijl, P.C.M., and and Nagae-Poetscher, L.M. (2005). *MRI Atlas of Human White Matter.* Amsterdam: Elsevier.

Neil, J.J. (2008). Diffusion imaging concepts for clinicians. *Journal of Magnetic Resonance Imaging* 27(1), 1-7. doi: 10.1002/jmri.21087.

Park, C.H., Kou, N., Boudrias, M.H., Playford, E.D., and Ward, N.S. (2013). Assessing a standardised approach to measuring corticospinal integrity after stroke with DTI. *Neuroimage Clinical* 2, 521-533. doi: 10.1016/j.nicl.2013.04.002.

Park, H.J., Westin, C.F., Kubicki, M., Maier, S.E., Niznikiewicz, M., Baer, A., et al. (2004). White matter hemisphere asymmetries in healthy subjects and in schizophrenia: a diffusion tensor MRI study. *Neuroimage* 23(1), 213-223. doi: 10.1016/j.neuroimage.2004.04.036.

Parker, G.D., Marshall, D., Rosin, P.L., Drage, N., Richmond, S., and Jones, D.K. (2013). A pitfall in the reconstruction of fibre ODFs using spherical deconvolution of diffusion MRI data. *Neuroimage* 65, 433-448. doi: 10.1016/j.neuroimage.2012.10.022.

Pasternak, O., Shenton, M.E., and Westin, C.-F. (Year). "Estimation of Extracellular Volume from Regularized Multi-shell Diffusion MRI", in: *Medical Image Computing and Computer-Assisted Intervention – MICCAI 2012*, eds. N. Ayache, H. Delingette, P. Golland & K. Mori: Springer Berlin Heidelberg), 305-312.

Pasternak, O., Sochen, N., Gur, Y., Intrator, N., and Assaf, Y. (2009). Free water elimination and mapping from diffusion MRI. *Magnetic Resonance in Medicine* 62(3), 717-730. doi: 10.1002/mrm.22055.

Pierpaoli, C., and Jones, C.K. (2004). "Removing CSF Contamination in Brain DT-MRIs by Using a Two-Compartment Tensor Model", in: *International Society for Magnetic Resonance in Medicine - ISMRM 2004.* (Kyoto, Japan).

Powell, J.L., Parkes, L., Kemp, G.J., Sluming, V., Barrick, T.R., and Garcia-Finana, M. (2012). The effect of sex and handedness on white matter anisotropy: a diffusion tensor magnetic resonance imaging study. *Neuroscience* 207, 227-242. doi: 10.1016/j.neuroscience.2012.01.016.

Puig, J., Pedraza, S., Blasco, G., Daunis-i-Estadella, J., Prats, A., Prados, F., et al. (2010). Wallerian Degeneration in the Corticospinal Tract Evaluated by Diffusion Tensor Imaging Correlates with Motor Deficit 30 Days after Middle Cerebral Artery Ischemic Stroke. *American Journal of Neuroradiology* 31(7), 1324.

Qiu, M., Darling, W.G., Morecraft, R.J., Ni, C.C., Rajendra, J., and Butler, A.J. (2011). White matter integrity is a stronger predictor of motor function than BOLD response in patients with stroke. *Neurorehabililation and Neural Repair* 25(3), 275-284. doi: 10.1177/1545968310389183.

Schaechter, J.D., Fricker, Z.P., Perdue, K.L., Helmer, K.G., Vangel, M.G., Greve, D.N., et al. (2009). Microstructural status of ipsilesional and contralesional corticospinal tract correlates with motor skill in chronic stroke patients. *Human Brain Mapping* 30(11), 3461-3474. doi: 10.1002/hbm.20770.

Schaechter, J.D., Perdue, K.L., and Wang, R. (2008). Structural damage to the corticospinal tract correlates with bilateral sensorimotor cortex reorganization in stroke patients. *Neuroimage* 39(3), 1370-1382. doi: 10.1016/j.neuroimage.2007.09.071.

Scherrer, B., Schwartzman, A., Taquet, M., Prabhu, S.P., Sahin, M., Akhondi-Asl, A., et al. (2013). "Characterizing the DIstribution of Anisotropic MicrO-structural eNvironments with Diffusion-Weighted Imaging (DIAMOND)," in *Medical Image Computing and Computer-Assisted Intervention – MICCAI 2013: 16th International Conference, Nagoya, Japan, September 22-26, 2013, Proceedings, Part III,* eds. K. Mori, I. Sakuma, Y. Sato, C. Barillot & N. Navab. (Berlin, Heidelberg: Springer Berlin Heidelberg), 518-526.

Sijbers, J., Den Dekker, A.J., Scheunders, P., and Van Dyck, D. (2004). Maximum likelihood estimation of signal amplitude and noise variance from MR data. *Magn Reson Med* 51(3), 586-594.

Song, J., Nair, V.A., Young, B.M., Walton, L.M., Nigogosyan, Z., Remsik, A., et al. (2015). DTI measures track and predict motor function outcomes in

stroke rehabilitation utilizing BCI technology. *Frontiers in Human Neuroscience* 9, 195. doi: 10.3389/fnhum.2015.00195.

Song, J., Young, B.M., Nigogosyan, Z., Walton, L.M., Nair, V.A., Grogan, S.W., et al. (2014). Characterizing relationships of DTI, fMRI, and motor recovery in stroke rehabilitation utilizing brain-computer interface technology. *Frontiers in Neuroengineering* 7, 31. doi: 10.3389/fneng.2014.00031.

Stinear, C.M., Barber, P.A., Smale, P.R., Coxon, J.P., Fleming, M.K., and Byblow, W.D. (2007). Functional potential in chronic stroke patients depends on corticospinal tract integrity. *Brain* 130(Pt 1), 170-180. doi: 10.1093/brain/awl333.

Taquet, M., Scherrer, B., Boumal, N., Peters, J.M., Macq, B., and Warfield, S.K. (2015). Improved fidelity of brain microstructure mapping from single-shell diffusion MRI. *Medical Image Analysis* 26(1), 268-286. doi: https://doi.org/10.1016/j.media.2015.10.004.

Teipel, S.J., Meindl, T., Wagner, M., Stieltjes, B., Reuter, S., Hauenstein, K.H., et al. (2010). Longitudinal changes in fiber tract integrity in healthy aging and mild cognitive impairment: a DTI follow-up study. *Journal of Alzheimer's Disease* 22(2), 507-522. doi: 10.3233/JAD-2010-100234.

Toga, A.W., and Thompson, P.M. (2003). Mapping brain asymmetry. *Nat Rev Neurosci* 4(1), 37-48. doi: 10.1038/nrn1009.

Tournier, J.D., Calamante, F., Gadian, D.G., and Connelly, A. (2004). Direct estimation of the fiber orientation density function from diffusion-weighted MRI data using spherical deconvolution. *Neuroimage* 23(3), 1176-1185. doi: 10.1016/j.neuroimage.2004.07.037.

Van den Bos, A. (2007). *Parameter Estimation for Scientific and Engineers.* Hoboken, NJ: Wiley.

Winston, G.P. (2012). The physical and biological basis of quantitative parameters derived from diffusion MRI. *Quantitative Imaging in Medicine and Surgery* 2(4), 254-265. doi: 10.3978/j.issn.2223-4292.2012.12.05.

Winters, C., van Wegen, E.E.H., Daffertshofer, A., and Kwakkel, G. (2015). Generalizability of the Proportional Recovery Model for the Upper Extremity After an Ischemic Stroke. *Neurorehabilitation and Neural Repair* 29(7), 614-622. doi: 10.1177/1545968314562115.

Yang, J., Poot, D.H.J., Caan, M.W.A., Su, T., Majoie, C.B.L.M., van Vliet, L.J., et al. (2016). Reliable Dual Tensor Model Estimation in Single and Crossing Fibers Based on Jeffreys Prior. *PLOS ONE* 11(10), e0164336. doi: 10.1371/journal.pone.0164336.

Yang, J., Poot, D.H.J., van Vliet, L.J., and Vos, F.M. (2015). Estimation of diffusion properties in three-way fiber crossings without overfitting. *Physics in Medicine and Biology* 60(23), 9123.

Yoshiura, T., Wu, O., Zaheer, A., Reese, T.G., and Sorensen, A.G. (2001). Highly diffusion-sensitized MRI of brain: Dissociation of gray and white matter. *Magnetic Resonance in Medicine* 45(5), 734-740. doi: 10.1002/mrm.1100.

Yu, C., Zhu, C., Zhang, Y., Chen, H., Qin, W., Wang, M., et al. (2009). A longitudinal diffusion tensor imaging study on Wallerian degeneration of corticospinal tract after motor pathway stroke. *Neuroimage* 47(2), 451-458. doi: 10.1016/j.neuroimage.2009.04.066.

Zhang, H., Schneider, T., Wheeler-Kingshott, C.A., and Alexander, D.C. (2012). NODDI: Practical in vivo neurite orientation dispersion and density imaging of the human brain. *NeuroImage* 61(4), 1000-1016. doi: https://doi.org/10.1016/j.neuroimage.2012.03.072.

4

Probabilistic tractography with model selection

Probability is the very guide of life.

Marcus Tullius Cicero

4 Probabilistic tractography in complex fiber orientations with automatic model selection.

Fiber tractography aims to reconstruct white matter (WM) connections in the brain. Challenges in these reconstructions include estimation of the fiber orientations in regions with multiple fiber populations, and the uncertainty in the fiber orientations as a result of noise. In this work, we use a range of multi-tensor models to cope with crossing fibers. The uncertainty in fiber orientation is captured using the Cramér-Rao lower bound. Furthermore, model selection is performed based on model complexity and goodness of fit. The performance of the framework on the fibercup phantom and human data was compared to the open source diffusion MRI toolkit Camino for a range of SNRs. Performance was quantified by using the Tractometer measures in the fibercup phantom and by comparing streamline counts of lateral projections of the corpus callosum (CC) in the human data. On the phantom data, the comparison showed that our method performs similar to Camino in crossing fiber regions, whilst performing better in a region with kissing fibers (median angular error of 0.73^o vs 2.7^o, valid connections of 57% vs 21% when seed is in the corresponding region of interest). Furthermore, the amount of counts in the lateral projections were found to be higher using our method (19 to 89% increase depending on a subject). Altogether, our method outperforms the reference method on both phantom and human data allowing for in-vivo probabilistic multi-fiber tractography with an objective model selection procedure.

4.1 Introduction

Diffusion weighted magnetic resonance imaging (dMRI) is a non-invasive technique which can be used for assessing tissue structure. Particularly, it measures the ability of water molecules to move freely in the surrounding tissue. Importantly, normal white matter (WM) shows high diffusivity along and slow across axons, whereas in gray matter (GM) the diffusion is more isotropic. As such, properties of WM tracts related to e.g. the fiber orientation, and fiber density can be estimated (Basser et al., 1994; Alexander et al., 2010). Fiber tractography algorithms strive to

reconstruct WM connections in the brain by following the estimated tract orientation.

Tractography algorithms can be roughly subdivided into two types: deterministic and probabilistic. Deterministic algorithms use line propagation techniques to generate streamlines from a seed region (Mori and van Zijl, 2002). However, noise in the dMRI acquisition can introduce uncertainties and possible errors in the generated streamlines (Jones, 2002). Alternatively, probabilistic tractography algorithms target to address this issue by modeling a probability density function (PDF) of the fiber orientations (Behrens et al., 2003). A density of streamlines can be obtained by sampling this PDF, which is assumed to relate to the probability of connection between voxels.

A classic way to estimate fiber orientations is to fit a single diffusion tensor (DT) to the signal in a voxel. The main assumptions of this approach are presence of a single Gaussian diffusion process in a voxel and correspondence of the principal eigenvector of the 3 x 3 DTs to the fiber orientation (Basser et al., 1994). However, it is well known that the single tensor model does not hold in voxels with non-Gaussian diffusion (Tuch et al., 2002), as is the case in voxels with multiple fiber populations. The prevalence of these multi-fiber voxels has been estimated to range from 33% up to ~90% of the WM voxels (Behrens et al., 2007; Jeurissen et al., 2013). Several methods have been developed to address the issue of multiple fiber populations in a voxel. For example, one can directly estimate the spin displacement probability (Jansons and Alexander, 2003; Tuch, 2004; Wedeen et al., 2005) or model the signal coming from different fiber compartments (Tuch et al., 2002; Kreher et al., 2005; Behrens et al., 2007).

Current methods to estimate the fiber orientation PDFs are based on the shape of the diffusion tensor (Parker et al., 2003), the variability between acquisitions (i.e. bootstrap methods) (Jones, 2008; Jeurissen et al., 2011), and the posterior probability of tensor parameters (Bayesian interference) (Behrens et al., 2003). Limitations of these methods include the increased scanning time (Chung et al., 2011) and long calculation times for Bayesian inference methods (Yang et al., 2016). Complementary, different model selection approaches exist that aim to select the model parameters best supported by the data (Behrens et al., 2007),

estimate the number of fiber compartments (Jeurissen et al., 2013), determine the type of diffusion (Alexander et al., 2002), and find a trade-off between goodness of fit and model complexity (Freidlin et al., 2007).

The aim of this work is to introduce a framework for model selection and probabilistic tractography with parsimonious model selection. Essentially, our approach takes uncertainties into account that are derived directly from the model fitting procedure. To achieve this we apply multi-tensor models, which model the signal as a combination of multiple fiber compartments and an isotropic compartment.

4.2 Methods

4.2.1 Models

The measured signal in a voxel S_j was modelled to originate from up to two fiber compartments and an isotropic compartment:

$$S_j = S_0 \left(\sum_{i=1,2} f_i \exp\left(-b_j \mathbf{g}_j^T \mathbf{D}_i \mathbf{g}_j\right) + f_{iso} \exp\left(-b_j D_{iso}\right) \right), \tag{4.1}$$

where S_0 denotes the signal without diffusion weighing, f_i and f_{iso} are the volume fractions of the different compartments, b_j stands for the strength of the diffusion gradient of the corresponding gradient direction $\boldsymbol{g}_j$, $\boldsymbol{D}_i$ is the 3 x 3 diffusion tensor of each fiber compartment, and lastly D_{iso} denotes the isotropic diffusion coefficient (Caan et al., 2010).

Parameters and constraints Practically, we fitted nine different diffusion models of increasing complexity to the data, see Table 4.1. Summary of the diffusion tensor models, their parameters and constraints. These models were based on the signal model of Equation 4.1. In the most conventional one, a single tensor model, we parametrized the diffusion tensor $\boldsymbol{D}_i$ with its eigenvalues λ_1, λ_2 and λ_3, and three angles θ, φ and ψ determining the tensor's orientation. Here, θ and φ represented the orientation of the principle eigenvector in spherical coordinates. The third angle ψ determined the rotation of the second and third eigenvectors around the first eigenvector. The described single tensor model can be expanded by adding an isotropic compartment.

Table 4.1. Summary of the diffusion tensor models, their parameters and constraints.

Model	Parameters	# Comp	Iso	Extra constraints
1	$\theta_1, \phi_1, \psi_1, \lambda_1, \lambda_2, \lambda_3, S_0$	1	No	
2	$\theta_1, \phi_1, \psi_1, \lambda_\parallel, \lambda_\perp, S_0$	1	No	$\lambda_2 = \lambda_3 = \lambda_\perp$
3	$\theta_1, \phi_1, \psi_1, \lambda_1, \lambda_2, \lambda_3, f, S_0$	2	Yes	
4	$\theta_1, \phi_1, \psi_1, \lambda_1, \lambda_2, \lambda_3, f, S_0$	2	Yes	$\lambda_2 + \lambda_3 + \lambda_3 = MDC$
5	$\theta_1, \phi_1, \psi_1, \lambda_\parallel, \lambda_\perp, f_{iso}, S_0$	2	Yes	$\lambda_2 = \lambda_3 = \lambda_\perp$
6	$\theta_1, \phi_1, \theta_2, \phi_2, \lambda_\parallel, \lambda_\perp, f_1, S_0$	2	No	$\lambda_{\perp_1} = \lambda_{\perp_2} = \lambda_\perp$
7	$\theta_1, \phi_1, \theta_2, \phi_2, \lambda_\parallel, \lambda_\perp, S_0$	2	No	$f_1 = f_2 = 0.5$
8	$\theta_1, \phi_1, \theta_2, \phi_2, \lambda_\parallel, \lambda_\perp, f_{iso}, f_1, S_0$	3	Yes	$\lambda_{\perp_1} = \lambda_{\perp_2} = \lambda_\perp$
9	$\theta_1, \phi_1, \theta_2, \phi_2, \lambda_\parallel, \lambda_{\perp_1}, \lambda_{\perp_2}, f_{iso}, f_1, S_0$	3	Yes	

Further constrained versions of the signal model of Equation 4.1 were used to characterize the signal in a crossing of two fibers. While doing so, we assumed that the axial diffusivities $\lambda_\parallel$ of the two anisotropic tensors are equal. Furthermore, the second and third eigenvector of each tensor were also taken to be the same and henceforth referred to as the radial diffusivity $\lambda_\perp$. We applied these constraints in the same way as in (Caan et al., 2010), to avoid degeneracy of the parameter estimation with our data.

Other constraints that were used in the models: the isotropic diffusion coefficient was set to that of free water $3 \cdot 10^{-3}$ mm^{2}s^{-1} and the sum of the volume fractions was set to one. The different diffusion models were fitted by maximum likelihood estimation assuming Rician distributed noise as in (Poot and Klein, 2015).

4.2.2 Model Selection

Clearly, unconstrained fitting the two tensor model in a region with just a single fiber population still results in overfitting. Therefore, we performed model selection with the aim to find the tensor model that best represents the underlying fiber population in each voxel.

ICOMP-TKLD We adopted the ICOMP-TKLD criterion for the model selection (Yang et al., 2015a). This criterion is an adapted version of the information

complexity (ICOMP) criterion (Bozdogan, 2000). The ICOMP-TKLD criterion performed model selection through balancing the goodness of the model fit and the model complexity. The goodness of fit was quantified by the log-likelihood of the model fit. In general, the goodness of fit is decreasing with increasing complexity.

The model complexity was captured in the total Kullback-Leibler divergence (TKLD) (Vemuri et al., 2011). This TKLD quantifies the interdependence between the model parameters, which is a direct measure of the model complexity. In other words, the more interdependent the parameters are, the higher the model complexity. Accordingly, a model in which the parameters are orthogonal and thus independent will have a complexity of zero (Yang et al., 2015b).

Formally, the ICOMP-TKLD criterion was defined as:

$$ICOMP_{TKLD}\left(\hat{\boldsymbol{\theta}}_i\right) = -2\log\left(L\left(\hat{\boldsymbol{\theta}}_i \mid \tilde{\mathbf{S}}\right)\right) + 2C_{tot}\left(\mathbf{I}^{-1}\left(\hat{\boldsymbol{\theta}}_i\right)\right). \tag{4.2}$$

Here, the first term quantified the goodness of fit where L is the likelihood of the fit of the parameter vector $\hat{\boldsymbol{\theta}}_i$ given the measured signal $\tilde{\mathbf{S}}$. The second term represents the model complexity, where C_{tot} denotes the TKLD which requires the inverse of the Fisher information matrix $\mathbf{I}^{-1}$ as an input.

4.2.3 Uncertainty in the fiber orientation

The previously described model selection essentially outputted the most appropriate model as estimates for the fiber orientation(s) in each voxel. These served as an input for our probabilistic tractography algorithm. The probabilistic tractography algorithm also needed a measure of the uncertainty in the estimated fiber orientations. In this work, we used the Cramér-Rao lower bound (CRLB) of each model parameter to provide an estimate of the variance in the estimated fiber orientations. This CRLB was obtained by inverting the Fisher information matrix. The diagonal of the resulting matrix contained lower bounds for the variance that could be obtained by an unbiased estimator on the given data (Sid et al., 2017). In our diffusion tensor models the angles θ and φ determine the fiber orientation. The uncertainty in these parameters was assumed to be normally distributed with a mean equal to the estimated parameter value, a variance equal to the CRLB of the parameter and a covariance obtained from the off-diagonal elements of the CRLB

matrix. This yielded a probability density function (PDF) of the fiber orientations at each voxel, that were sampled during tractography.

Tractography algorithm Our tractography algorithm is a standard line propagation algorithm with a fixed step size (Mori and van Zijl, 2002). The probabilistic aspect of the tractography was reflected in the placement of seed points and the sampling of the fiber orientation PDFs from the fiber compartment(s) at each step. The starting points for the streamlines were placed at a random position inside the seed voxels, as this allowed us to sample the variation in streamlines based on their starting position. The streamlines were propagated by comparing the direction of the last step in the streamline with a sample from the fiber orientation PDF of each compartment in the voxel. A step was taken in the direction of the sample that made the smallest angle with the previous step. Propagation of the fiber was stopped when the angle between successive steps was larger than 80 degrees, the streamline exited the brain mask or the streamline looped back on itself. In our tractography we generated 5000 streamlines per seed voxel to obtain sufficient sampling of the fiber orientation PDFs.

4.2.4 Benchmarking

The performance of our tractography algorithm was assessed by comparing it with the open source dMRI toolkit Camino (Cook et al., 2006), which also allows for probabilistic multi-fiber tractography.

We performed a quantitative and qualitative comparison between the two tractography frameworks. In the quantitative comparison we used the reconstructed version of the fibercup phantom (Neher et al., 2015) with multiple b-values (1500/2000 s/mm2). The fibercup phantom is shown in Figure 4.1. The ground truth of this phantom was used to evaluate the tractography algorithms using measures from the tractometer, which is an online evaluation tool for tractography algorithms (Côté et al., 2013). These measures assessed the performance of the algorithms by quantifying global measures, such as the percentage of the valid bundle covered by streamlines (average bundle coverage or ABC), the percentage of invalid bundles covered by streamlines (No bundle coverage) and, the angular error of the generated streamlines. ROI specific measures that were used were the number of streamlines that either correctly connect ROIs (Valid connections or

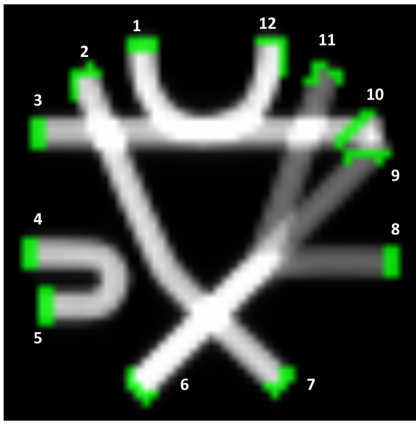

Figure 4.2. The fibercup phantom with numbered ROIs.

VC), do not reach another ROI (No connection or NC) and incorrectly connect ROIs (invalid connections or IC). Baseline (BL) tractography was performed, i.e. without additional noise, as well tractography at range of SNR values to investigate the sensitivity of the tractography algorithms to noise (Table 4.2. Signal-to-noise ratios for the different noise scenarios.).

The qualitative comparison was performed on data from 5 healthy controls with multiple b-values (1000/2000 s/mm^2). The scans were acquired on a 3T MRI scanner (Discovery MR750, GE Medical Systems). 40 gradient directions were used for the diffusion weighted acquisitions combined with five non-diffusion weighted acquisitions per b-value. The SNR values for the b = 0, 1000, and 2000 s/mm^2 acquisitions were estimated to be 41, 20 and 12 respectively. Seed regions were placed in the corticospinal tract (CST) and the corpus callosum (CC). We examined the lateral projections of the CC into the pre-central gyrus to assess the performance of the methods on in-vivo fiber crossings.

Table 4.2. Signal-to-noise ratios for the different noise scenarios.

	b=0	b=1500	b=2000
Noise scenario 1 (N1)	39	11	7
Noise scenario 2 (N2)	26	7	5

4.3 Results

Benchmarking The results for the global tractometer measures are shown in Table 4.3. The table shows that our method had a lower median angular error than Camino. The average bundle coverage of Camino was slightly higher but

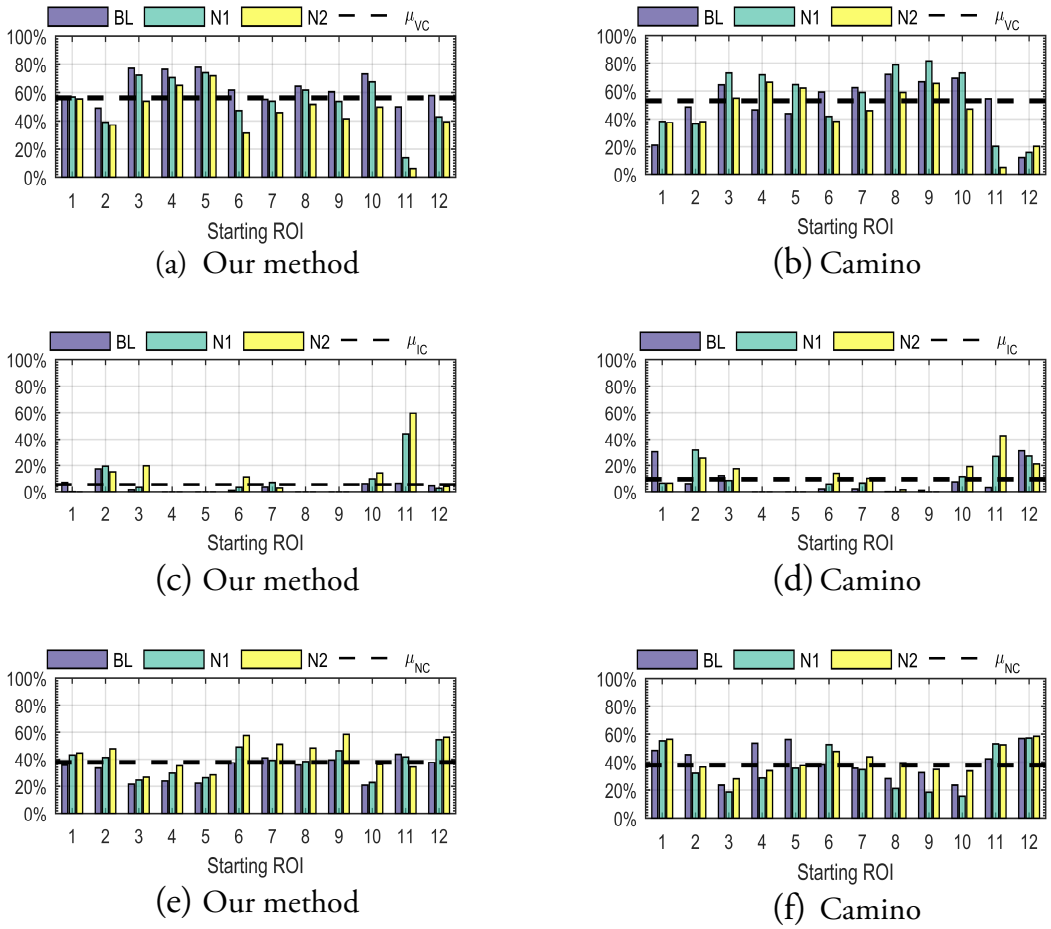

(a) Our method (b) Camino

(c) Our method (d) Camino

(e) Our method (f) Camino

Figure 4.3. The percentage of valid connections (a,b), invalid connections (c,d) and no connections (e,f) per seed region for the baseline (BL) and different noise levels (N1,N2,) of the fibercup phantom. The dashed lines represent the average percentage of connections for all ROIs.

simultaneously the no bundle coverage of Camino was markedly higher than our method for all noise levels.

Table 4.3. Results for the median angular error, average bundle coverage and no bundle coverage for the baseline (BL) and different noise levels (N1,N2) of the fibercup phantom.

	Median angular error			Average bundle coverage			No bundle coverage		
	BL	N1	N2	BL	N1	N2	BL	N1	N2
Our method	0.73^0	1.6^0	2.8^0	87.0%	84.4%	83.2%	10.0%	12.7%	15.0%
Camino	2.7^0	2.7^0	4.2^0	95.3%	88.7%	90.4%	47.7%	27.5%	32.0%

Figure 4.3 shows that on average the percentage of valid connections decreased for increasing noise levels, whilst the percentage of invalid and no connections increased. We used a Wilcoxon rank sum test to test whether the perceived difference in the connection types between the two methods was significant. The

results are shown in Table 4.4. This table demonstrates that the two methods differed most significantly in terms of valid and no connection percentage.

Human data An example of the crossing of the CC and CST streamlines is shown in Figure 4.4. There seemed to be more streamlines from the CC that crossed over the CST estimated by our algorithm than by the Camino algorithm. We have quantified this by determining the average number of streamlines passing through the fiber crossing. The results are shown in Table 4.5.

Table 4.4. P-values for the ROIs where the difference in performance of both methods is statistically significant.

	Our method better					Camino better			
ROI	1	5	8	11	12	7	8	9	11
Valid connections	$6.4 \cdot 10^{-9}$	$6.4 \cdot 10^{-9}$	x	x	$6.4 \cdot 10^{-9}$	x	0.0043	$6.4 \cdot 10^{-9}$	x
Invalid connections	0.0043	x	$6.4 \cdot 10^{-9}$	x	$6.4 \cdot 10^{-9}$	x	x	x	0.0043
No connections	$6.4 \cdot 10^{-9}$	$6.4 \cdot 10^{-9}$	x	$5.6 \cdot 10^{-5}$	$6.4 \cdot 10^{-9}$	0.0043	0.0043	$6.4 \cdot 10^{-9}$	x

Table 4.5. The average streamline count from the CC passing the crossing with the CST.

	Control 1	Control 2	Control 3	Control 4	Control 5
Our method	37	30	123	41	358
Camino	31	17	66	27	278

4.4 Discussion

Benchmarking The global tractometer measures showed that the median angular error for our method is consistently lower than that of Camino. This could be attributed to the different methods used for estimating the fiber uncertainty. Notably, the fiber orientation PDFs in Camino are based on the link between the relative magnitude and orientations of the DT's second and third eigenvectors and the uncertainty in fiber orientation (Parker et al., 2003). This shape of the tensor might be invariant at lower noises levels, therefore introducing a higher angular error. Our method derives the uncertainty from the CRLB, whose value decreases with lower noise levels (Sid et al., 2017). The higher uncertainty in fiber orientation in Camino also explains the higher average bundle coverage, as it allows

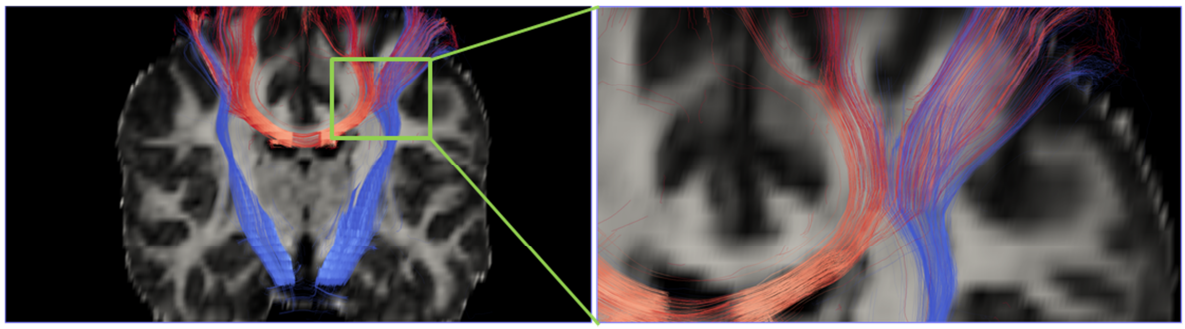

(a) Our method

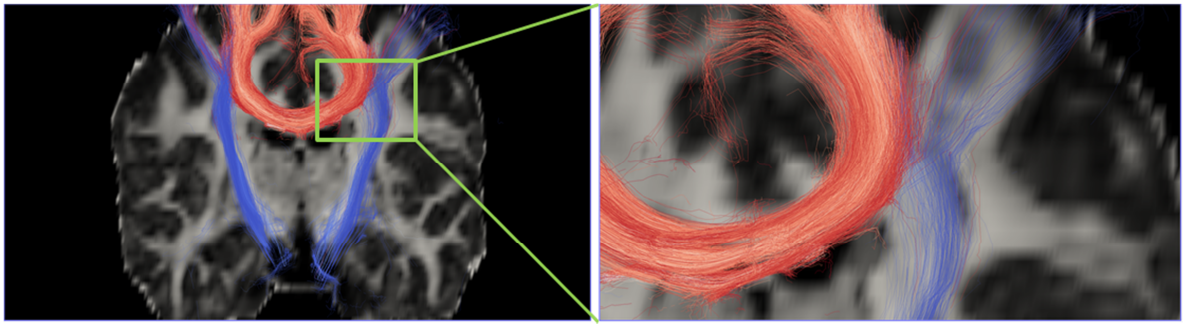

(b) Camino

Figure 4.4. Tractography outputs for the CC seed region (Red) and the CST seed region (Blue) in a coronal slice, overlaid with a fractional anisotropy map.

the tractography to explore more voxels. However, this also leads to a higher no bundle coverage which is undesirable.

From the ROI specific tractometer measures (Table 4.4 and Figure 4.3) we can see that the ROIs where our method performs better contain a highly curved bundle (ROI 4 and 5) and a bundle with kissing fibers (ROI 1 and 12). Camino performs better in ROIs with a long straight section such as ROI 8 and 9. Both methods seem to perform similarly in the ROIs with crossing fibers.

The observed decrease in valid connections with noise level, especially the one in ROI 11 (see Figure 4.3), is due to not discerning the fiber crossing by both our method and Camino's. In the case of Camino, which selects models based on fitted diffusion type (e.g. Non-Gaussian or Gaussian diffusion), the diffusion in the crossing is considered to be merely Gaussian (Alexander et al., 2002). The erroneous classification in our model selection stems from the effect of noise on the log likelihood the different model fits. This log-likelihood converges to similar

values for all models, effectively causing our model selection to pick the simplest (Gaussian) model.

Overall, our method performs either better or similarly to Camino software while having lower no bundle coverage.

Human data As our method was applied to human data more fibers were tracked across the fiber crossing than with Camino. In this region we observed that the magnitude of the second eigenvector was similar to that of the first eigenvector. In Camino this leads to an increased uncertainty, hence, fewer fibers passing the crossing. Performance of our method is not reduced as the uncertainty is based on the noise level and not tensor shape.

Limitations There are two limitations to the use of our method for probabilistic tractography. First of all, the data needs to have multiple b-values, which preferably consist of a low b-value of at least 1000 s/mm^2 and a high b-value of about 2000 s/mm^2. This is necessary to fit the more complex dual tensor models (Caan et al., 2010). Secondly, there is the influence of noise on the model selection. This limitation was observed in a crossing with lower diffusivity in the fiber cup phantom and resulted in selection of single tensor models. Still, the performance on the human data, which is comparable in SNR to most modern dMRI acquisitions, suggests that tracking across in-vivo crossings is very well possible.

Our results both on the fibercup phantom and especially on the human data suggest that sophisticated diffusion tensor reconstruction techniques combined with model selection procedures can lead to improved fiber tractography outcomes.

References

Alexander, D.C., Barker, G.J., and Arridge, S.R. (2002). Detection and modeling of non-Gaussian apparent diffusion coefficient profiles in human brain data. *Magnetic Resonance in Medicine* 48(2), 331-340. doi: 10.1002/mrm.10209.

Alexander, D.C., Hubbard, P.L., Hall, M.G., Moore, E.A., Ptito, M., Parker, G.J.M., et al. (2010). Orientationally invariant indices of axon diameter and density from diffusion MRI. *NeuroImage* 52(4), 1374-1389. doi: https://doi.org/10.1016/j.neuroimage.2010.05.043.

Basser, P.J., Mattiello, J., and LeBihan, D. (1994). MR diffusion tensor spectroscopy and imaging. *Biophysical Journal* 66(1), 259-267. doi: https://doi.org/10.1016/S0006-3495(94)80775-1.

Behrens, T.E., Berg, H.J., Jbabdi, S., Rushworth, M.F., and Woolrich, M.W. (2007). Probabilistic diffusion tractography with multiple fibre orientations: What can we gain? *Neuroimage* 34(1), 144-155. doi: 10.1016/j.neuroimage.2006.09.018.

Behrens, T.E., Woolrich, M.W., Jenkinson, M., Johansen-Berg, H., Nunes, R.G., Clare, S., et al. (2003). Characterization and propagation of uncertainty in diffusion-weighted MR imaging. *Magn Reson Med* 50(5), 1077-1088. doi: 10.1002/mrm.10609.

Bozdogan, H. (2000). Akaike's Information Criterion and Recent Developments in Information Complexity. *Journal of Mathematical Psychology* 44(1), 62-91. doi: https://doi.org/10.1006/jmps.1999.1277.

Caan, M.W.A., Khedoe, H.G., Poot, D.H.J., den Dekker, A.J., Olabarriaga, S.D., Grimbergen, K.A., et al. (2010). Estimation of Diffusion Properties in Crossing Fiber Bundles. *IEEE Transactions on Medical Imaging* 29(8), 1504-1515.

Chung, H.W., Chou, M.C., and Chen, C.Y. (2011). Principles and Limitations of Computational Algorithms in Clinical Diffusion Tensor MR Tractography. *American Journal of Neuroradiology* 32(1), 3.

Cook, P., Bai, Y., Nedjati-Gilani, S., Seunarine, K., Hall, M., Parker, G., et al. (2006). "Camino: open-source diffusion-mri reconstruction and processing", in: *14th scientific meeting of the international society for magnetic resonance in medicine.*).

Côté, M.-A., Girard, G., Boré, A., Garyfallidis, E., Houde, J.-C., and Descoteaux, M. (2013). Tractometer: Towards validation of tractography pipelines. *Medical Image Analysis* 17(7), 844-857. doi: https://doi.org/10.1016/j.media.2013.03.009.

Freidlin, R.Z., Ozarslan, E., Komlosh, M.E., Chang, L.C., Koay, C.G., Jones, D.K., et al. (2007). Parsimonious model selection for tissue segmentation and classification applications: a study using simulated and experimental DTI data. *IEEE Trans Med Imaging* 26(11), 1576-1584. doi: 10.1109/TMI.2007.907294.

Jansons, K.M., and Alexander, D.C. (2003). Persistent angular structure: new insights from diffusion magnetic resonance imaging data. *Inverse Problems* 19(5). doi: 10.1088/0266-5611/19/5/303.

Jeurissen, B., Leemans, A., Jones, D.K., Tournier, J.-D., and Sijbers, J. (2011). Probabilistic fiber tracking using the residual bootstrap with constrained spherical deconvolution. *Human Brain Mapping* 32(3), 461-479. doi: 10.1002/hbm.21032.

Jeurissen, B., Leemans, A., Tournier, J.-D., Jones, D.K., and Sijbers, J. (2013). Investigating the prevalence of complex fiber configurations in white matter tissue with diffusion magnetic resonance imaging. *Human Brain Mapping* 34(11), 2747-2766. doi: 10.1002/hbm.22099.

Jones, D.K. (2002). Determining and visualizing uncertainty in estimates of fiber orientation from diffusion tensor MRI. *Magnetic Resonance in Medicine* 49(1), 7-12. doi: 10.1002/mrm.10331.

Jones, D.K. (2008). Tractography gone wild: probabilistic fibre tracking using the wild bootstrap with diffusion tensor MRI. *IEEE Trans Med Imaging* 27(9), 1268-1274. doi: 10.1109/TMI.2008.922191.

Kreher, B.W., Schneider, J.F., Mader, I., Martin, E., Hennig, J., and Il'yasov, K.A. (2005). Multitensor approach for analysis and tracking of complex fiber configurations. *Magnetic Resonance in Medicine* 54(5), 1216-1225. doi: 10.1002/mrm.20670.

Mori, S., and van Zijl, P.C.M. (2002). Fiber tracking: principles and strategies – a technical review. *NMR in Biomedicine* 15(7 - 8), 468-480. doi: 10.1002/nbm.781.

Neher, P.F., Descoteaux, M., Houde, J.-C., Stieltjes, B., and Maier-Hein, K.H. (2015). Strengths and weaknesses of state of the art fiber tractography pipelines – A comprehensive in-vivo and phantom evaluation study using Tractometer. *Medical Image Analysis* 26(1), 287-305. doi: https://doi.org/10.1016/j.media.2015.10.011.

Parker, G.J.M., Haroon, H.A., and Wheeler-Kingshott, C.A.M. (2003). A framework for a streamline-based probabilistic index of connectivity (PICo) using a structural interpretation of MRI diffusion measurements. *Journal of Magnetic Resonance Imaging* 18(2), 242-254. doi: 10.1002/jmri.10350.

Poot, D.H., and Klein, S. (2015). Detecting statistically significant differences in quantitative MRI experiments, applied to diffusion tensor imaging. *IEEE Trans Med Imaging* 34(5), 1164-1176. doi: 10.1109/TMI.2014.2380830.

Sid, F.A., Abed-Meraim, K., Harba, R., and Oulebsir-Boumghar, F. (2017). Analytical performance bounds for multi-tensor diffusion-MRI. *Magnetic Resonance Imaging* 36, 146-158. doi: https://doi.org/10.1016/j.mri.2016.10.014.

Tuch, D.S. (2004). Q-ball imaging. *Magnetic Resonance in Medicine* 52(6), 1358-1372. doi: 10.1002/mrm.20279.

Tuch, D.S., Reese, T.G., Wiegell, M.R., Makris, N., Belliveau, J.W., and Wedeen, V.J. (2002). High angular resolution diffusion imaging reveals intravoxel white matter fiber heterogeneity. *Magnetic Resonance in Medicine* 48(4), 577-582. doi: 10.1002/mrm.10268.

Vemuri, B.C., Liu, M., Amari, S., and Nielsen, F. (2011). Total Bregman divergence and its applications to DTI analysis. *IEEE Trans Med Imaging* 30(2), 475-483. doi: 10.1109/TMI.2010.2086464.

Wedeen, V.J., Hagmann, P., Tseng, W.-Y.I., Reese, T.G., and Weisskoff, R.M. (2005). Mapping complex tissue architecture with diffusion spectrum magnetic resonance imaging. *Magnetic Resonance in Medicine* 54(6), 1377-1386. doi: 10.1002/mrm.20642.

Yang, J., Poot, D.H.J., Caan, M.W.A., Su, T., Majoie, C.B.L.M., van Vliet, L.J., et al. (2016). Reliable Dual Tensor Model Estimation in Single and Crossing Fibers Based on Jeffreys Prior. *PLOS ONE* 11(10), e0164336. doi: 10.1371/journal.pone.0164336.

Yang, J., Poot, D.H.J., Caan, M.W.A., Vos, F.M., and van Vliet, L.J. (Year). "Rank-2 model-order selection in diffusion tensor MRI: Information complexity based on the total kullback-leibler divergence", in: *IEEE 12th International Symposium on Biomedical Imaging (ISBI)*).

Yang, J., Poot, D.H.J., van Vliet, L.J., and Vos, F.M. (2015b). Estimation of diffusion properties in three-way fiber crossings without overfitting. *Physics in Medicine and Biology* 60(23), 9123.

5

Dynamic information flow based on EEG and diffusion MRI

We must become the change we want to see.

Mahatma Gandhi

5 Dynamic information flow based on EEG and diffusion MRI: proof-of-principle study

In hemiparetic stroke, functional recovery of paretic limb may occur with the reorganization of neural networks in the brain. Neuroimaging techniques, such as magnetic resonance imaging (MRI), have a high spatial resolution which can be used to reveal anatomical changes in the brain following a stroke. However, low temporal resolution of MRI provides less insight of dynamic changes of brain activity. In contrast, electro-neurophysiological techniques, such as electroencephalography (EEG), have an excellent temporal resolution to measure such transient events, however are hindered by its low spatial resolution. This proof-of-principle study assessed a novel multimodal brain imaging technique namely Variational Bayesian Multimodal Encephalography (VBMEG), which aims to improve the spatial resolution of EEG for tracking the information flow inside the brain and its changes following a stroke. The limitations of EEG are complemented by constraints derived from anatomical MRI and diffusion weighted imaging (DWI). EEG data were acquired from individuals suffering from a stroke as well as able-bodied participants while electrical stimuli were delivered sequentially at their index finger in the left and right hand, respectively. The locations of active sources related to this stimulus were precisely identified, resulting in high Variance Accounted For (VAF above 80%). An accurate estimation of dynamic information flow between sources was achieved in this study, showing a high VAF (above 90%) in the cross-validation test. The estimated dynamic information flow was compared between chronic hemiparetic stroke and able-bodied individuals. The results demonstrate the feasibility of VBMEG method in revealing the changes of information flow in the brain after stroke. This study verified the VBMEG method as an advanced computational approach to track the dynamic information flow in the brain following a stroke. This may lead to the development of a quantitative tool for monitoring functional changes of the cortical neural networks after a unilateral brain injury and therefore facilitate the research into, and the practice of stroke rehabilitation.

5.1 Introduction

Stroke is a sudden interruption of the blood supply to the brain due to a vessel occlusion or rupture ((WHO), 2015). After the incident, most survivors suffer from hemiparesis, making it more difficult to perform activities of daily living. Clinical tests, such as Fugl-Meyer motor scores, indicate the severity of neural impairment following a stroke, but do not provide insight to the changes within the brain that occur after the incident and during recovery (Gladstone et al., 2002). Brain plasticity or neuroplasticity refers to the ability of the brain to reorganize neuronal connections, triggered by goal-oriented and environment-induced experiences – thus learning and adapting (Arya et al., 2011). The problem of understanding how the brain reconfigures itself following a stroke may be approached in different ways. One of the main strategies is to investigate brain responses to external stimuli. This can be achieved with various non-invasive brain imaging techniques such as electroencephalography (EEG) and functional magnetic resonance imaging (fMRI) (Bandara et al., 2016; Weinstein et al., 2017).

Mapping from the measured scalp EEG signals to their cortical sources is called an inverse problem, which is inherently ill-posed due to a limited number of measurement electrodes in comparison to the large number of active sources in the cortex (Wendel et al., 2009). Thus, precise source localization is a key challenge for EEG. Despite its poor spatial resolution, the major advantage of EEG is its temporal resolution in the order of milliseconds, which allows capturing fast dynamics of neuronal activity in the brain. A recent review of stroke rehabilitation indicated that the assessment of electrical neuronal activity with EEG may provide a precise way of measuring dynamic neural processes and thereby providing biomarkers for time-dependent brain plasticity during spontaneous neurobiological recovery (Ward, 2017b). In contrast, the spatial resolution of fMRI is in the order of 2-3 mm, which is much higher than that of EEG. However, the temporal resolution of fMRI is relatively low because the hemodynamic response reaches its peak around 5-6 seconds after the neural activity. Moreover, the fMRI is an indirect measure of electrical neuronal activity in the brain (Heeger et al., 2000).

Additional to the functional brain imaging approaches, anatomical brain imaging techniques are also often used in the stroke research (Qiu et al., 2011; Song et al.,

2012; Song et al., 2015; Wirsich et al., 2017). For example, commonly used T_1-weighted structural MRI allows obtaining the high-resolution detailed brain structure. Diffusion-weighted MRI (dMRI) is another anatomical acquisition that is typically used to infer white matter connections between cortical regions (Owen et al., 2017). Anatomical brain imaging techniques reflect the anatomical changes in the brain following a stroke; however, they cannot provide direct insight into functional changes brain activity caused by a brain lesion (Boyd et al., 2017).

As discussed, each brain imaging technique has its pros and cons (Ward, 2015; Boyd et al., 2017). Nowadays, it has become clear that combining different imaging modalities may improve our understanding of the brain as a complex biological system and its functions (Arikan, 2011). The excellent temporal resolution of EEG provides unique advantage for monitoring dynamic changes of neuronal activity at the cortex following a stroke. Nevertheless, the underdetermined nature of the inverse problem of EEG calls for structural, physiological and functional information to be combined to better estimate the location of active sources at the cortex and the causal interactions between sources, i.e., effective connectivity, related to a specific form of stimulus. Various computational approaches such as dynamic causal modeling (DCM) and conditional Granger causality analysis have been proposed and used to estimate the effective connectivity (Bajaj et al., 2015; Schulz et al., 2016; Wang et al., 2016). However, most of the current methods either require prior assumptions on the model structure (e.g., DCM) or exclusively rely on the signal correlations without considering anatomical constraints in the model (e.g., Granger causality analysis). Among the state-of-the-art methods, the Variational Bayesian Multimodal Encephalography (VBMEG) method has shown potential both in locating the active cortical sources and in identifying neural pathways (both physically and causally) between them, without involving prior assumptions on the model structure. A physiologically constrained Bayesian estimation algorithm is used to locate active cortical sources. Combining them with white matter tracks estimated from dMRI, a linear connectome dynamics (LCD) model is built to infer causal interactions between active cortical sources (Friston, 2011). Such a method allows tracking the information flow through the neural fibers within the brain network. The VBMEG method was initially proposed to investigate the dynamic cortical

activity of healthy participants during a face recognition task (Fukushima et al., 2015). VBMEG has been tested in both simulations (Sato et al., 2004; Aihara et al., 2012) and healthy volunteer studies (Yoshioka et al., 2008; Yoshimura et al., 2012; Nakamura et al., 2015; Yoshimura et al., 2017); their main focus was on muscle activity reconstruction and visual stimuli analysis with or without structural and functional MRI constraints. Nevertheless, as a novel brain imaging method, the clinical value of the VBMEG method is yet to be demonstrated regarding its potential to investigate functional brain changes following a brain disease such as a stroke.

Therefore, the present work serves as a proof-of-principle study demonstrating the feasibility of the VBMEG method to estimate active cortical sources and their dynamic interactions in stroke participants during a sensory stimulation task. The high-density EEG, anatomic MRI, and diffusion MRI data were collected from both able-bodied and stroke participants. EEG was recorded when the participants were receiving electrical finger stimulation. The accuracy of EEG source localization and dynamic information flow estimation within the VBMEG method was evaluated by the Variance Accounted For (VAF). The VAF indicates how much cortical activity and brain dynamics can be explained by the VBMEG method. The estimated dynamic information flow was compared between two chronic hemiparetic stroke survivors and two able-bodied individuals to demonstrate the feasibility of the VBMEG method in revealing functional cortical network changes post hemiparetic stroke. This proof-of-principle study is a critical prerequisite for applying the VBMEG on a large database to identify a quantitative biomarker for assessing neurological impairment and exploring neurobiological recovery following a stroke.

5.2 Materials and methods

5.2.1 Subjects

Two chronic stroke survivors and two age-matched able-bodied individuals were included in this proof-of-principle study. The participants were recruited with informed consent and permission of the Medical Ethics Committee of the Vrije Universiteit Medical Center, Amsterdam. The trial protocol was registered on 23 October 2013 at the Netherlands Trial Register (identifier NTR4221). Inclusion

criteria for the subjects suffering from chronic stroke were 1) upper limb paresis, 2) ability to sit without support (National Institutes of Health Stroke Scale item 5a/b > 0), 3) age over 18, 4) single ischemic hemispheric stroke, 5) more than six months post stroke. Exclusion criteria were 1) previously existing pathological neurological conditions or orthopedic limitations of the upper limb that would affect the results, 2) botulin toxin injections or medication that may have influenced upper limb function in the past three months, 3) general MRI contraindications (claustrophobia, pacemaker or other metallic implants), and 4) absence of history of epilepsy or seizures. All participants are in the age range of 55-70 in this study. The information of lesion side in the brain and clinical assessment for stroke survivors is provided in the Table 5.1. Both stroke participants had lesions in the posterior limb of internal capsule, but in different hemispheres, as shown in Figure 5.1.

The finger stimulation experiment and EEG data acquisition were performed in a conversion van which was designed to execute measurements at geographical locations convenient for the participants. MR images were acquired on another day after the EEG recording was completed at VU University Medical Center at Amsterdam. The two stroke participants were chronic and the above measurements were done more than 6 years post stroke, meaning that their recovery had plateaued.

Table 5.1 Information of stroke subjects. FM: Fugl-Meyer Upper Extremity Assessment Score, EmNSA: the Erasmus MC modification of the Nottingham Sensory Assessment.

Subject	Lesion side	FM-UE	EmNSA	Year of stroke
Stroke 1	Right	58	8	2009
Stroke 2	Left	66	8	2009

5.2.2 Electrical finger stimulation and EEG acquisition

The experiment was performed within a NEN1010 approved measurement van. During the experiment, participants were sitting comfortably with their hands and forearms positioned on their lap with the fingers facing upward (supine position).

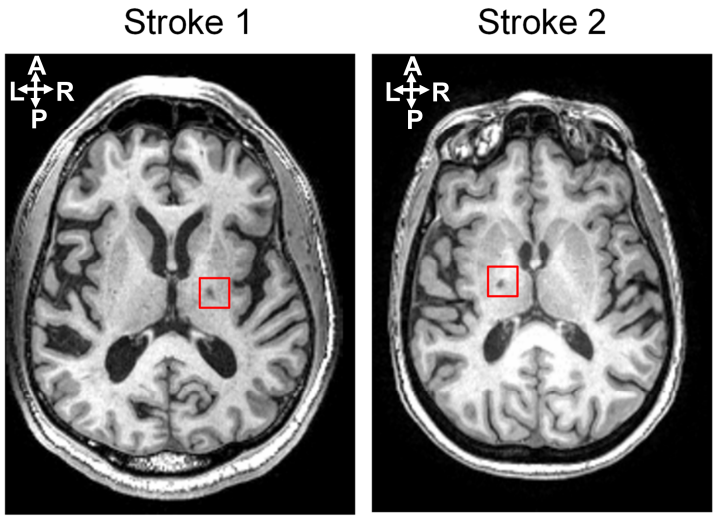

Figure 5.1 Lesion locations for two stroke subjects shown on an axial slice of the T1-weighted anatomic images.

Between forearm and lap, a pillow was placed to secure a stable position and comfort. Index fingers of both hands were stimulated with a randomized order in healthy controls and stroke patients with bipolar stimulation using a battery-powered electrical stimulator (Micromed, Brain quick, Treviso, Italy). The anodal electrode (size 1 cm) was placed on most distal phalange and cathode on the second distal phalange with an inter-electrode distance of approximately 1 cm (Kalogianni et al., 2018a).This placement is chosen to reduce the likelihood of anodal block (Cruccu et al., 2008). A monophasic anodic rectangular electrical pulse of 400 ⊠s width and a stimulation intensity of two times the sensation threshold was chosen. The sensation threshold was defined as the level at which the subject was able to sense half of the 10 given pulses (Jones and Tan, 2013). The chosen stimulation did not cause any pain or heat feeling to the participants.

The finger stimulation was repeated during 500 trials for each hand. During the stimulation, the EEG data were recorded with a 64-channel EEG system (TMSi, Netherlands) with ground electrode placed at the left mastoid, and online referenced to the common average. Sampling rate was 1024 Hz. Apart from antialiasing filters, no other filters were applied online. Positions of the EEG electrodes for every subject were measured with the ANT Neuro Xensor system (ANT Neuro, Enschede, Netherlands). The experimental setup (e.g. EEG cap placement and preparation, etc.) and finger stimulation had a typical duration of 50

min per participant. This short experimental time is plausible for stroke participants without any physical or mental fatigue.

5.2.3 EEG pre-processing

EEG data were preprocessed using EEGLAB (Delorme and Makeig, 2004), which is an open source toolbox running in the MATLAB environment. Continuous EEG data was band-pass filtered between 1 and 30 Hz to remove possible slow trends in the data (e.g., blood pressure, heartbeat, and breathing) and high-frequency fluctuations in event-related potentials, and then down-sampled to 512 Hz. EEG epochs were extracted using a window analysis time of 250 ms, with 50 ms before stimulus and 200 ms after stimulus. The artifact caused by electrical stimulus was removed by a blanking window from 10 ms before the stimulus to 10 ms after the stimulus. Then the gap was filled by a 3-order autoregressive model. Independent Component Analysis (ICA) algorithm (Delorme and Makeig, 2004) was used to remove the components of eye-blinks and movements (Li et al., 2006). After the artifact removal, the baseline correction was applied to each epoch using the signal from 50 ms to 10 ms before the stimulus. The epochs for the same experimental conditions were averaged in each subject, time-locked to the onset of the stimulus to extract the event-related potential (ERP).

5.2.4 MRI acquisition and preprocessing

Image acquisition was performed with a 3T MRI scanner (Discovery MR750, GE Medical Systems) at VU University Medical Center. Anatomical T1-weighted acquisition had the following settings: TE=3.22 ms, TR=8.21 ms, flip angle 12^{o}, imaging matrix = 256 x 256 x 172, resolution 1 mm^3. The diffusion-weighted MRI (dMRI) acquisition protocol involved 40 non-collinear gradient directions uniformly sampled over a sphere for each of two b-values: 1000 and 2000 s/mm2; TE=100 ms, TR=7200 ms, voxel size 2.5×2.5×2.5 mm^3, 52 consecutive slices, acquisition time 12,5 min. This allowed for whole brain coverage. Data for each b-value were acquired as separate scans together with five non-diffusion weighted images (i.e., per b-value).

The dMRI data were preprocessed using FSL v5.0 (http://fsl.fmrib.ox.ac.uk/fsl/) (Jenkinson et al., 2012). The acquired DWIs were corrected for motion and eddy current distortion by affine co-registration to the reference b_0-image (using FSL eddy_correct). Gradient directions were reoriented according to the rotation

component of the affine transformation. Diffusion tensor fitting and fractional anisotropy (FA) were calculated using FSL, and fiber tracking was performed with MRTrix software v0.2.10 (http://jdtournier.github.io/mrtrix-0.2/index.html).

5.2.5 VBMEG Method

The VBMEG method is constituted by a hierarchical Variational Bayesian (hVB) estimation of cortical sources as proposed by Sato et al. (2004) and a dynamic estimation of the information flow traveling from one source to another (Fukushima et al., 2015). In contrast to the original work from Sato et al. (2004), prior knowledge obtained from functional MRI was not included in hVB estimation. In this study, the source localization and dynamic information flow estimation were performed using VBMEG toolbox with default settings, using pre-processed EEG data, built leadfield matrix and fiber tracking results. The VBMEG toolbox and documentation are available online (http://vbmeg.atr.jp/docs/v2/static/vbmeg_users_manual.html, http://vbmeg.atr.jp/download2/). The general overview of the VBMEG method is provided in Figure 5.2.

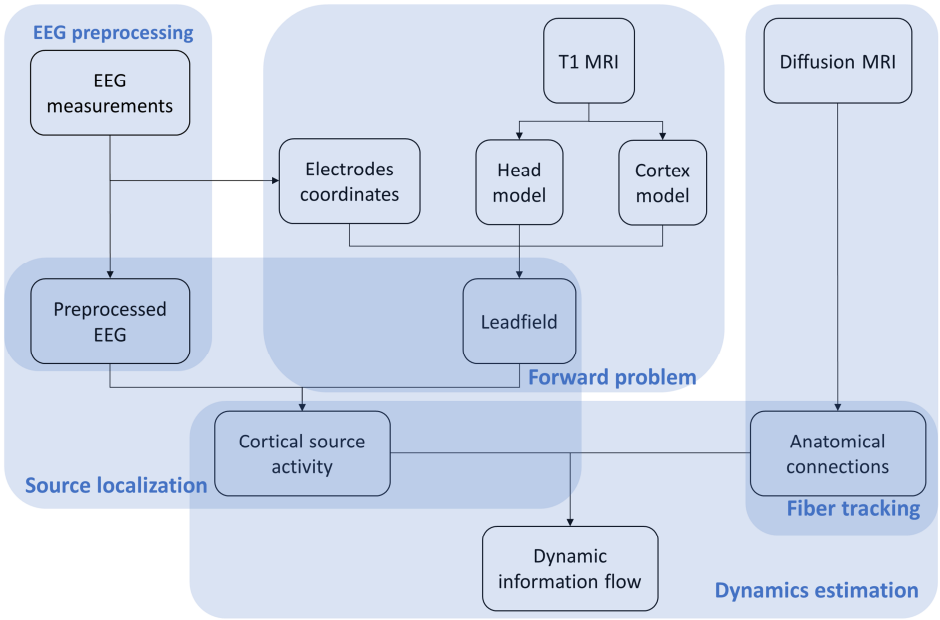

Figure 5.2 Workflow of the VBMEG method. EEG, anatomic and diffusion weighted MRIs are first preprocessed. Then EEG sources are estimated using hVB approach. By combining sources and anatomical connections extracted from diffusion MRI, the linear connectome dynamics model is built leading to the estimation of dynamic information flow traveling between sources. The results are visualized individually for each subject dataset.

5.2.6 Source localization

An individual head model for each subject was built using the T1 MR image for EEG source localization. Freesurfer (Reuter et al., 2012), an MRI processing software, was used to construct a polygon model of cortical surface, label the cortex surface anatomically, and extract the inner skull surface and outer scalp surface from the T1 image. Then a three-layer (CSF, skull, and scalp) head model was built using boundary element method (BEM) by VBMEG toolbox (Fukushima et al., 2015). 10000 vertices on the cortex surface were chosen as possible dipole sources, and the leadfield matrix was built based on the position of dipole sources and EEG electrodes, as well as the head model by VBMEG toolbox. The conductivity of CSF, skull, and scalp was set as 0.62, 0.03 and 0.62 s/m respectively as the default setting in the toolbox (ATR, 2017). As both stroke participants have small white matter lesions in the deep brain area (see Figure 5.1), their lesions would not affect EEG source localization.

The inverse calculation was performed using the hVB method to estimate the cortical source of EEG activity. The hVB is an altered version of the MNE method similar in structure to the Wiener filter, which intends to use the current variance to regularize the solution of the L_2 – reconstruction problem (Sato et al., 2004). Nevertheless, because the true current variance is unknown, the hVB method places a hierarchical prior on the current variance and estimates it iteratively using an Automatic Relevance Determination (ARD) model (Neal, 1996). The hVB method differentiates itself further from the MNE method in that it places a smoothness constraint in the currents, ensuring that neighboring active sources are correlated (Sato et al., 2004). The source activity was estimated with pre-processed EEG signals and estimated leadfield matrix using the hVB method, which is implemented in the VBMEG toolbox.

5.2.7 Dynamic information flow estimation

The dynamic information flow was estimated by a linear connectome dynamics (LCD) model (as a variant of multivariate autoregressive, MAR model) to determine whether causal interactions exist between active cortical sources (Fukushima et al., 2015). The time window for dynamic analysis is around 0-200 ms post stimulation for the length of 102 samples (sampling rate: 512 Hz). An anatomical constraint was applied to the LCD model based on the fiber tracking results from diffusion MRI, so only the anatomically connected sources have the

non-zero weights. For fiber tracking, the cortical surface was parcellated into 250 equally distributed target regions of interest (ROIs) based on the diffusion MRI data. The remaining cortex vertices were clustered into these ROIs based on their spatial proximity. The source activity of these ROIs was calculated as the mean of contained dipole moments. Thus, there are 250 variables in the LCD model. Fibers connecting these ROIs through white matter were tracked using MRtrix 0.2. The fiber tracking results provide information about the presence of fiber connections between ROIs as well as the length of the fibers. The time lags in the LCD model were estimated based on the length of fiber connection using the theoretical conduction velocity of axon equal to 6 m/s (Fukushima et al., 2015). Only the terms with specific time lags were included in the LCD model, therefore the order for inter-variable interaction is one. In this case, the estimated LCD model could be represented by a 2-D matrix for inter-source dynamics. The intra-source dynamics was set as a second-order interaction. The LCD weights were estimated based on fiber connections and their corresponding time lag using an L_2-regularized least-squares method with the default regularization parameter (0.01) (Golub and Reinsch, 1971). These LCD weights represented the estimated dynamic information flow between cortical sources.

5.2.8 Model evaluation

The accuracy of source localization and dynamic information flow estimation was evaluated by calculating the Variance Accounted For (VAF) (Vlaar et al., 2017; Kalogianni et al., 2018b). For source localization, the estimated sources were used to generate an estimated EEG signal $\hat{\boldsymbol{M}} = \boldsymbol{L}\hat{\boldsymbol{S}}$, which was compared with collected EEG signal $\boldsymbol{M}$. For the ith EEG channel, $\boldsymbol{VAF}_{\boldsymbol{M}_i}$ was defined as:

$$\boldsymbol{VAF}_{\boldsymbol{M}_i} = \left(1 - \frac{\mathrm{var}\left(\boldsymbol{M}_i - \hat{\boldsymbol{M}}_i\right)}{\mathrm{var}\left(\boldsymbol{M}_i\right)}\right) \cdot 100\% \,.$$

The time window was chosen as from 0-200ms. As EEG channels on the non-active areas are not representative, the VAF for source localization $\boldsymbol{VAF}_{\boldsymbol{M}}$ was defined as the median (instead of mean) of $\boldsymbol{VAF}_{\boldsymbol{M}_i}$ across all EEG channels. For dynamic information flow estimation, one step forward (2 ms) of source activity $\hat{\boldsymbol{S}}$ was estimated by the LCD model. The estimated source activity was compared with

the results $\boldsymbol{S}$ from source localization. For a specific time point *t*, the $\boldsymbol{VAF_S(t)}$ was defined as:

$$\boldsymbol{VAF_S(t)} = \left(1 - \frac{\mathrm{var}\left(\boldsymbol{S(t)} - \hat{\boldsymbol{S}}\boldsymbol{(t)}\right)}{\mathrm{var}\left(\boldsymbol{S(t)}\right)}\right) \cdot 100\% \ ,$$

where $\boldsymbol{S(t)}$ and $\hat{\boldsymbol{S}}\boldsymbol{(t)}$ are vectors containing all source activities resulting from source localization and estimated from LCD model respectively, and $\boldsymbol{t}$ is the time going from 0-200ms. The VAF for dynamic information flow $\boldsymbol{VAF_S}$ was defined as the mean of $\boldsymbol{VAF_S(t)}$ in the time window.

As the accuracy of the LCD model can be affected by the signal to noise ratio (SNR), the signal to noise ratio of the EEG recording was also calculated. The SNR is defined as follows:

$$\boldsymbol{SNR} = \frac{\boldsymbol{A_{RMS_{signal}}}}{\boldsymbol{A_{RMS_{noise}}}} ,$$

where A_{rms} is the root mean square amplitude. To intuitively show the signal level, signal percentage was calculated by

$$\boldsymbol{P_{signal}} = \frac{\boldsymbol{A_{RMS_{signal}}}}{\boldsymbol{A_{RMS_{signal}}} + \boldsymbol{A_{RMS_{noise}}}} \cdot 100\%$$

5.3 Results

The results of the method application are illustrated in four cases: for two able-bodied individuals and two chronic stroke subjects.

In Figure 5.3 the ERP of a control and a stroke subject are presented. In line with the literature (Oniz et al., 2016; Zhang et al., 2016), a positive-going peak around 50 ms (P50) and a negative-going peak around 100 ms (N100) were identified in the ERP for both control and stroke. Additionally, we provide the ERP topographies at the latency of P50 in Figure 5.4. Both controls have similar topographies with large ERP values at the sensorimotor area of the contralateral hemisphere. This result is consistent with previous studies (Desmedt and Cheron, 1980; Buchner et al., 1995; Druschky et al., 2003). Individual differences are

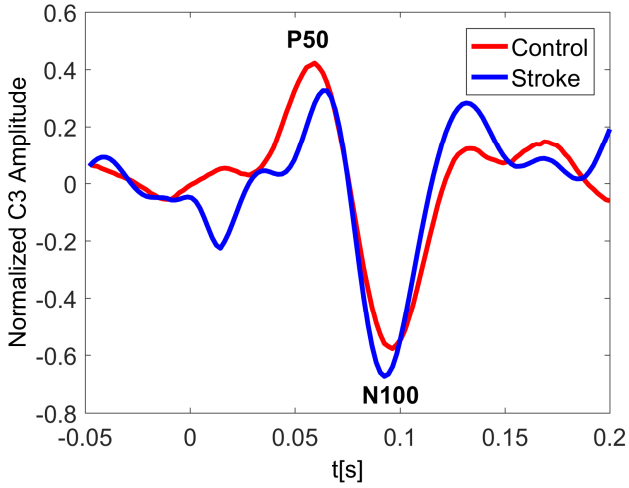

Figure 5.3 Normalized C3 Amplitude for control and stroke with stimulus on right hand. The ERP plotting at C3 shows great similarity for both control and stroke. The latency of P50 peak for stroke is slightly larger than that of control.

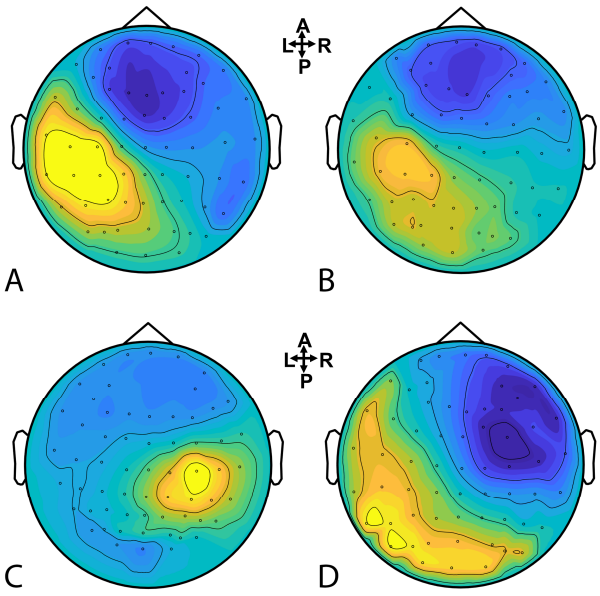

Figure 5.4 Brain topographies of the P50 peak for control and stroke subjects when a dominant hand (for controls) and an affected hand (for strokes) are stimulated. (A-B): controls, (C): stroke 1, (D): stroke 2.

shown in stroke patients, which may be related to subject-specific lesion load and recovery.

The VAF of EEG source localization is shown in Table 5.2, where we can see the VAF of source localization is higher than 80 % for all subjects.

Figure 5.5 shows the estimated dynamic information flow for each subject for finger stimulation at the dominant hand for control subjects, and at the affected hand for stroke participants. It also schematically depicts the anatomic connections

between the active sources. The information flow is shown only at the contralateral hemisphere in the control subjects, while at the both hemispheres in the stroke participants. In the time period between P50 and N100 peaks, information flow occurs in the ipsilateral (contralesional) hemisphere, i.e. the left hemisphere for stroke subject 1 and the right hemisphere for stroke subject 2.

Table 5.2 The VAF of EEG source localization (inverse model) for each subject.

Subject	VAF, Right Hand	VAF, Left Hand
Control 1	94.49 %	96.28 %
Control 2	93.64 %	92.27 %
Stroke 1	90.03 %	87.12 %
Stroke 2	85.63 %	83.79 %

The VAF of dynamic information flow estimation is provided in Table 5.3, where the VAF is higher than 90% for all subjects. Additionally, we also provide the SNR for all subjects in Table 5.4. Although the SNR for the stroke subjects is slightly lower than the controls, the signal percentage is above 88% for all subjects. To determine the baseline value of VAF when the input signal of the model is random, we replaced ERP signals with white noise. The same estimation and prediction process were repeated 100 timed with different noise realizations to determine the baseline. The estimated VAF obtained from this baseline test was around zero. Therefore, the high VAF from our dynamic information flow estimation, with respect to EEG source activity, can prove the significance of our results by comparing it to this baseline.

For each subject, estimated coefficients matrices of the LCD model are presented in Figure 5.6, where we can see that increased inter-hemisphere interactions are shown for the stroke participants. This increase is also characterized by the number and percentage of the non-zero LCD model coefficients within and between hemispheres as shown in Table 5.5.

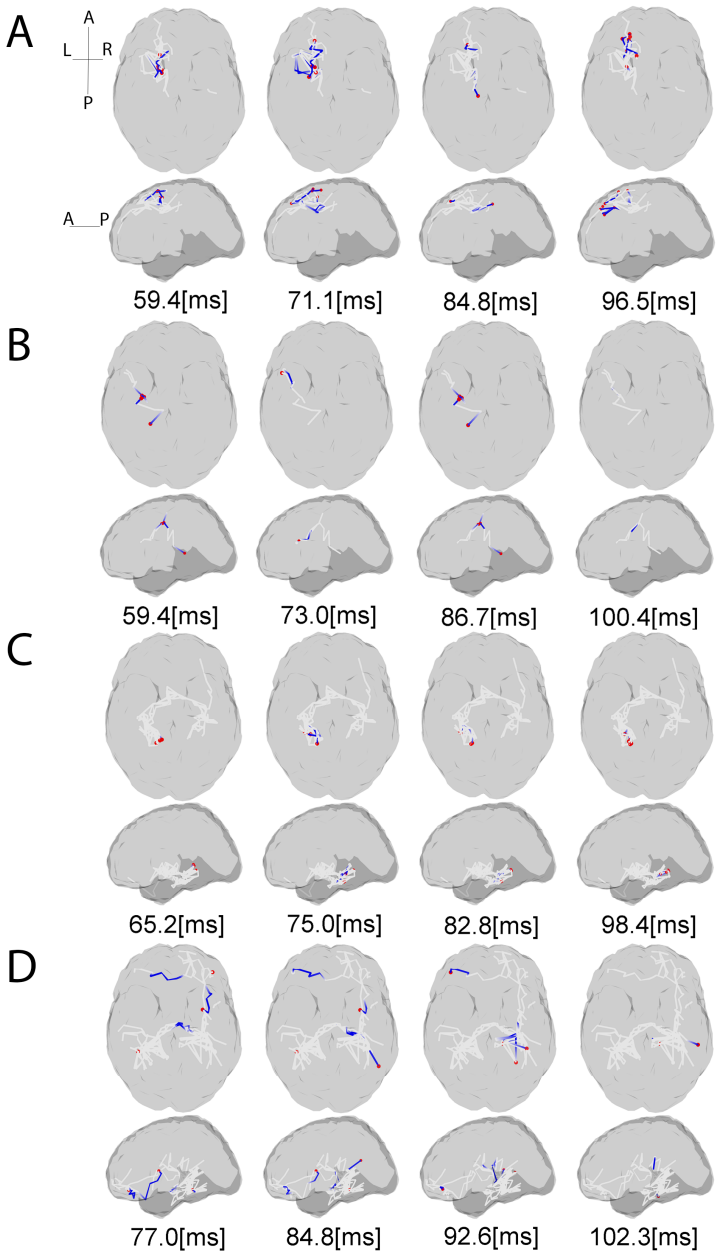

Figure 5.5 Source interactions estimated from LCD model. The plots show the information flow between P50 and N100 for each subject and anatomic connections between the active sources estimated via white matter tractography based on the individual dMRI acquisitions. The gray lines indicate the whole fiber network involved in the transmission of somatosensory information flow through the brain. The blue lines show the currently active fibers, and red dots are the currently active sources on the cortex at the specific time points. The 'active sources' here denotes the sources have electrical neural activities at the presented time point, while 'active fibers' indicate the fibers where the information flow is travelling through. For each subject projection of all axial slices (top) and of all sagittal slices (bottom) are shown. (A-B): controls, (C): stroke 1, (D): stroke 2. For the full dynamics visualizations please refer to the Supplementary material of (Filatova et al., 2018b)

Table 5.3. The average VAF of the dynamic model estimation with standard deviation for all subjects

Subject	VAF Right Hand		VAF Left Hand	
	mean	std	mean	std
Control 1	97.77 %	12.42 %	97.77 %	12.41 %
Control 2	97.58 %	10.00 %	97.78 %	12.42 %
Stroke 1	92.30 %	14.80 %	93.75 %	12.06 %
Stroke 2	91.69 %	11.58 %	92.86 %	10.47 %

Table 5.4. Signal to noise ratio of data acquisition in each subject when the corresponding hand was stimulated. In Stroke 1 case left hand was impaired. In Stroke 2 case right hand was impaired.

Subject	Right Hand		Left Hand	
	SNR (dB)	Signal percentage	SNR (dB)	Signal percentage
Control 1	14.22	96.35 %	13.76	95.97 %
Control 2	13.45	95.68 %	15.28	97.12 %
Stroke 1	7.64	85.30 %	8.62	87.92 %
Stroke 2	9.92	90.76 %	8.71	88.13 %

Table 5.5. Number and percentage of intra-hemispheric vs. inter-hemispheric interactions represented by non-zero LCD model coefficients.

	intra-hemispheric interactions		inter-hemispheric interactions	
	Number of interactions	Percentage	Number of interactions	Percentage
Control 1	4956	89.3%	594	10.7%
Control 2	4930	93.51%	342	6.49%
Stroke 1	11868	84.18%	2230	15.82%
Stroke 2	11274	76.51%	3462	23.49%

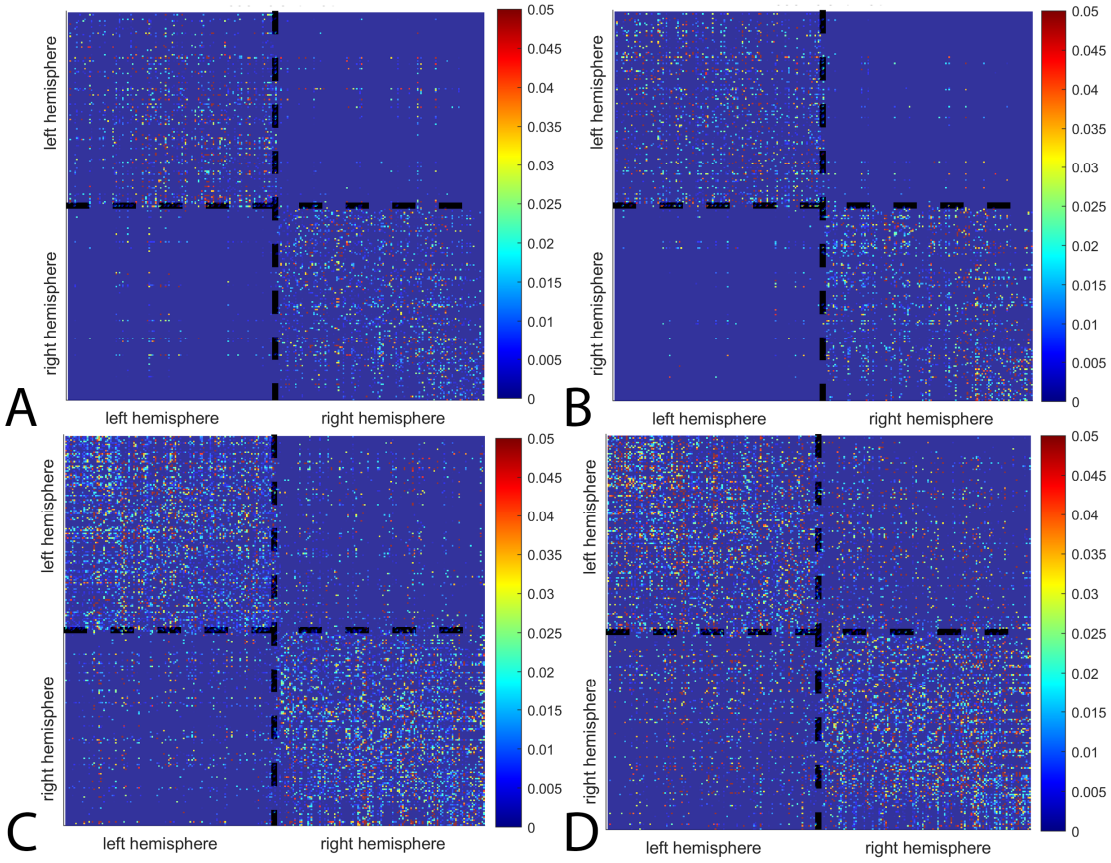

Figure 5.6 Matrices of the LCD model coefficients for controls (A and B) and stroke participants (C and D).

To illustrate how the anatomical priors used in VBMEG improves the estimation of dynamic information flow, we also used a conventional method based on correlation metrics (Greicius et al., 2003) to estimate brain functional connectivity without involving anatomical constraints. As shown in Figure 5.7, numerous spurious connectivity was estimated between the sources, for which there is no physical pathway connection. It is also quantified in Table 5.6 as the number of false positives and false discovery rate.

Table 5.6. Number of false positives (FP) and false discovery rate, i.e. FP/(FP + TP) × 100%, generated by correlation metrics without involving anatomical constraints. TP: True positive.

	Number of false positives	False discovery rate
Control 1	5342	49.05 %
Control 2	3598	40.56 %
Stroke 1	2084	12.88%
Stroke 2	2896	16.42%

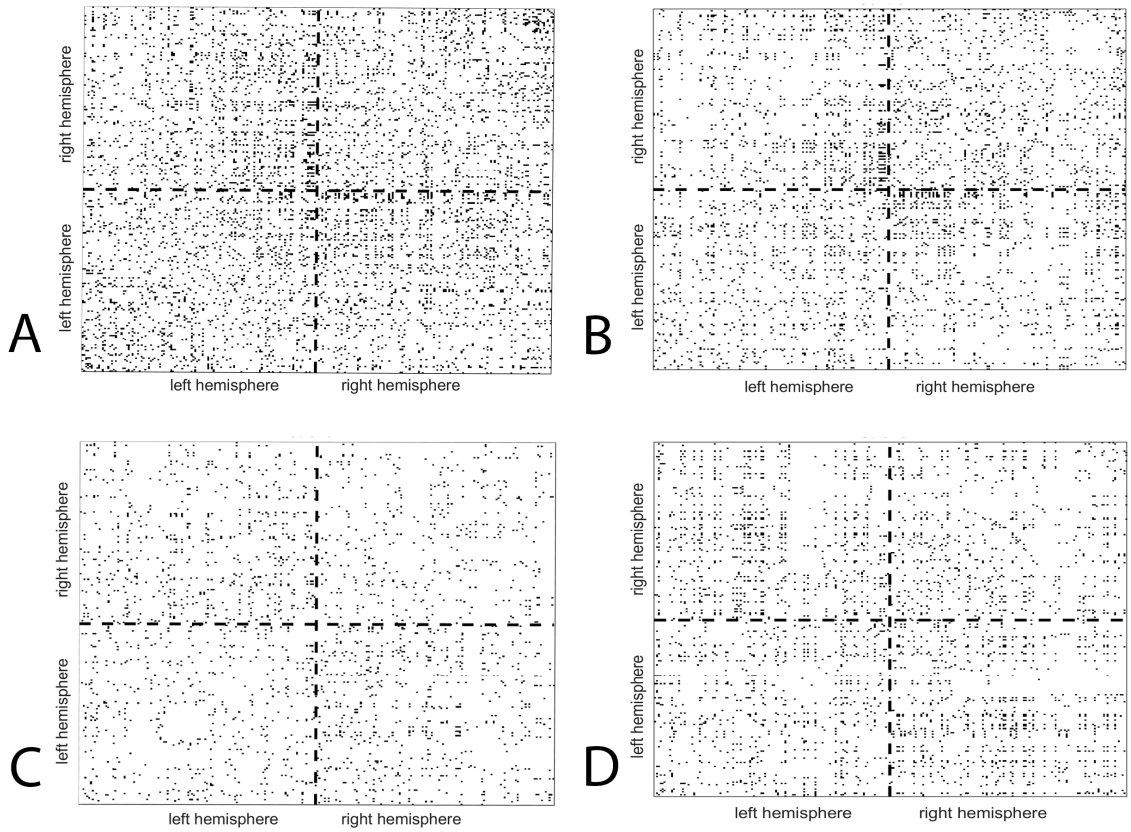

Figure 5.7 False positives (indicated by the black dots in the maps) of functional connectivity generated by correlation metrics without involving anatomical constraints: (A-B): controls, (C): stroke 1, (D): stroke 2.

5.4 Discussion

The present work aimed to test the two-stage estimation procedure of the VBMEG method, consisting of an estimation of EEG sources and a dynamic estimation of the information flow between them, in both able-bodied individuals and stroke participants. This study is a proof of principle for the clinical applicability of VBMEG method, not only demonstrating its new application regarding the somatosensory stimulations but also indicating its potential for the study of hemiparetic stroke, which has not been done in previous studies.

The estimation of the activation causality between sources provides insight on functional integration between cortical areas. The selection of strong fiber pairs between estimated sources constrains the solution space. Only the sources having the anatomical connection are included in the estimation of dynamic information flow, which controls the type I error in the MAR modeling. In the VBMEG

method, assumptions were made regarding the spatial sparseness and smoothness of the currents, as well as regarding the noise distribution being Gaussian and temporally uncorrelated. However, different noise models can potentially lead to different estimation results, and as long as a "true model" is not known, there will always be uncertainty regarding the possibility of fitting the noise in the solution. Therefore, a quantitative evaluation is needed to assess how much task-relevant cortical source activity and dynamics were captured in the VBMEG method. In this proof of principle study, we assessed the performance of EEG source localization and LCD modeling in the VBMEG method by the variance accounted for (VAF) (Vlaar et al., 2017; Kalogianni et al., 2018b). The VAF is a summary of how much of the variability of the data can be explained by a fitted model. High VAF for both source localization and LCD modeling was reported in all tested datasets, indicating the VBMEG method can precisely capture the task-relevant cortical source activity and the dynamics in the brain network.

In terms of stroke research, many efforts have been previously made to develop advanced methods based on fMRI to investigate reorganization of the sensorimotor system following a stroke (Grefkes and Fink, 2011). However, the poor temporal resolution of fMRI limits its ability to capture fast somatosensory information flow between cortical regions, which typically occurs in less than a hundred milliseconds. Therefore, a dynamic method based on EEG is highly desired for studying stroke. Most existing methods computing EEG source interactions are based on signal correlation/coherence (Srinivasan et al., 2007; Smit et al., 2008) or purely signal-driven MAR modelling (Baccalá and Sameshima, 2001; Kamiński et al., 2001; Blinowska et al., 2004; Bressler and Seth, 2011) without referring to anatomical pathways in the brain (Friston, 2011; Sakkalis, 2011). When compared to a conventional method based on correlation metrics (Greicius et al., 2003), it is clear that our method combining the anatomic constraints provided a way to avoid spurious connectivity estimations as shown in Figure 5.7.

For the able-bodied individuals, the estimated cortical sources and dynamic information flow are found only at the sensorimotor areas contralateral to the finger stimulation. This result is consistent with previous electro-neurophysiological studies (Jamali and Ross, 2013; Porcaro et al., 2013; Kalogianni et al., 2018a), showing that the somatosensory information is processed by brain regions predominantly contralateral to the stimulated hand. Conversely, in chronic

hemiparetic stroke participants, the activation of brain activity occurs in both hemispheres, with information flow transmitted from the contralateral (ipsilesional) to the ipsilateral (contralesional) hemisphere in the time period between P50 and N100 whereas in control participants cortical activity stays over the contralateral hemisphere. The result of dynamic information flow indicates that reconfiguration of the sensory network following a stroke. Two chronic stroke survivors have the Fugl-Meyer upper extremity scores of 58 and 66, respectively, and the Erasmus MC modifications to the Nottingham Sensory Assessment (EmNSA) of 8 (see Table 5.1). Thus, the reconfiguration of the sensory network occurs even in well-recovered individuals with hemiparetic stroke as shown in this study. Similar findings were previously reported in an animal model (Winship and Murphy, 2009). Regarding previous EEG/MRI studies in human participants the focus is on revealing cortical reconfiguration only of a motor network (Ward, 2015). There is growing evidence indicating an increased usage of ipsilateral (contralesional) cortical motor network associated with the loss of independent joint control (van Kordelaar et al., 2012; van Kordelaar et al., 2013; van Kordelaar et al., 2014) or the expression of the flexion synergy in the paretic upper limb following hemiparetic stroke (Yao et al., 2009; Wilkins et al., 2017; McPherson et al., 2018). However, less is known regarding changes of somatosensory cortical networks in this cohort (Gurari et al., 2017; Vlaar et al., 2017; Gurari et al., 2018). Our results could provide new evidence of reconfiguration of somatosensory cortical networks in individuals with hemiparetic stroke, which cannot be revealed by current clinical assessments. The reconfiguration of somatosensory cortical network may contribute to our understanding of time-dependent mechanisms during recovery of the sensory as well as motor function post hemiparetic stroke (Nelles et al., 1999; Ward, 2017a). A better understanding of the recovery of somatosensory function, based on connectivity, is imperative as it serves as an essential feedback channel for the control of movement (Todorov and Jordan, 2002; Scott, 2004). Thus, the VBMEG has potential to evolve into a new neuroimaging tool to monitor cortical network changes post hemiparetic stroke and thus improving our understanding of stroke recovery.

It is worth to discuss the pros and cons of the presented work, in order to point out possible future directions. This work presented a multi-modal brain imaging method which combines anatomical and physiological information from MRI and

EEG. Different from conventional EEG connectivity methods that are purely based on mathematical modelling and signal correlation, our method considers physical connections between cortical sources (obtained from dMRI), which reduces the chance of false positive in connectivity assessment, as indicated by Figure 5.7 and Table 5.6. This allows for a comprehensive way to track neural information flow traveling between cortical regions through neural tracts, which, to the best of our knowledge, has never been realized before in other methods. Moreover, compared to the fMRI-based connectivity methods, this EEG-dMRI combined method is able to provide a fine temporal resolution to capture fast somatosensory information flow in the brain, which occurs at the timescale in order of milliseconds.

Nevertheless, the current work has several limitations and could be improved in following directions:

- Ideally, the presented method could be configured in a way that simultaneously estimates EEG sources and dynamic information flow, known as "one-step" strategy (Fukushima et al., 2015). However, the implementation of one-step strategy has yet to be improved and validated[3]. Therefore, in this study, we employed the "two-step" strategy where the EEG source localization and dynamic information were performed sequentially.
- In the future, we will also consider improving our method by estimating tissue conductivity in a subject-specific way. This can be done using the electrical impedance tomography as introduced by (Dabek et al., 2016) . That will allow a more precise head modelling for EEG source localization.
- Additionally, the white matter conduction velocity could be better estimated in the future by considering the change of fiber myelination after stroke.
- In the current study, we applied our method to stroke patients with small white matter lesions. Thus, the head modeling and EEG source localization would not be affected by the lesion. In the future, the finite element model can be built for precise head modeling, in particular for the patients who also have gray matter lesions. This will also require additional methodological improvements to allow for cortical parcellation. To the best of our knowledge, the currently available approaches are not equipped to solve this problem.

[3] http://vbmeg.atr.jp/docs/v2/static/vbmeg_users_manual.html#toc9

- As a proof of principle study, we did not aim to make general conclusions regarding reorganization of the information flow between neural networks in the brain after stroke. Current results can be considered as a multiple-case study used for the introduction of our methodology as well as provides a preliminary assessment of the ability of our approach. Therefore, no conclusions on a group level can be drawn yet neither for the able-bodied individuals, nor for the stroke survivors. However, we do consider this as an objective for the future application of our method, in order to develop a sensitive biomarker for assessing brain function and reorganization after a hemiparetic stroke. Increase in the inter-hemispheric cross talk after stroke, as indicated by Figure 5.6 and Table 5.5, might be considered a candidate for such a biomarker.
- Regarding our results on EEG source localization and information flow, the stimulation to either the left or right hand leads to similar responses in the contralateral hemisphere in able-bodied individuals. Therefore, we did not further investigate the effect of handedness in this study. Furthermore, there are a few previous neuroimaging studies investigated the effects of handedness on the human brain. For example, differences in volumes of grey and white matter areas were detected by Herve et al. (2006). A voxel-based statistical analysis found higher FA in the left arcuate fasciculus in consistent right-handers (Buchel et al., 2004), but this was not confirmed in a study from Park and colleagues (Park et al., 2004). Right hand preference might be expected to result from asymmetries in the motor cortex. However, it is more strongly correlated with asymmetries in language-processing structures (Toga and Thompson, 2003). A more recent study by Powell et al. (2012) suggests a greater effect of gender than handedness, based on a DTI analysis. All in all, results regarding handedness effects on the brain have not been entirely consistent across different studies. Based on new evidence from (Filatova et al., 2018), it is very likely that the influence of stroke is significantly higher than the effect of handedness. In the future, we would like to further justify this assumption on a larger sample size using our method.

5.5 Conclusion

This study provides a proof-of-principle assessment on the VBMEG method. Our experimental results indicate that VBMEG method can capture the task-relevant cortical source activity and estimate the dynamic information flow in neural networks at the brain. Application of the VBMEG method to the data recorded

from stroke participants demonstrates the potential of monitoring dynamic brain activity and revealing the reconfiguration of somatosensory cortical networks following a hemiparetic stroke. In the future, we plan to apply this method to a larger sample size to identify quantitative biomarkers for the assessment of sensory impairment after a unilateral brain injury. Furthermore, the inclusion of this novel imaging method in future clinical trials starting at the acute phase following a hemiparetic stroke is likely to advance our understanding of the neurobiological recovery. In conclusion, the use of the VBMEG method is expected to provide novel quantitative means to assess and subsequently develop more effective neurorehabilitation approaches.

5.6 Acknowledgements

Authors would like to thank people in the 4D-EEG consortium for data collection and useful discussions.

References(WHO), W.H.O. (2015). *Stroke, Cerebrovascular accident* [Online]. Available: http://www.who.int/topics/cerebrovascular_accident/en/ [Accessed 1 May 2018].

Aihara, T., Takeda, Y., Takeda, K., Yasuda, W., Sato, T., Otaka, Y., et al. (2012). Cortical current source estimation from electroencephalography in combination with near-infrared spectroscopy as a hierarchical prior. *NeuroImage* 59(4), 4006-4021. doi: https://doi.org/10.1016/j.neuroimage.2011.09.087.

Arikan, K. (2011). Multimodal Brain Imaging. *Clinical EEG and neuroscience* 42(2), x.

Arya, K.N., Pandian, S., Verma, R., and Garg, R.K. (2011). Movement therapy induced neural reorganization and motor recovery in stroke: A review. *Journal of Bodywork and Movement Therapies* 15(4), 528-537. doi: https://doi.org/10.1016/j.jbmt.2011.01.023.

ATR (2017). *VBMEG user's manual* [Online]. ATR Neural Information Analysis Labs, Kyoto, Japan. Available: http://vbmeg.atr.jp/docs/v2/static/vbmeg_users_manual.html#head_model [Accessed 19 July 2018].

Baccalá, L.A., and Sameshima, K. (2001). Partial directed coherence: a new concept in neural structure determination. *Biological Cybernetics* 84(6), 463-474. doi: 10.1007/PL00007990.

Bajaj, S., Butler, A.J., Drake, D., and Dhamala, M. (2015). Brain effective connectivity during motor-imagery and execution following stroke and rehabilitation. *Neuroimage Clin* 8, 572-582. doi: 10.1016/j.nicl.2015.06.006.

Bandara, D.S.V., Arata, J., and Kigichi, K. (Year). "Task based motion intention prediction with EEG signals", in: *2016 IEEE International Symposium on Robotics and Intelligent Sensors (IRIS)*), 57-60.

Blinowska, K.J., Kus, R., and Kaminski, M. (2004). Granger causality and information flow in multivariate processes. *Phys Rev E Stat Nonlin Soft Matter Phys* 70(5 Pt 1), 050902. doi: 10.1103/PhysRevE.70.050902.

Boyd, L.A., Hayward, K.S., Ward, N.S., Stinear, C.M., Rosso, C., Fisher, R.J., et al. (2017). Biomarkers of stroke recovery: Consensus-based core recommendations from the Stroke Recovery and Rehabilitation Roundtable. *Neurorehabilitation and neural repair* 31(10-11), 864-876.

Bressler, S.L., and Seth, A.K. (2011). Wiener-Granger causality: a well established methodology. *Neuroimage* 58(2), 323-329. doi: 10.1016/j.neuroimage.2010.02.059.

Buchel, C., Raedler, T., Sommer, M., Sach, M., Weiller, C., and Koch, M.A. (2004). White matter asymmetry in the human brain: a diffusion tensor MRI study. *Cereb Cortex* 14(9), 945-951. doi: 10.1093/cercor/bhh055.

Buchner, H., Adams, L., Müller, A., Ludwig, I., Knepper, A., Thron, A., et al. (1995). Somatotopy of human hand somatosensory cortex revealed by dipole source analysis of early somatosensory evoked potentials and 3D-NMR tomography. *Electroencephalography and Clinical Neurophysiology/Evoked Potentials Section* 96(2), 121-134. doi: https://doi.org/10.1016/0168-5597(94)00228-7.

Cruccu, G., Aminoff, M.J., Curio, G., Guerit, J.M., Kakigi, R., Mauguiere, F., et al. (2008). Recommendations for the clinical use of somatosensory-evoked potentials. *Clinical Neurophysiology* 119(8), 1705-1719. doi: https://doi.org/10.1016/j.clinph.2008.03.016.

Dabek, J., Kalogianni, K., Rotgans, E., van der Helm, F.C.T., Kwakkel, G., van Wegen, E.E.H., et al. (2016). Determination of head conductivity frequency response in vivo with optimized EIT-EEG. *NeuroImage* 127, 484-495. doi: https://doi.org/10.1016/j.neuroimage.2015.11.023.

Delorme, A., and Makeig, S. (2004). EEGLAB: an open source toolbox for analysis of single-trial EEG dynamics including independent component analysis. *Journal of Neuroscience Methods* 134(1), 9-21. doi: https://doi.org/10.1016/j.jneumeth.2003.10.009.

Desmedt, J.E., and Cheron, G. (1980). Somatosensory evoked potentials to finger stimulation in healthy octogenarians and in young adults: Wave forms, scalp topography and transit times of pariental and frontal components. *Electroencephalography and Clinical Neurophysiology* 50(5), 404-425. doi: https://doi.org/10.1016/0013-4694(80)90007-3.

Druschky, K., Kaltenhäuser, M., Hummel, C., Druschky, A., Huk, W., Neundörfer, B., et al. (2003). Somatosensory evoked magnetic fields following passive movement compared with tactile stimulation of the index finger. *Experimental Brain Research* 148(2), 186-195. doi: 10.1007/s00221-002-1293-4.

Filatova, O.G., van Vliet, L.J., Schouten, A.C., Kwakkel, G., van der Helm, F.C.T., and Vos, F.M. (2018). Comparison of Multi-Tensor Diffusion Models' Performance for White Matter Integrity Estimation in Chronic Stroke. *Frontiers in Neuroscience* 12(247). doi: 10.3389/fnins.2018.00247.

Friston, K.J. (2011). Functional and effective connectivity: a review. *Brain connectivity* 1(1), 13-36.

Fukushima, M., Yamashita, O., Knösche, T.R., and Sato, M.-a. (2015). MEG source reconstruction based on identification of directed source interactions

on whole-brain anatomical networks. *NeuroImage* 105, 408-427. doi: https://doi.org/10.1016/j.neuroimage.2014.09.066.

Gladstone, D.J., Danells, C.J., and Black, S.E. (2002). The Fugl-Meyer assessment of motor recovery after stroke: a critical review of its measurement properties. *Neurorehabilitation and neural repair* 16(3), 232-240.

Golub, G.H., and Reinsch, C. (1971). "Singular Value Decomposition and Least Squares Solutions," in *Handbook for Automatic Computation: Volume II: Linear Algebra,* eds. J.H. Wilkinson, C. Reinsch, F.L. Bauer, A.S. Householder, F.W.J. Olver, H. Rutishauser, K. Samelson & E. Stiefel. (Berlin, Heidelberg: Springer Berlin Heidelberg), 134-151.

Grefkes, C., and Fink, G.R. (2011). Reorganization of cerebral networks after stroke: new insights from neuroimaging with connectivity approaches. *Brain* 134(Pt 5), 1264-1276. doi: 10.1093/brain/awr033.

Greicius, M.D., Krasnow, B., Reiss, A.L., and Menon, V. (2003). Functional connectivity in the resting brain: A network analysis of the default mode hypothesis. *Proceedings of the National Academy of Sciences of the United States of America* 100(1), 253-258. doi: 10.1073/pnas.0135058100.

Gurari, N., Drogos, J.M., and Dewald, J.P. (2017). Individuals with chronic hemiparetic stroke can correctly match forearm positions within a single arm. *Clinical Neurophysiology* 128(1), 18-30.

Gurari, N., Drogos, J.M., Lopez, S., and Dewald, J.P. (2018). Impact of motor task execution on an individual's ability to mirror forearm positions. *Experimental brain research*, 1-13.

Heeger, D.J., Huk, A.C., Geisler, W.S., and Albrecht, D.G. (2000). Spikes versus BOLD: what does neuroimaging tell us about neuronal activity? *Nature neuroscience* 3(7), 631.

Herve, P.Y., Crivello, F., Perchey, G., Mazoyer, B., and Tzourio-Mazoyer, N. (2006). Handedness and cerebral anatomical asymmetries in young adult males. *Neuroimage* 29(4), 1066-1079. doi: 10.1016/j.neuroimage.2005.08.031.

Jamali, S., and Ross, B. (2013). Somatotopic finger mapping using MEG: Toward an optimal stimulation paradigm. *Clinical Neurophysiology* 124(8), 1659-1670.

Jenkinson, M., Beckmann, C.F., Behrens, T.E., Woolrich, M.W., and Smith, S.M. (2012). Fsl. *Neuroimage* 62(2), 782-790. doi: 10.1016/j.neuroimage.2011.09.015.

Jones, L.A., and Tan, H.Z. (2013). Application of Psychophysical Techniques to Haptic Research. *IEEE Transactions on Haptics* 6(3), 268-284. doi: 10.1109/TOH.2012.74.

Kalogianni, K., Daffertshofer, A., van der Helm, F.C., Schouten, A.C., and de Munck, J.C. (2018a). Disentangling Somatosensory Evoked Potentials of the Fingers: Limitations and Clinical Potential. *Brain Topography* 31(3), 498–512

Kalogianni, K., de Munck, J.C., Nolte, G., Vardy, A.N., van der Helm, F.C., and Daffertshofer, A. (2018b). Spatial resolution for EEG source reconstruction—A simulation study on SEPs. *Journal of neuroscience methods* 301, 9-17.

Kamiński, M., Ding, M., Truccolo, W.A., and Bressler, S.L. (2001). Evaluating causal relations in neural systems: Granger causality, directed transfer function and statistical assessment of significance. *Biological Cybernetics* 85(2), 145-157. doi: 10.1007/s004220000235.

Li, Y., Ma, Z., Lu, W., and Li, Y. (2006). Automatic removal of the eye blink artifact from EEG using an ICA-based template matching approach. *Physiological measurement* 27(4), 425-436. doi: https://doi.org/10.1088/0967-3334/27/4/008.

McPherson, J.G., Chen, A., Ellis, M.D., Yao, J., Heckman, C., and Dewald, J.P. (2018). Progressive recruitment of contralesional cortico - reticulospinal pathways drives motor impairment post stroke. *The Journal of physiology* 596(7), 1211-1225.

Nakamura, M., Yanagisawa, T., Okamura, Y., Fukuma, R., Hirata, M., Araki, T., et al. (2015). Categorical discrimination of human body parts by magnetoencephalography. *Frontiers in Human Neuroscience* 9(609). doi: 10.3389/fnhum.2015.00609.

Neal, R.M. (1996). *Bayesian Learning for Neural Networks.* Springer, New York, NY.

Nelles, G., Spiekermann, G., Jueptner, M., Leonhardt, G., Müller, S., Gerhard, H., et al. (1999). Reorganization of sensory and motor systems in hemiplegic stroke patients: a positron emission tomography study. *Stroke* 30(8), 1510-1516.

Oniz, A., Inanc, G., Guducu, C., and Ozgoren, M. (2016). Brain responsiveness to non-painful tactile stimuli prior and during sleep. *Sleep and Biological Rhythms* 14(1), 87-96.

Owen, M., Ingo, C., and Dewald, J.P.A. (2017). Upper Extremity Motor Impairments and Microstructural Changes in Bulbospinal Pathways in Chronic Hemiparetic Stroke. *Frontiers in Neurology* 8, 257.

Park, H.J., Westin, C.F., Kubicki, M., Maier, S.E., Niznikiewicz, M., Baer, A., et al. (2004). White matter hemisphere asymmetries in healthy subjects and in

schizophrenia: a diffusion tensor MRI study. *Neuroimage* 23(1), 213-223. doi: 10.1016/j.neuroimage.2004.04.036.

Porcaro, C., Coppola, G., Pierelli, F., Seri, S., Di Lorenzo, G., Tomasevic, L., et al. (2013). Multiple frequency functional connectivity in the hand somatosensory network: an EEG study. *Clinical Neurophysiology* 124(6), 1216-1224.

Powell, J.L., Parkes, L., Kemp, G.J., Sluming, V., Barrick, T.R., and Garcia-Finana, M. (2012). The effect of sex and handedness on white matter anisotropy: a diffusion tensor magnetic resonance imaging study. *Neuroscience* 207, 227-242. doi: 10.1016/j.neuroscience.2012.01.016.

Qiu, M., Darling, W.G., Morecraft, R.J., Ni, C.C., Rajendra, J., and Butler, A.J. (2011). White matter integrity is a stronger predictor of motor function than BOLD response in patients with stroke. *Neurorehabililation and Neural Repair* 25(3), 275-284. doi: 10.1177/1545968310389183.

Reuter, M., Schmansky, N.J., Rosas, H.D., and Fischl, B. (2012). Within-subject template estimation for unbiased longitudinal image analysis. *Neuroimage* 61(4), 1402-1418. doi: 10.1016/j.neuroimage.2012.02.084.

Sakkalis, V. (2011). Review of advanced techniques for the estimation of brain connectivity measured with EEG/MEG. *Comput Biol Med* 41(12), 1110-1117. doi: 10.1016/j.compbiomed.2011.06.020.

Sato, M.-a., Yoshioka, T., Kajihara, S., Toyama, K., Goda, N., Doya, K., et al. (2004). Hierarchical Bayesian estimation for MEG inverse problem. *NeuroImage* 23(3), 806-826. doi: https://doi.org/10.1016/j.neuroimage.2004.06.037.

Schulz, R., Buchholz, A., Frey, B.M., Bönstrup, M., Cheng, B., Thomalla, G., et al. (2016). Enhanced Effective Connectivity Between Primary Motor Cortex and Intraparietal Sulcus in Well-Recovered Stroke Patients. *Stroke* 47(2), 482.

Scott, S.H. (2004). Optimal feedback control and the neural basis of volitional motor control. *Nature Reviews Neuroscience* 5(7), 532.

Smit, D.J., Stam, C.J., Posthuma, D., Boomsma, D.I., and de Geus, E.J. (2008). Heritability of "small-world" networks in the brain: a graph theoretical analysis of resting-state EEG functional connectivity. *Hum Brain Mapp* 29(12), 1368-1378. doi: 10.1002/hbm.20468.

Song, F., Zhang, F., Yin, D.-Z., Hu, Y.-S., Fan, M.-X., Ni, H.-H., et al. (2012). Diffusion Tensor Imaging for Predicting Hand Motor Outcome in Chronic Stroke Patients. *Journal of International Medical Research*, 126-133.

Song, J., Nair, V.A., Young, B.M., Walton, L.M., Nigogosyan, Z., Remsik, A., et al. (2015). DTI measures track and predict motor function outcomes in

stroke rehabilitation utilizing BCI technology. *Frontiers in Human Neuroscience* 9, 195. doi: 10.3389/fnhum.2015.00195.

Srinivasan, R., Winter, W.R., Ding, J., and Nunez, P.L. (2007). EEG and MEG coherence: measures of functional connectivity at distinct spatial scales of neocortical dynamics. *J Neurosci Methods* 166(1), 41-52. doi: 10.1016/j.jneumeth.2007.06.026.

Todorov, E., and Jordan, M.I. (2002). Optimal feedback control as a theory of motor coordination. *Nature neuroscience* 5(11), 1226.

Toga, A.W., and Thompson, P.M. (2003). Mapping brain asymmetry. *Nat Rev Neurosci* 4(1), 37-48. doi: 10.1038/nrn1009.

van Kordelaar, J., van Wegen, E., and Kwakkel, G. (2014). Impact of Time on Quality of Motor Control of the Paretic Upper Limb After Stroke. *Archives of Physical Medicine and Rehabilitation* 95(2), 338-344. doi: https://doi.org/10.1016/j.apmr.2013.10.006.

van Kordelaar, J., van Wegen, E.E.H., Nijland, R.H.M., Daffertshofer, A., and Kwakkel, G. (2013). Understanding Adaptive Motor Control of the Paretic Upper Limb Early Poststroke: The EXPLICIT-stroke Program. *Neurorehabilitation and Neural Repair* 27(9), 854-863. doi: 10.1177/1545968313496327.

van Kordelaar, J., van Wegen, E.E.H., Nijland, R.H.M., de Groot, J.H., Meskers, C.G.M., Harlaar, J., et al. (2012). Assessing Longitudinal Change in Coordination of the Paretic Upper Limb Using On-Site 3-Dimensional Kinematic Measurements. *Physical Therapy* 92(1), 142-151. doi: 10.2522/ptj.20100341.

Vlaar, M.P., Solis-Escalante, T., Dewald, J.P., van Wegen, E.E., Schouten, A.C., Kwakkel, G., et al. (2017). Quantification of task-dependent cortical activation evoked by robotic continuous wrist joint manipulation in chronic hemiparetic stroke. *Journal of neuroengineering and rehabilitation* 14(1), 30.

Wang, L., Zhang, J., Zhang, Y., Yan, R., Liu, H., and Qiu, M. (2016). Conditional Granger Causality Analysis of Effective Connectivity during Motor Imagery and Motor Execution in Stroke Patients. *BioMed Research International* 2016, 9. doi: 10.1155/2016/3870863.

Ward, N.S. (2015). Does neuroimaging help to deliver better recovery of movement after stroke? *Current opinion in neurology* 28(4), 323-329.

Ward, N.S. (2017a). Restoring brain function after stroke—bridging the gap between animals and humans. *Nature Reviews Neurology* 13(4), 244.

Ward, N.S. (2017b). Restoring brain function after stroke — bridging the gap between animals and humans. *Nature Reviews Neurology* 13, 244. doi: 10.1038/nrneurol.2017.34.

Weinstein, M., Green, D., Rudisch, J., Zielinski, I.M., Benthem-Muniz, M., Jongsma, M.L.A., et al. (2017). Understanding the relationship between brain and upper limb function in children with unilateral motor impairments: A multimodal approach. *Eur J Paediatr Neurol*. doi: 10.1016/j.ejpn.2017.09.012.

Wendel, K., Väisänen, O., Malmivuo, J., Gencer, N.G., Vanrumste, B., Durka, P., et al. (2009). EEG/MEG source imaging: methods, challenges, and open issues. *Computational intelligence and neuroscience* 2009, 13.

Wilkins, K.B., Owen, M., Ingo, C., Carmona, C., Dewald, J., and Yao, J. (2017). Neural plasticity in moderate to severe chronic stroke following a device-assisted task-specific arm/hand intervention. *Frontiers in neurology* 8, 284.

Winship, I.R., and Murphy, T.H. (2009). Remapping the somatosensory cortex after stroke: insight from imaging the synapse to network. *The Neuroscientist* 15(5), 507-524.

Wirsich, J., Ridley, B., Besson, P., Jirsa, V., Benar, C., Ranjeva, J.P., et al. (2017). Complementary contributions of concurrent EEG and fMRI connectivity for predicting structural connectivity. *Neuroimage* 161, 251-260. doi: 10.1016/j.neuroimage.2017.08.055.

Yao, J., Chen, A., Carmona, C., and Dewald, J.P. (2009). Cortical overlap of joint representations contributes to the loss of independent joint control following stroke. *Neuroimage* 45(2), 490-499.

Yoshimura, N., DaSalla, C.S., Hanakawa, T., Sato, M.-a., and Koike, Y. (2012). Reconstruction of flexor and extensor muscle activities from electroencephalography cortical currents. *NeuroImage* 59(2), 1324-1337. doi: https://doi.org/10.1016/j.neuroimage.2011.08.029.

Yoshimura, N., Tsuda, H., Kawase, T., Kambara, H., and Koike, Y. (2017). Decoding finger movement in humans using synergy of EEG cortical current signals. *Scientific Reports* 7(1), 11382. doi: 10.1038/s41598-017-09770-5.

Yoshioka, T., Toyama, K., Kawato, M., Yamashita, O., Nishina, S., Yamagishi, N., et al. (2008). Evaluation of hierarchical Bayesian method through retinotopic brain activities reconstruction from fMRI and MEG signals. *NeuroImage* 42(4), 1397-1413. doi: https://doi.org/10.1016/j.neuroimage.2008.06.013.

Zhang, D., Xu, F., Xu, H., Shull, P.B., and Zhu, X. (2016). Quantifying different tactile sensations evoked by cutaneous electrical stimulation using electroencephalography features. *International journal of neural systems* 26(02), 1650006.

6

From acute to chronic stroke

The future is fluid. Each act, each decision, and each development creates new possibilities and eliminates others. The future is ours to direct.

Jacque Fresco

6 A longitudinal diffusion MRI study: case studies from acute to chronic stroke

In this chapter multiple case-studies of stroke recovery in six individuals are presented. Based on the results of Chapter 3, two multi-compartment models were applied to the diffusion magnetic imaging (dMRI) data of stroke survivors acquired longitudinally throughout their recovery.

6.1 Introduction

Stroke is a major cause of disability in the developed world. Up to 80% of the stroke survivors suffer from upper limb paresis (Kwakkel et al., 2003; Dobkin, 2005). Prognosis for upper limb motor recovery is mainly determined within the first hours and days after the onset of brain ischemia. It was suggested in (Winters et al., 2015) that the outcome of motor recovery of the upper paretic limb measured at 6 months may be predictable within the first 72 hours post stroke. Moreover, the extent of recovery in the majority of the patients is an almost fixed amount of about 70% of the totally possible change. There is a number of mechanisms which can account for damage reversibility of infarcted motor control areas post stroke such as: salvation of penumbral tissue and elevation of diaschisis (Buma et al., 2013).

Unfortunately, about one third of the patients does not fit this proportional model of spontaneous recovery. A better insight into how neuronal networks change, starting from the acute phase after stroke onset, could help to understand the underlying recovery mechanisms in these nonfitters. Additionally, prognostic models might be improved by an enhanced understanding of these mechanisms. Furthermore, having improved biomarkers of spontaneous recovery from diffusion Magnetic Resonance Imaging (dMRI) early after stroke could support assessing the impact of applied rehabilitative interventions. The importance of dMRI stems from evidence that changes in white matter (WM) structures may be observed in

diffusion tensor imaging (DTI) data prior to clinical onset of diseases and before becoming evident in conventional MRI.

In recent years, more and more studies have emerged investigating longitudinal alterations in stroke survivors (Ward et al., 2003; Pannek et al., 2009; Groisser et al., 2014; Ma et al., 2014; Vlaar, 2017) or even patients suffering a transient ischemic attack (Ferris et al., 2017). A limitation of the previous assessments of WM microstructural changes, and also in the cases of longitudinal measurements, is in using conventional, so-called single b-value dMR imaging methods (Pannek et al., 2009; Yu et al., 2009). An accurate study into white matter alterations after stroke benefits from advanced imaging techniques enabling sophisticated modeling (Filatova et al., 2018). We intend to study neurological alterations after stroke longitudinally by measuring structural features using dMRI starting within the first five days post-stroke. As swelling reaches its maximum around 5-7 days post-stroke and then decreases, we should be able to observe changes in the diffusivity parameters, for example, fractional anisotropy increase and therefore decrease of the brain asymmetry due to stroke (Warach et al., 1996; Bhagat et al., 2008). Accordingly, dMRI and clinimetric information were measured four times during the first half year post stroke starting within five days of the incident. Our aim is to study anatomic changes occurring in the brain during stroke recovery based on dMRI. We hypothesize that there is a common pattern of recovery reflected in WM diffusion properties that can be captured early on after stroke. Such a metric could be represented either by initial brain asymmetry measures or their changes between the first two measurement points.

6.2 Methods

6.2.1 Cohort and study design

Subjects were included after informed consent and with permission of the Medical Ethics Committee of the Vrije Universiteit Medical Center, Amsterdam, and the Board of the Reinier de Graaf Gasthuis hospital, Delft. The trial protocol was registered on 23 October 2013 at the Netherlands Trial Register (identifier NTR4221) and amended on April 4, 2016, to include longitudinal dMRI measurements. Inclusion criteria for the subjects suffering from stroke were: upper limb paresis, ability to sit without support (National Institutes of Health Stroke

Scale item 5 a/b > 0), age >18, first-ever ischemic hemispheric stroke, <5 days post stroke. Exclusion criteria were: previously existing pathological neurological conditions or orthopedic limitations of the upper limb that would affect the results, botuline-toxine injections or medication that may have influenced upper limb function in the past three months, general MRI contra indications (claustrophobia, pacemaker or other metallic implants), high risk of epilepsy. Clinimetric measurements were scheduled as close to the dMRI acquisition date as possible.

Patients (n=18) were consecutively included from November 30, 2016 to March 21, 2018. However, 12 dropped out at different stages of the study: 1 wrong stroke diagnosis, 1 death, 2 repeated strokes in the course of the study, 1 skin rash, 1 claustrophobia (unknown at the inclusion time), 6 patients were too burdened by the study (project protocol included clinimetric and electroencephalographic measurements in addition to the MRI acquisitions).

6.2.2 MRI protocol

Image acquisition was performed with a 3T MRI scanner (Philips Achieva, Philips Healthcare, Best, The Netherlands). The diffusion-weighted MRI (dMRI) acquisition protocol had 40 non-collinear gradient directions uniformly sampled over a sphere for each of two b-values, 1000 and 2000 s/mm^2, acquired in a single scan; TE=100 ms, TR= 6506 ms, imaging matrix = 96x96, 50 consecutive slices with a thickness of 2.5 mm and slice spacing 2.5 mm. One image per acquisition had no diffusion weighting, i.e. b=0 s/mm^2.

6.2.3 Data preprocessing

Preprocessing was done similarly to Chapter 3, (Filatova et al., 2018). However, a main difference was the fact that scans corresponding to different b-values were acquired simultaneously, so that their co-registration was not needed.

dMRI data were preprocessed using FSL v5.0 (http://fsl.fmrib.ox.ac.uk/fsl/, (Jenkinson et al., 2012)). The acquired DWIs were corrected for motion and eddy current distortion by affine coregistration to the reference b0-image (using FSL eddy_correct). Gradient directions were reoriented according to the rotation component of the affine transformation. Based on the results of Chapter 3, two diffusion models were fitted to the data: single tensor with isotropic compartment and bi-tensor with isotropic compartment (Caan et al., 2010). The maximum

diffusivity of the tensor compartment in both models was limited by the diffusivity of free water at body temperature, ~$3 \cdot 10^{-3}$ mm^2/s.

6.2.4 Registration

Separate fractional anisotropy (FA) and radial diffusivity (RD) images were derived for each diffusion model and each subject. All FA images were co-registered to the Montreal Neurological Institute (MNI) space using an affine registration with 12 degrees of freedom as implemented in FSL v5.0 (Jenkinson et al., 2012). Subsequently, the same transformation was applied to the rest of the parameter maps (RD, volume fractions, etc.). Similarly to the previous cross-sectional analysis (Chapter 3), areas with high volume fraction of the isotropic compartment (f_{iso}) determined by the bi-tensor model were excluded from the analysis.

The JHU white-matter tractography atlas (https://neurovault.org/collections/264/) was projected onto the data to determine location of the common WM tracts. This tractography atlas contains 20 labeled white matter structures. It was generated by averaging the results of deterministic tractography in 28 normal subjects (mean age 29, M:17, F:11) (Mori et al., 2005). Several symmetric WM tracts in this atlas were considered in our analysis. Their functional roles are summarized in Table 3.1 of this thesis. Additionally, the atlas contains delineations of forceps major and forceps minor. Based on the results of Chapter 3, we considered diffusion measure changes only in corticospinal tract and superior longitudinal fasciculus, because those WM structures were most affected by stroke.

6.2.5 Data analysis

As concluded from the cross-sectional analysis, FA and RD are the properties most strongly reflecting WM changes after stroke compared to the control population. That is why for every tract and for all subjects we calculated the mean values of FA, RD and f_{iso}. After that, we determined asymmetries of the mean tract values between contralesional (healthy) and ipsilesional (impaired) hemispheres, which were normalized to the interval between -1 and 1. For example, for FA it was defined as $\boldsymbol{FA}_{asymmetry} = \frac{\left(\boldsymbol{FA}_{healthy} - \boldsymbol{FA}_{impaired}\right)}{\left(\boldsymbol{FA}_{healthy} + \boldsymbol{FA}_{impaired}\right)}$. This allowed making sure that subject outcomes are comparable despite individual differences of the absolute values of diffusion measures between subjects.

6.3 Results

The characteristics of the 6 patients were : 1 female; median age: 63 (IQR: 59 – 69.25); 2/6 patients had an impaired right hand; for 3/6 patients the dominant hand was impaired. Four diffusion-weighted MRI (dMRI) scans were acquired within 5 days, at 5, 12 and 26 weeks post stroke. Further information regarding patient inclusion and initial measurements is presented in Table 6.1. Notes on lesion location are presented in Table 6.2.

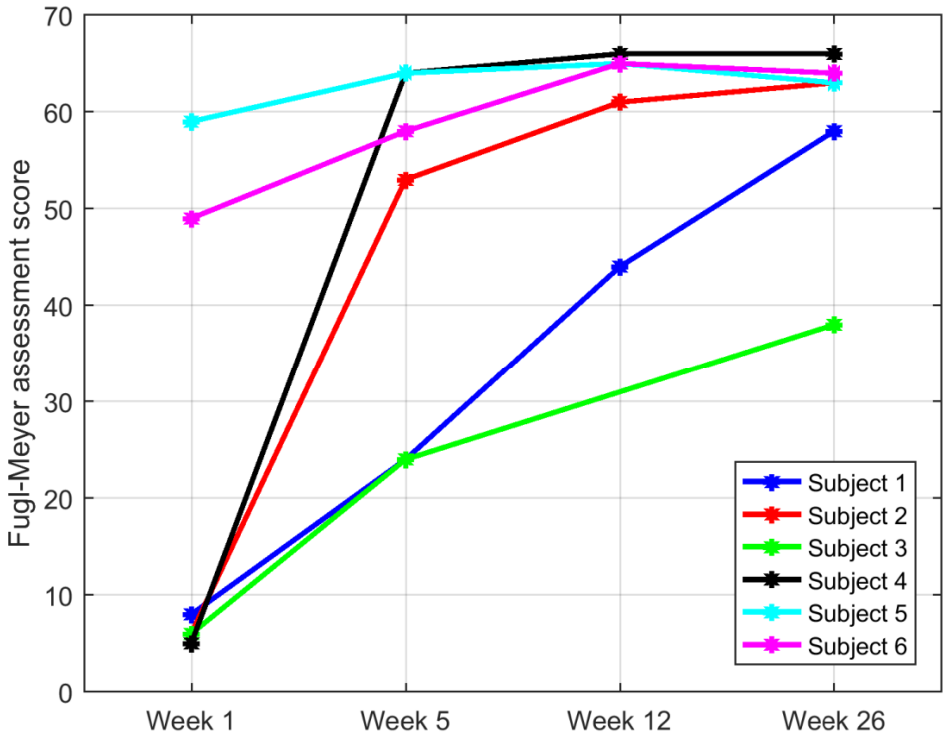

Figure 6.1. Fugl-Meyer upper extremity score of the subjects as a function of time since stroke (week) are indicated. Maximal FMA score is 66 points. Colors represent different subjects. For Subject 3 the third measurement (week 12) is missing.

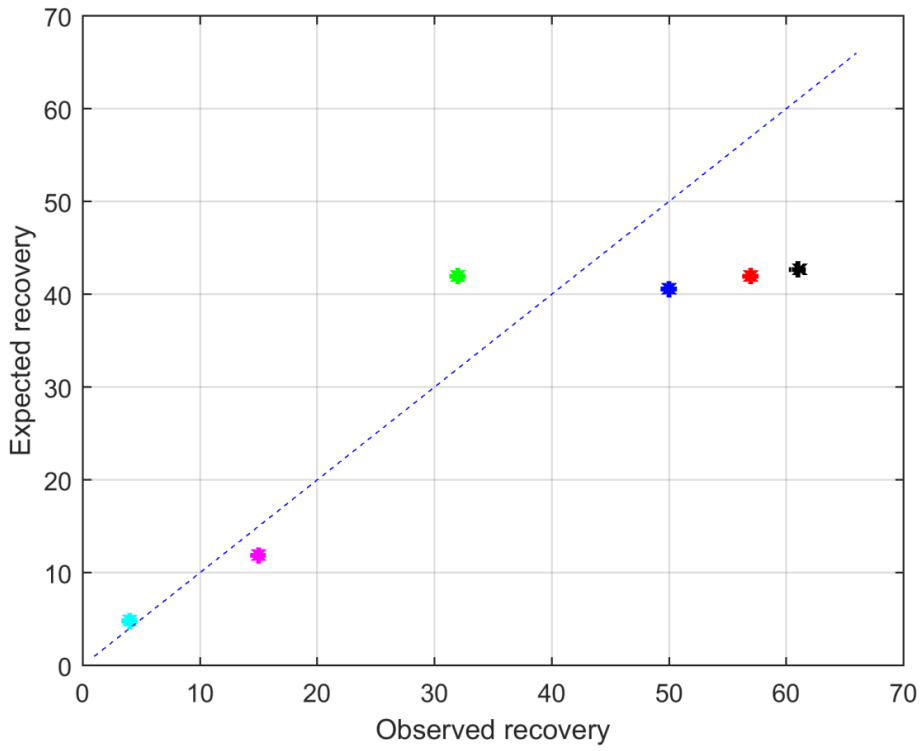

Figure 6.2. Change of the Fugl-Meyer upper extremity score between T4 and T1 in each subject represents observed recovery. Expected recovery is computed based on the 70% rule as $0.7 \cdot (\boldsymbol{FMA}_{\text{max}} - \boldsymbol{FMA}_{\text{initial}})$. Maximal FMA score is 66 points. Colors represent different subjects.

Table 6.1. Patient demographic information.

Patient number	Stroke date	Inclusion date	First MRI date	First clinimetrics date
1	7.03.2017	08.03.2017	09.03.2017	10.03.2017
2	25.03.2017	27.03.2017	28.03.2017	27.03.2017
3	12.08.2017	12.08.2017	15.08.2017	12.08.2017
4	15.08.2017	17.08.2017	18.08.2017	17.08.2017
5	20.08.2017	23.08.2017	24.08.2017	23.08.2017
6	15.10.2017	16.10.2017	16.10.2017	17.10.2017

Table 6.2. Lesion location per subject.

Patient number	Lesion location
1	Basal ganglia, right hemisphere
2	Small areas in frontal and parieto-occipital lobes, right
3	Thalamus, right
4	Small lacunar infarct (no CT representation), left
5	Internal capsule and sub-insular, right
6	Small lacunar infarct (no CT representation), left

Fugle-Meyer assessment (FMA) score of the study participants over time is presented in Figure 6.1. For subject 3, clinimetrics of week 12 is missing. For subjects 1 and 3 no dMRI was acquired at 12 weeks. These data are missing due to unavailability of the patients in the week required by the protocol. In all of the plots points and/or lines of the same color represent the same subject.

Figure 6.2 shows how recovery of the subjects in this study relates to the so-called proportional recovery rule. According to this rule, patients achieve about 70% of their maximum recovery as indicated by the FMA score. Among our subjects only Subject 3, depicted in green, did not fit this rule.

Time trajectories of each patient of f_{iso}, FA and RD asymmetries in two white matter tracts, corticospinal tract (CST) and superior longitudinal fasciculus (SLF), are presented in Figure 6.3 (single tensor plus isotropic compartment) and Figure 6.4 (bi-tensor with isotropic compartment).

When compared to the outcomes of the cross-sectional study (Chapter 3), individual patient outcomes for both $FA_{asymmetry}$ and $RD_{asymmetry}$ fall outside the range of the corresponding measures for the control subjects. Except for the increased $FA_{asymmetry}$ and $RD_{asymmetry}$ compared to the controls, no clear recovery pattern of these was observed in neither CST nor SLF for both models. Pearson correlations computed between these asymmetries at week 1 and FMA at week 26 were not statistically significant. The same holds for the correlations of the asymmetry changes between week 5 and week 1 and patient FMA at week 26. However, a rapid decrease in the asymmetry of f_{iso} for subjects 1, 2, 4 and 6 can be observed with both employed models. Subjects 3 and 5 demonstrate a less prominent decrease. Even in the latter two subjects, the lowest asymmetry value of f_{iso} corresponds to the time point with the highest measured FMA score.

6.4 Discussion

In the present preliminary study we studied microstructural changes occurring in the brain during stroke recovery as assessed by diffusion-weighted MRI measured at four time points in the first six month of recovery starting within 5 days after stroke.

Based on the tract-based spatial statistics, (Koyama and Domen, 2017) suggested that interhemispheric ratio of FA in CST and SLF could be a predictor of cognitive

function and extremity function. In case of cognitive processing assessment, the same two tracts were found to play an important role: CST for the psychomotor speed and SLF for the executive functioning (Biesbroek et al., 2018). Therefore, based on the recent stroke literature and our previous results, we investigated the behavior of diffusion measures' asymmetries in CST and SLF.

Despite the original hypothesis, no clear relation was found between the FA and RD asymmetries at week 1 or their changes between week 1 and week 5 and the FMA scores at week 26. However, the results show that the asymmetry in the volume fraction of the isotropic compartment between the contra- and ipsilesional hemispheres rapidly decreases during the first weeks of recovery. This may indicate that the white matter tissue swelling decreases in the affected hemisphere thus leading to the improved motor performance. Moreover, the isotropic compartment might be a biomarker of the vasogenic edema post stroke.

This study has a number of limitations. The most prominent drawback is the small sample size with a group consisting of the patients well-recovered at the half-year mark. This was caused by the low inclusion and high drop-out rates of the study. Furthermore, from a methodological point of view, especially at the early stages post stroke, it is more desirable to measure MRI and clinimetrics on the same day, which was not the case in our protocol. According to (Thomas et al., 2018), even the time of day at which the patient was scanned may play a role with the diffusivity measures. Although the exact underlying mechanism is not known, radial and axial diffusivities increase from the afternoon to the morning hours.

Despite the limitations, the unclear pattern of recovery observed in this work could also be caused by the biological differences between the patients. Lesion location and volume vary between the patients, but are important indicators of the nature and severity of post-stroke impairment (Wu et al., 2015). Moreover, all the stroke participants exhibited extremely high levels of recovery, even exceeding the 70% recovery rule prediction. According to the current recovery prediction modelling, patients with initial FMA scores under 17 points have low chances of good motor recovery. In two out of the six considered patients lesions were not visible on the clinical CT scans. Four patients had initially low FMA scores with three of them

reaching above 50 points at the end of the observation period. This most probably led to a study cohort biased towards a good motor outcome.

In the study of Boscolo Galazzo and colleagues a similar longitudinal design was used with measurements within 1 week, at 1 month and 6 months (Boscolo Galazzo et al., 2018). They were able to quantify the remodeling of WM tracts and even grey matter regions involved in motor recovery after ischemic stroke in 10 stroke patients and 10 control participants. However, their acquisition consisted of 258 diffusion directions and 34 non-zero diffusion weightings (b-values) allowing to apply generalized diffusivity measures such as generalized fractional anisotropy, propagator anisotropy, etc. In our case even with the very limited study population and much less extensive acquisition protocol we are able to detect microstructural changes based on the water content in the affected brain.

In conclusion, we did not find significant correlations between diffusion measures and FMA score. However, we visually observe trends that could be of high interest for clinical application. Our study was very limited in its design regarding the number of subjects, we therefore recommend to perform longitudinal study with a larger sample size.

6.5 Conclusions

- No clear patterns in FA and RD asymmetry changes were observed during longitudinal dMRI measurements of stroke recovery.
- Initial asymmetry change in volume fraction of an isotropic compartment, i.e. tissue swelling, could be a useful outcome predictor for an upper extremity recovery
- Further investigation of the WM changes in the bigger sample of the **diverse** population of stroke survivors and larger sample sizes are necessary to achieve further insights into stroke recovery mechanisms.

References

Bhagat, Y.A., Hussain, M.S., Stobbe, R.W., Butcher, K.S., Emery, D.J., Shuaib, A., et al. (2008). Elevations of diffusion anisotropy are associated with hyper-acute stroke: a serial imaging study. *Magnetic Resonance Imaging* 26(5), 683-693. doi: 10.1016/j.mri.2008.01.015.

Biesbroek, J.M., Leemans, A., den Bakker, H., Duering, M., Gesierich, B., Koek, H.L., et al. (2018). Microstructure of Strategic White Matter Tracts and Cognition in Memory Clinic Patients with Vascular Brain Injury. *Dementia and Geriatric Cognitive Disorders* 44(5-6), 268-282. doi: 10.1159/000485376.

Boscolo Galazzo, I., Brusini, L., Obertino, S., Zucchelli, M., Granziera, C., and Menegaz, G. (2018). On the Viability of Diffusion MRI-Based Microstructural Biomarkers in Ischemic Stroke. *Frontiers in Neuroscience* 12, 92.

Buma, F., Kwakkel, G., and Ramsey, N. (2013). Understanding upper limb recovery after stroke. *Restor Neurol Neurosci* 31(6), 707-722. doi: 10.3233/RNN-130332.

Caan, M.W.A., Khedoe, H.G., Poot, D.H.J., den Dekker, A.J., Olabarriaga, S.D., Grimbergen, K.A., et al. (2010). Estimation of Diffusion Properties in Crossing Fiber Bundles. *IEEE Transactions on Medical Imaging* 29(8), 1504-1515.

Dobkin, B.H. (2005). Clinical practice. Rehabilitation after stroke. *N Engl J Med* 352(16), 1677-1684. doi: 10.1056/NEJMcp043511.

Ferris, J.K., Edwards, J.D., Ma, J.A., and Boyd, L.A. (2017). Changes to white matter microstructure in transient ischemic attack: A longitudinal diffusion tensor imaging study. *Human Brain Mapping* 38(11), 5795-5803. doi: 10.1002/hbm.23768.

Filatova, O.G., van Vliet, L.J., Schouten, A.C., Kwakkel, G., van der Helm, F.C.T., and Vos, F.M. (2018). Comparison of Multi-Tensor Diffusion Models' Performance for White Matter Integrity Estimation in Chronic Stroke. *Frontiers in Neuroscience* 12(247). doi: 10.3389/fnins.2018.00247.

Groisser, B.N., Copen, W.A., Singhal, A.B., Hirai, K.K., and Schaechter, J.D. (2014). Corticospinal tract diffusion abnormalities early after stroke predict motor outcome. *Neurorehabilitation and Neural Repair* 28(8), 751-760. doi: 10.1177/1545968314521896.

Jenkinson, M., Beckmann, C.F., Behrens, T.E., Woolrich, M.W., and Smith, S.M. (2012). Fsl. *Neuroimage* 62(2), 782-790. doi: 10.1016/j.neuroimage.2011.09.015.

Koyama, T., and Domen, K. (2017). Diffusion Tensor Fractional Anisotropy in the Superior Longitudinal Fasciculus Correlates with Functional Independence Measure Cognition Scores in Patients with Cerebral Infarction. *Journal of Stroke and Cerebrovascular Diseases* 26(8), 1704-1711. doi: https://doi.org/10.1016/j.jstrokecerebrovasdis.2017.03.034.

Kwakkel, G., Kollen, B.J., van der Grond, J., and Prevo, A.J. (2003). Probability of regaining dexterity in the flaccid upper limb: impact of severity of paresis and time since onset in acute stroke. *Stroke* 34(9), 2181-2186. doi: 10.1161/01.STR.0000087172.16305.CD.

Ma, C., Liu, A., Li, Z., Zhou, X., and Zhou, S. (2014). Longitudinal study of diffusion tensor imaging properties of affected cortical spinal tracts in acute and chronic hemorrhagic stroke. *Journal of Clinical Neuroscience* 21(8), 1388-1392. doi: 10.1016/j.jocn.2013.11.032.

Mori, S., Wakana, S., van Zijl, P.C.M., and and Nagae-Poetscher, L.M. (2005). *MRI Atlas of Human White Matter.* Amsterdam: Elsevier.

Pannek, K., Chalk, J.B., Finnigan, S., and Rose, S.E. (2009). Dynamic corticospinal white matter connectivity changes during stroke recovery: a diffusion tensor probabilistic tractography study. *J Magn Reson Imaging* 29(3), 529-536. doi: 10.1002/jmri.21627.

Thomas, C., Sadeghi, N., Nayak, A., Trefler, A., Sarlls, J., Baker, C.I., et al. (2018). Impact of time-of-day on diffusivity measures of brain tissue derived from diffusion tensor imaging. *NeuroImage* 173, 25-34. doi: https://doi.org/10.1016/j.neuroimage.2018.02.026.

Vlaar, M. (2017). *Characterizing Cortical Responses Evoked by Robotic Joint Manipulation after Stroke.* TU Delft.

Warach, S., Dashe, J.F., and Edelman, R.R. (1996). Clinical Outcome in Ischemic Stroke Predicted by Early Diffusion-Weighted and Perfusion Magnetic Resonance Imaging: A Preliminary Analysis. *Journal of Cerebral Blood Flow and Metabolism* (16), 53-59.

Ward, N.S., Brown, M.M., Thompson, A.J., and Frackowiak, R.S.J. (2003). Neural correlates of motor recovery after stroke: a longitudinal fMRI study. *Brain : a journal of neurology* 126(0 11), 2476-2496. doi: 10.1093/brain/awg245.

Winters, C., van Wegen, E.E.H., Daffertshofer, A., and Kwakkel, G. (2015). Generalizability of the Proportional Recovery Model for the Upper Extremity After an Ischemic Stroke. *Neurorehabilitation and Neural Repair* 29(7), 614-622. doi: 10.1177/1545968314562115.

Wu, O., Cloonan, L., Mocking, S.J.T., Bouts, M.J.R.J., Copen, W.A., Cougo-Pinto, P., et al. (2015). The role of acute lesion topography in initial

ischemic stroke severity and long-term functional outcomes. *Stroke; a journal of cerebral circulation* 46(9), 2438-2444. doi: 10.1161/STROKEAHA.115.009643.

Yu, C., Zhu, C., Zhang, Y., Chen, H., Qin, W., Wang, M., et al. (2009). A longitudinal diffusion tensor imaging study on Wallerian degeneration of corticospinal tract after motor pathway stroke. *Neuroimage* 47(2), 451-458. doi: 10.1016/j.neuroimage.2009.04.066.

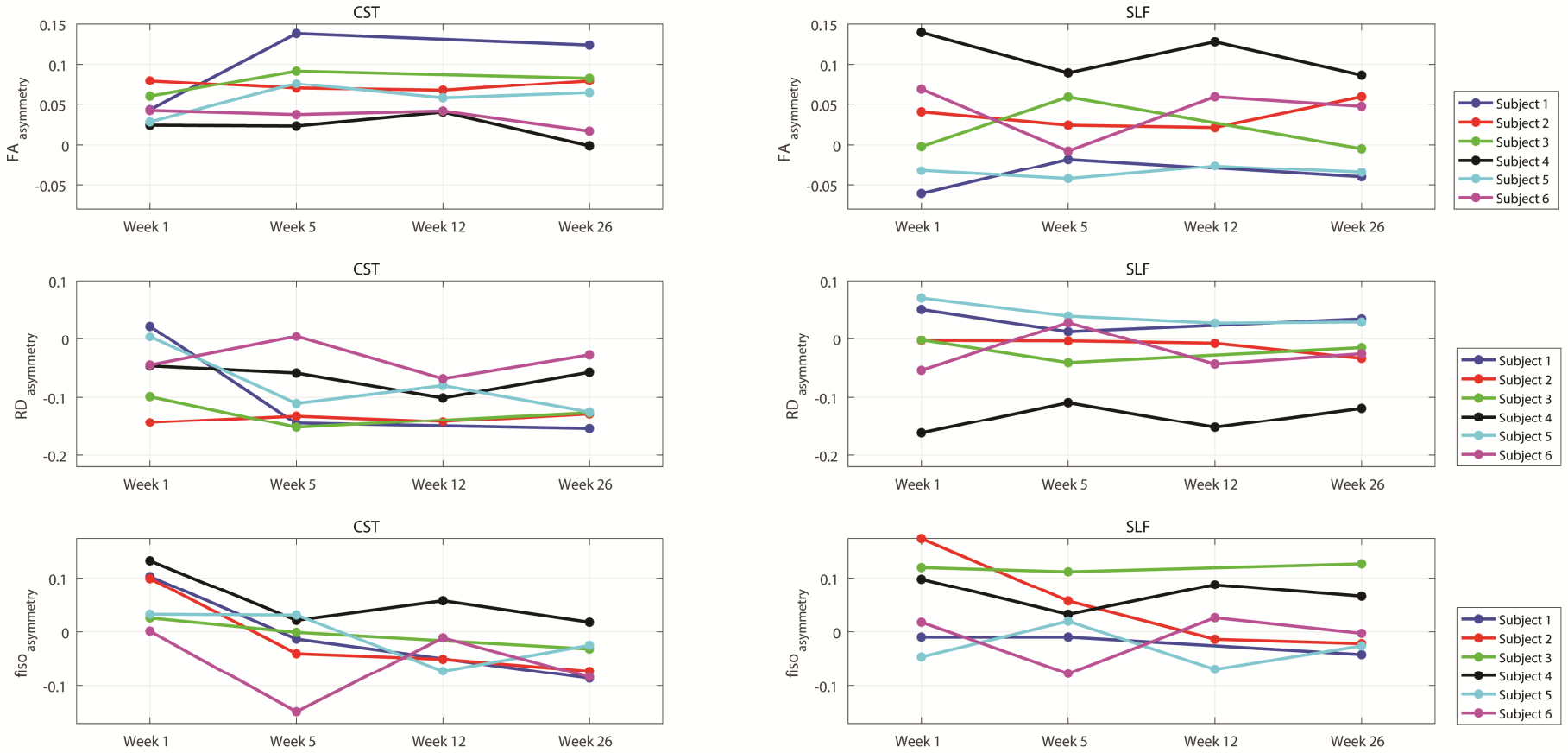

Figure 6.3 Evolution over time of FA, RD and f_{iso} asymmetries in the corticospinal tract (left) and superior longitudinal fasciculus (right) estimated by the single tensor model with isotropic compartment.

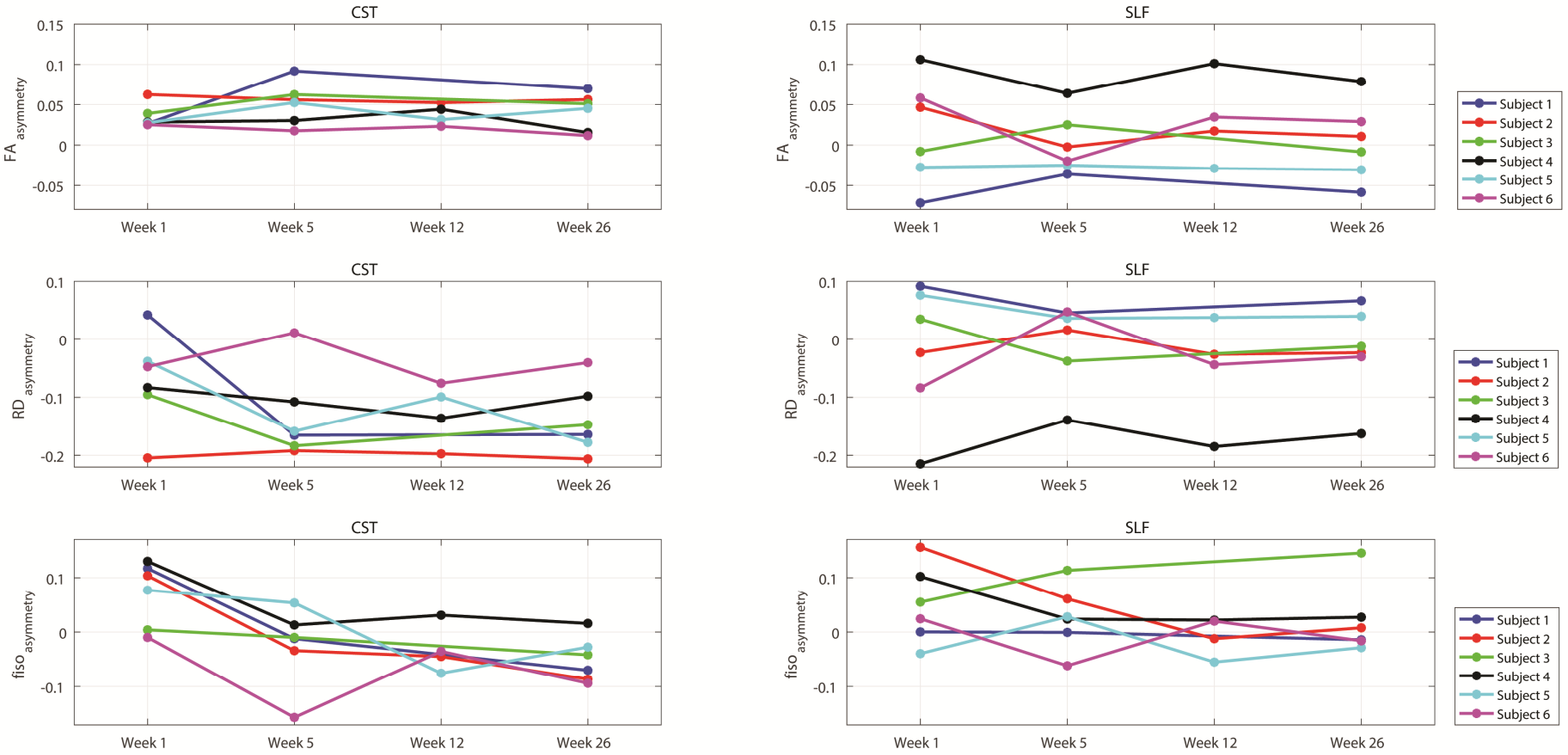

Figure 6.4 Evolution over time of FA, RD and f_{iso} asymmetries in the corticospinal tract (left) and superior longitudinal fasciculus (right) estimated by the bi-tensor with isotropic compartment.

7 Conclusion and outlook

Life is the art of drawing sufficient conclusions from insufficient premises.

Samuel Butler

7 Conclusion and outlook

In the past decades diffusion-weighted MRI has grown and matured as a unique non-invasive technique to assess the white matter microstructure of the brain. This thesis focused on brain dMRI analysis and aimed to enhance the understanding of the white matter changes in clinical populations, namely, patients with attention deficit hyperactivity disorder (ADHD) and in stroke survivors. In this chapter, I will highlight the conclusions of my work; discuss the relationship between the results obtained in separate chapters and give recommendations for the future developments in the field.

Figure 7.1 schematically describes relations between the chapters of this thesis in terms of the study design (cross-sectional or longitudinal) and the type of the methodology being used (established in the field or novel).

What catches the eye in Figure 7.1 is that the top right quadrant of the scheme is empty: novel methods described in Chapters 4 and 5 have not yet been applied to the data acquired in a longitudinal manner.

By combining methodology for assessing dynamic information flow in the brain, introduced in Chapter 5, with the longitudinal measurements, as presented in Chapter 6, a deeper insight into structure-function coupling in the stroke survivors' population can be gained. It remains unclear whether the higher level of interhemispheric integration demonstrated in the proof-of-principle study in this thesis is generalizable to the wider range of stroke patients. Moreover, how such an integration may occur and at what stage during the course of recovery would be an important direction of investigation. This project set out to enable determination of realistic therapeutic goals and selection of particular rehabilitation approaches. Speculatively speaking, it could happen that certain types of therapy lead to normalization of the brain information flow thus ensuring better patient outcomes. Or, perhaps, even higher levels of interhemispheric communication could mean more efficient motor performance of the patients as the contralesional hemisphere takes over functions of the affected hemisphere. Approaches described in this thesis

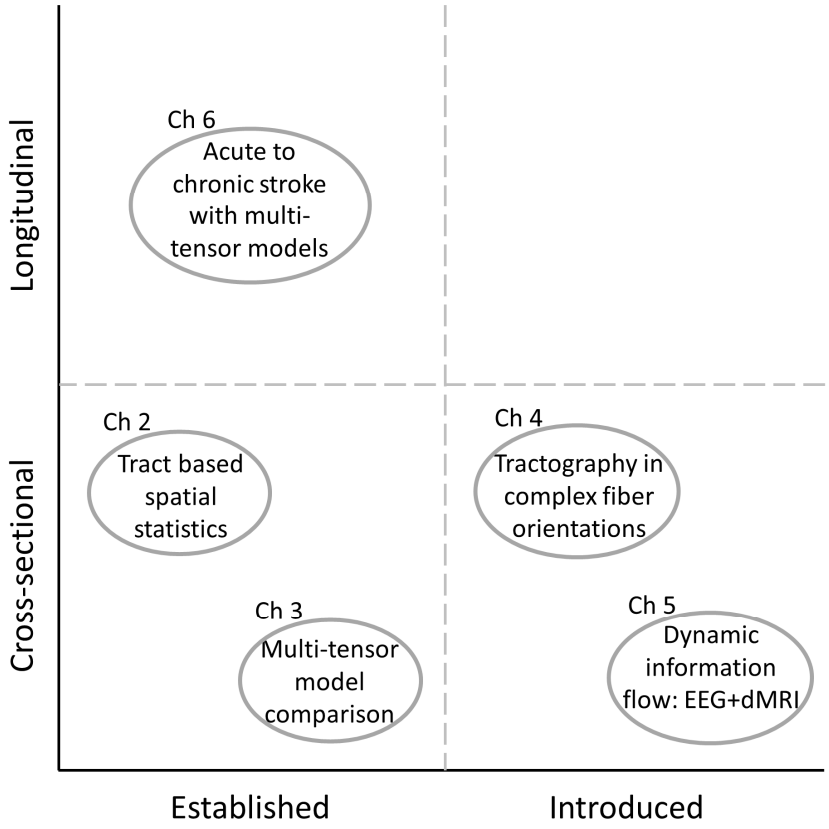

Figure 7.1 Schematic representation of the chapters of this thesis in terms of the study design (cross-sectional or longitudinal) and the type of the methodology being used (established in the field or novel).

could be used to search for answers to these questions and further development of both neuroscience and rehabilitation fields.

On the other hand, it is also possible to apply the tractography approach with an automatic model selection to longitudinal measurements. However, when attempting to compare outcomes in the same pixel or region of interest, one should make sure that diffusion measures are comparable over multiple time points. The difficulty is that they could be estimated through different models and the exact ways to deal with this issue need to be investigated to draw any meaningful conclusions. One approach to resolve this could be based on spatially consistent model selection inspired, for example, by Chapter 4 of (Arkesteijn, 2018).

Let us now discuss the results of each chapter in more detail.

7.1 Voxel-based morphometry of dMRI in ADHD patients

Despite the increased number of subjects being diagnosed with ADHD, safety studies on the effect of stimulant medication on the development of the adolescent brain remain scarce. In Chapter 2, dMRI is employed in a randomised clinical trial to study the influence of stimulant medication on the WM and its age modulated effects. Our results provide some direction regarding safety of methylphenidate hydrochloride use during brain development indicating positive effects on brain white matter FA in children suffering from ADHD. As for the long-term, the significance of these findings still remains to be established.

The study design was strong, especially in terms of minimizing confounders such as age and gender. However, the applied acquisition protocol with a single diffusion weighting value (b=1000 s/mm^2) limits possibilities for the more advanced diffusion modeling that could further improve interpretability of the results.

With that in mind, and based on experiences of colleagues working on studies such as the Rotterdam scan study (Ikram et al., 2015), one should develop the protocol for a study based on the expected outcome measures. In the Chapters 3, 4 and 6 of this thesis a protocol with two diffusion weightings was used to allow for more freedom for interpreting diffusion measures. Namely, a more extensive protocol made it possible to apply models taking into account additional physical processes such as fiber crossings and the presence of free water in the tissue.

7.2 Chronic stroke: diffusion modeling

In Chapter 3, we evaluated the influence of stroke on white matter tracts based on interhemispheric asymmetry of diffusion properties. This analysis was done using four tensor-based diffusion models in order to determine their performance when relating WM properties with the clinical outcome of chronic stroke patients.

Particularly, we studied the asymmetries of FA, MD, AD and RD in nine symmetric WM structures. Our results indicated that FA and RD asymmetries may be most predictive for white matter alterations after stroke. Moreover, multi-compartment models accounting for the free-water diffusion allowed for a more sensitive evaluation of the tract properties. We found that not only the corticospinal

tract, but also the superior longitudinal fasciculus is significantly affected by stroke as indicated by the group comparison between patients and controls. This supports the hypothesis previously discussed in literature that stroke leads to alterations in the brain even in the areas distal to the lesion location. A limitation of this study is a relatively small sample size which does not allow to investigate further statistics such as an interaction between the handedness of the subjects, lesion location and brain asymmetry.

Given this information at the chronic stroke stage, multi-compartment diffusion models should be tested in stroke patients longitudinally, starting from the acute phase.

7.3 Multi-tensor tractography with model selection

So far, we have concluded that multi-compartment models are useful tools to investigate WM properties in stroke. However, it is also important to take into account brain anatomy at different locations. For example, corpus callosum is the inter-hemispheric tract and its body does not contain fiber crossings. It is thus superfluous to fit a crossing-fiber model to the data of this tract. On the other hand, the corticospinal tract and various association fibers encounter many crossings over their length and it is advantageous to model that as well.

In Chapter 4, we introduce a framework for model selection and probabilistic tractography and assess the performance of this approach quantitatively using artificial phantom data as well more qualitatively in healthy subjects' scans by counting the number of fibers estimated over one crossing of major white matter tracts. We employ the information complexity criterion that balances the goodness of the model fit and the model complexity. This way the selection procedure outputs the model, which is best supported by the available data. The resulting fiber orientations and CRLB-based variance of the estimated fiber orientations serve as inputs for the probabilistic tractography algorithm.

Our framework allowed achieving a lower median angular error and a better performance for the highly curved fibers and the kissing fibers of the fibercup phantom compared to the Camino software. As for the in-vivo measurements of

healthy controls, we were consistently able to track more fibers across the corticospinal tract and corpus callosum than Camino. These results indicate that employing model selection as a part of a dMRI analysis pipeline is beneficial for achieving accurate estimations of white matter properties.

7.4 Brain dynamics estimation

Lesions affect anatomical brain networks resulting in functional disturbances of brain systems and their behavior (Alstott et al., 2009). In Chapter 5 we demonstrated the feasibility of estimating dynamic interactions of cortical sources during sensory stimulation, with the aid of dMRI-based anatomic constraints. First, sources of the brain activity were estimated from EEG recordings at different time points. Then anatomic connections and their length were derived using white matter tractography. Only sources connected by tractography are included in the estimation of dynamic information flow and time delays are estimated based on the connection length. This helps to control the type I error in multivariate autoregressive modeling.

This approach is first applied to the EEG recordings of healthy controls. The results show contralateral activation patterns consistent with findings in literature. In chronic hemiparetic stroke participants, the activation of brain activity occurs in both hemispheres, with information flow running through the ipsilateral (contralesional) hemisphere. Performance of the method is evaluated by estimating the variance accounted for in the source localization and dynamics estimation. Despite the linear nature of the multivariate autoregressive model, an average variance accounted for (VAF) of over 90% is achieved for the dynamics estimation, with about 97% VAF in controls and about 91% in stroke patients.

Our results indicate that reconfiguration of the sensory network may occur following a stroke. This suggests a direction for identifying quantitative biomarkers to assess sensory impairment after a unilateral brain injury. Application of this methodology to a large database of measurements can be a first step to achieve further understanding of the brain reorganization and recovery mechanisms post-stroke.

7.5 Stroke recovery

In Chapter 6, based on the results of Chapter 3, a single tensor model with an isotropic compartment and a bi-tensor model with an isotropic compartment were applied to the dMRI data acquired longitudinally during recovery of stroke patients. Asymmetries of FA, RD and f_{iso} were assessed in the corticospinal tract and the superior longitudinal fasciculus of these patients at each time point.

No relation was found between the patient motor outcome and initial FA and RD asymmetries or the patterns of their change in time. The asymmetry in the volume fraction of the isotropic compartment between the hemispheres showed rapid decrease during the first weeks of recovery indicating the decrease in tissue swelling. This was associated with the increased FMA scores of patients. All in all, a larger and more varied sample size is necessary for generalizing the conclusions about the microstructural changes during stroke recovery.

7.6 Final remarks

Diffusion-weighted MRI of the brain's white matter is a widely applied technique for research purposes. However, it is not yet a common clinical tool and still needs to find a place in the standard toolbox of radiologists and neurologists. For a stroke patient arriving to a hospital, computed tomography (CT) is the first modality of choice all over the world to differentiate hemorrhagic and ischemic strokes. Clinical utilization of dMRI is much more rare despite its ability to dramatically alter ischemic stroke care by early detection of ischemic changes in the brain tissue and differentiating them from other stroke-mimicking events (Birenbaum et al., 2011).

Lack of studies proving how complex diffusion modeling can be helpful in rehabilitation and the absence of readily available analysis software solutions are among the obstacles for translating research knowledge on dMRI into clinical practice. Moreover, to assess brain microstructure based on the dMRI, appropriate acquisition protocols should be used.

This thesis studies how outcomes of different multi-compartment models relate to patient outcomes and developing the tools to gain insight into the disease impact and patient recovery process. Combining functional causality and structural

connectivity is one of the ways to get a more comprehensive understanding of stroke.

A general difficulty in human neuroscience research is the absence of a ground truth, making it even more difficult to interpret the results of image analysis and modeling approaches. One way to overcome this problem is to look into simulated or animal data. At the same time, attempting to do so in patient measurements will certainly add another level of complexity.

On a more general level, we aim at improving patient prognostic models so that for every patient the possible extent of recovery would be clear at a very early stage. The better prognosis is made, the more personalized rehabilitation therapy can be. However, what will we do when they become very precise on individual level? Which approach will be taken in cases when almost no recovery will be predicted for a specific person? To my opinion scientific development means that awareness of such questions needs to be increased not only in daily practice of clinical doctors, but of technical researchers as well.

Currently, one of the biggest challenges is translation of knowledge gathered via basic and applied research into clinical use. That is why, in my view, translational research is where the biggest impact can be made in the near future. To be successful, such an interdisciplinary field requires combined efforts of researchers and clinicians. Frequently, researchers are interested in developing new technology and studying fundamental biological mechanisms by means of modeling or nowadays widely popular machine learning approaches. On the other hand, the primary concern of clinicians is their patients' well-being, which may cause reluctance in adopting new techniques and devices. Therefore, a change of the mindset needs to happen at both sides of the spectrum. Many problems that are being solved and presented in scientific forums and conferences form an important step in this direction. I find that we need to start with the question or need from the clinical perspective and then work towards addressing it with technological advances. The research community should rise to the challenge of generalizing algorithms to clinically relevant data, handling patient-specific results and non-standard anatomy. One of the most difficult parts is demonstrating that what we

develop has benefits when used in the clinic and addressing the above-mentioned problems can be another step in this direction. And that is what clinicians should be open to.

Hopefully, insights presented in this thesis can be employed to bring dMRI analysis closer to rehabilitation of stroke patients in clinical practice, with the ultimate goal of facilitating more personalized treatments.

References

Alstott, J., Breakspear, M., Hagmann, P., Cammoun, L., and Sporns, O. (2009). Modeling the impact of lesions in the human brain. *PLoS Comput Biol* 5(6), e1000408. doi: 10.1371/journal.pcbi.1000408.

Arkesteijn, G.A.M. (2018). *Application of sophisticated models for conventional diffusion-weighted MRI data.*

Birenbaum, D., Bancroft, L.W., and Felsberg, G.J. (2011). Imaging in Acute Stroke. *Western Journal of Emergency Medicine* 12(1), 67-76.

Ikram, M.A., van der Lugt, A., Niessen, W.J., Koudstaal, P.J., Krestin, G.P., Hofman, A., et al. (2015). The Rotterdam Scan Study: design update 2016 and main findings. *European Journal of Epidemiology* 30, 1299-1315. doi: 10.1007/s10654-015-0105-7.

Summary

Human brain consists of grey and white matter. Grey matter largely forms the outer layer of the brain, and is responsible for decision making and functioning of the human body. Complementary, the white matter (WM) contains the communication pathways between the grey matter areas. Diffusion-weighted magnetic resonance imaging (dMRI) is an imaging modality allowing to model the brain's white matter structures by making the MRI acquisition sensitive to diffusion processes. When brain structure is altered due to pathology, it can be assessed and quantified by analysing dMRI data.

This thesis investigates the influence of stroke on the brain's white matter structure based on dMRI-measurements and functional properties measured with EEG. This work is part of the 4D EEG project, one of the aims of which was to evaluate outcomes of the stroke patients in terms of their WM integrity and brain function.

To gain a better understanding of the commonly used analysis techniques, conventional dMRI data of patients with Attention Deficit Hyperactivity Disorder (ADHD) were analyzed. This study evaluated whether the effects of stimulant ADHD medication on the brain were modulated by the age of the patients. The results demonstrate a different *change* in WM properties of children after treatment than the *change* in adults treated with the same medication. (Chapter 2)

Traditional diffusion tensor imaging (DTI) models water diffusion with one Gaussian profile. However, multiple brain regions contain complex white matter configurations such as crossing or kissing fibers. Moreover, edema is present in the brain of stroke survivors, especially around the lesion site. Such physical properties can be modeled with multi-compartment models in which crossings and free water diffusion are explicitly accounted for. Comparing four models of increasing complexity, starting with a conventional DTI model, suggested that more elaborate approaches, involving free water modeling, better relate to the clinical outcome of the patients. By assessing interhemispheric

asymmetry of diffusion measures in patients compared to healthy age-matched individuals, superior longitudinal fasciculus was identified as a tract affected by stroke in addition to the well-known effects on the corticospinal tract. (Chapter 3)

In addition to directly quantifying mean diffusion properties of various tracts, WM pathways can be reconstructed based on the computed diffusion directions. A novel framework was introduced for probabilistic tractography in complex fiber orientations with parsimonious model selection. The proposed approach outperforms an existing state-of-the-art method on both phantom and human data allowing for in-vivo probabilistic multi fiber tractography. (Chapter 4)

Previous works on stroke suggested that existence of the intact sensory pathways from the periphery to the motor cortex could serve as a proxy for the motor function recovery. A novel method was developed combining diffusion-weighted MRI with electroencephalography (EEG). Responses of different cortical areas to the external stimulation were measured using EEG while anatomic connections between those areas were estimated using dMRI-based tractography. This study demonstrated the feasibility of estimating active cortical sources and their dynamic interactions in stroke patients during a sensory stimulation task. In the future, this could allow monitoring dynamic brain activity and identifying quantitative biomarkers to assess sensory impairment following a hemiparetic stroke. (Chapter 5)

Finally, six stroke patients were tracked with dMRI throughout the recovery process starting within five days post-stroke and until six months post-stroke. Analysis of the multi-compartment models accounting for the free water compartment (determined in Chapter 3) did not reveal a common pattern of the recovery in terms of the mean diffusion statistics' asymmetry of superior longitudinal fasciculus and corticospinal tract. However, a rapid decrease in the free water asymmetry during the first five weeks post-stroke seemed to be coupled with the substantial improvement in the patients' motor performance. This suggests that decrease in tissue swelling is associated with spontaneous neurological recovery of the patients. (Chapter 6)

To conclude, this thesis related diffusion-weighted imaging measures with patient outcomes and introduced frameworks to enhance our insight into the impact and recovery of stroke. We anticipate that in the future it may help to set realistic rehabilitation goals and to facilitate selection of more personalized rehabilitation approaches.

Acknowledgments

This is both the easiest and the most difficult part of writing the thesis. On one hand, it is an opportunity to express my gratitude to all the people who helped, supported, encouraged and kept me (mostly) sane during the past four years. On the other hand, it is hard to do so in just a few paragraphs.

First of all, I would like to thank my promotors prof. Frans van der Helm and prof. Lucas van Vliet, as well as my co-promotors dr. Frans Vos and dr. Alfred Schouten for the opportunity to work at TU Delft and to do research together with them.

Dear Frans H, it has been an eventful and interesting journey to work under your supervision. Thank you for always being critical and challenging towards my work.

Dear Lucas, it has been a great honor to be your PhD student. I will never forget your full support to finish my thesis on time. Your feedback during the bi-weekly progress meetings really kept me motivated and encouraged.

Dear Frans V, thank you for your daily support and words of wisdom when they were most needed. It was a great learning experience for me to work with you. I appreciate your patience and guidance.

Dear Alfred, you have always been very approachable and eager to help or share knowledge. At all times, you were an affable face no matter what.

Second, I would like to express my gratitude to all my co-authors, including the master and bachelor students who worked with me, for our at times heated discussions. Be that on the mathematical content, clinical relevance, physiology or MR measurements, it lead to improvements and better understanding of the 'what' and 'why' of the work.

My best thoughts and gratitude to all the patients and healthy volunteers who dedicated their time to the 4D EEG experiments under frequently very challenging conditions of their lives. Moreover, I would like to thank all the doctors, nurses, MR technicians and other personnel of RdGG, VUmc and AMC who were instrumental in gathering data without which this thesis would not be possible.

I would like to thank all the people from 4D EEG project. Working in this big collaboration was an exciting and fruitful experience for me. I will never forget our monthly meetings and Skyping with Jules and Jun from Northwestern. Gert, Erwin, Jan, Carel, Aukje, Sarah, Dirk, Juhani, Caroline, Lucas and Ines – thank you for our discussions and all the hard work. And, of course, big thanks to Mique, especially for our Chicago adventures.

Warmest thanks to my colleagues from QI and BME for all the lunches, coffees, days out and other social activities we had together. Being part of two departments means that I got to work with almost twice the number of great people. At BME Nadia, Martijn, Mark, Yuan, Teo, Joost, Jantsje, Pavlo, Nurhan, Hoda, Ronald, Ingrid, Bram, Teun, Marta, Ivan and many more were always ready to share a joke, a coffee or the latest scientific paper. Thanks to Sabrina, Hanneke and a huge group of BME secretariat for always making sure that things run smoothly.

I would like to thank all the QI members for the Friday drinks, board game nights, Halloween onesies, 'secret Sinterklaas' poems and lots of other activities I probably forgot to mention. Anna, Jelle H, Jeroen H, Jelle S, Robert M. and Christiaan for our discussions about (PhD) life, complaining about graduate school and just being great office mates. Nadya for nice 'Russian' discussions and for the Dutch speaking club. Thanks 'team MRI' Joor, Willem, Tian, Jeroen S, Dirk, Robiel, Jianfei for exchanging ideas, going to courses and code discussions. Tom for always having a minute to talk about life, mortgages, houses, cats and more. Gyllion for discussing art, languages and literature. All the other colleagues: Alois, Annelies, Babak, Bernd, Boling, Edwin, Ellen, Jaap, Jelena, Jeroen K, Jos, Joost, Juan Pedro, Kedir, Mohammed, Mojtaba, Hamid, Pierre, Rasmus, Richard, Robert N, Ronald, Sjoerd, Taylor, Ted, Yan and Zhang. Hope I did not forget anyone and sorry if I did.

Hanne, Hans, Andrea and Luc, I would not have even started doing this PhD without working with you. Thanks for believing in me.

Adrian, Maxime, Danielle, Duygu, Mathias, Roxane, Shekoofeh, Ben and the rest of the MICCAI Student Board over the years, I learned a ton from you. Thanks for the Hangouts, late conference nights and organizing so many events together!

Markus, thank you for in-depth discussions about life and career. Also for believing in my crazy idea and organizing TOP GRAD with me.

Kristina, Valeriu, Masha, Patricio, Inga, Maxim, Tamerlan, Alex, Sultan, Aleksandra, Julia, Eugenia, Lena thank you for being a great counterbalance for all the academic struggles.

All my friends in Odessa, thank you for being part of my life for so long that many of you have even started families with the cutest future physicists and mathematicians ☺ Valentin, Daria, Kirill, Aleksey, Anna, Yuriy and many more: it is impossible to mention all your names here, but you know that I appreciate your support.

Valeriy Koleboshin, Pavel Viktor, Vadim Manakin – thanks for being the best physics teachers. You were the ones who set me on the path towards research.

Finally, I want to thank my family, especially my parents Olga and Grygoriy, for their unwavering love and support. Родители, спасибо за вашу поддержку и словом, и делом. Без вас все эти достижения были бы невозможны.

Last, but definitely not least, I would like to thank Oleg, my dearest husband. You have always been my constant, a shoulder to cry on, a partner, a friend, help and support, even in designing the cover of this thesis. I am very grateful to the fate that we found each other.

About the author

Lena Filatova was born on August 14, 1989 in Odessa, Ukraine.

In June 2010, Lena obtained her Bachelor degree in applied mathematics from Odessa I. I. Mechnikov National University, Ukraine. From September 2010 to September 2012, Lena did her master in industrial and applied mathematics at Eindhoven University of Technology, The Netherlands. Lena then worked as a Professional Doctorate in Engineering trainee in healthcare systems design program at the Electrical Engineering department of the same university. Her project was focused on cardiac image analysis. From October 2014 till October 2018, she did her PhD project jointly at the Biomechanical Engineering Group and at the Quantitative Imaging Group, Delft University of Technology. She was involved in the EU-funded 4D EEG project working on analysis of diffusion-weighted magnetic resonance imaging.

Publications

Filatova, O.G., van Vliet, L.J., Schouten, A.C., Kwakkel, G., van der Helm, F.C.T., and Vos, F.M. (2018a). Comparison of Multi-Tensor Diffusion Models' Performance for White Matter Integrity Estimation in Chronic Stroke. *Frontiers in Neuroscience* 12(247). doi: 10.3389/fnins.2018.00247.

Filatova, O.G.*, Yang, Y.*, Dewald, J.P.A., Tian, R., Maceira-Elvira, P., Takeda, Y., et al. (2018b). Dynamic information flow based on EEG and diffusion MRI in stroke: a proof-of-principle study. *Frontiers in Neural Circuits*. doi: 10.3389/fncir.2018.00079.

Versteeg, E., Vos, F.M., Kwakkel, G., van der Helm, F.C.T., Arkesteijn, J.A.M., and **Filatova, O.G.** (2018c). "Probabilistic Tractography for Complex Fiber Orientations with Automatic Model Selection", in: *Computational Diffusion MRI, MICCAI 2017*, eds. E. Kaden, F. Grussu, L. Ning, C.M.W. Tax & J. Veraart: Springer International Publishing), 117-128.

Bouziane, C.*, **Filatova, O.G.***, Schrantee, A., Caan, M.W.A., Vos, F.M., Reneman, L. A randomized controlled trial on the effects of Methylphenidate on brain white matter development. (*submitted*)